

Probing spin, charge, and orbital degrees of freedom in complex transition-metal oxide heterostructures by x-ray spectroscopy



Eva Benckiser

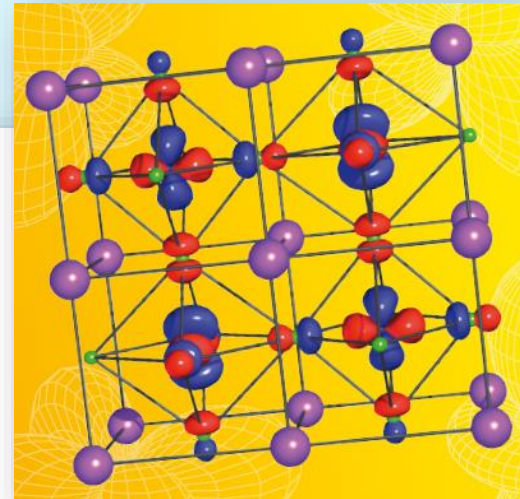
Max Planck Institute for Solid State Research, Stuttgart, Germany

September 20, 2023

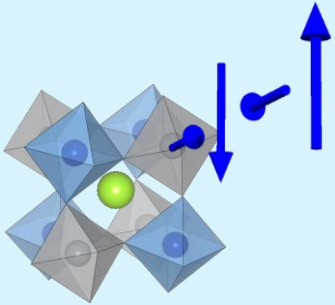
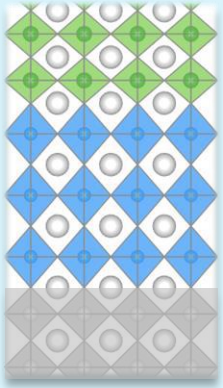
Autumn School on Correlated Electrons

Orbital Physics in Correlated Matter

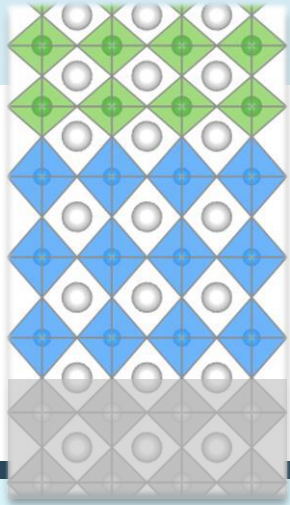
18 – 22 September 2023
Forschungszentrum Jülich



Outline

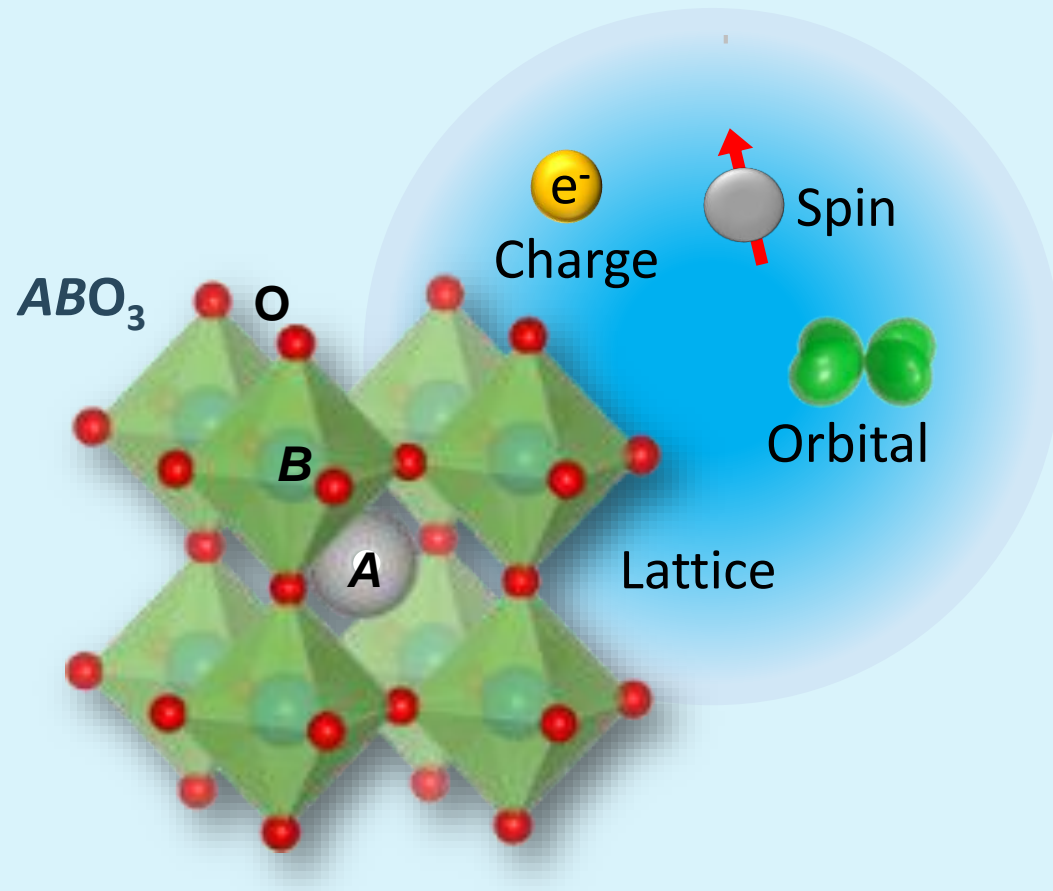


- I. **Complex oxide heterostructure** with correlated spin, charge, orbital, and lattice degrees of freedom
- II. **How can we probe spin, charge, and orbital degrees of freedom by x-ray spectroscopy?**
 - X-ray absorption spectroscopy (XAS) with polarized soft x-rays
 - Resonant x-ray reflectometry (XRR)
 - Resonant elastic x-ray scattering (REXS)
- III. **Case studies:**
 - **Interfacial doping** in cuprate-nickelate hybrid structures
 - **Orbital reflectometry** of nickelate and vanadate superlattices
 - Noncollinear **magnetic order** in nickel oxide heterostructures



Complex oxide heterostructure

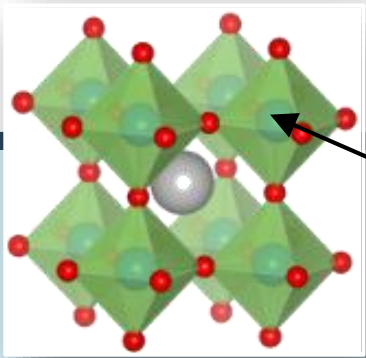
3d transition-metal oxide perovskites



- **Large variety of interesting quantum states:** Magnetism, Mott transitions, superconductivity, (multiferro)electrics, ...
- **facile chemical substitution**
- Flexible and comparatively **simple structure**
- **cube-on-cube** combination of different compounds in heterostructures.

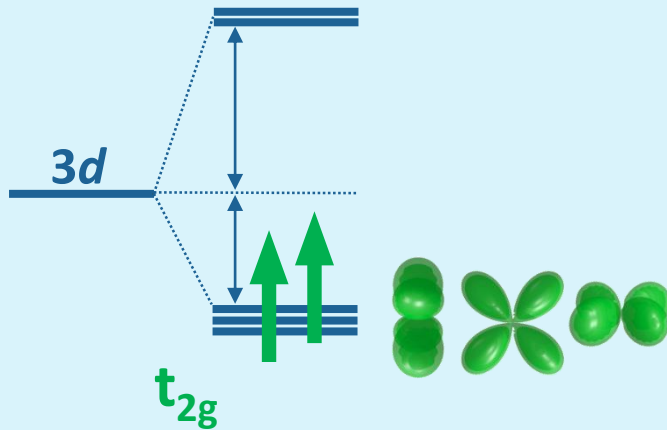
→ **Building blocks of our heterostructures**

Two prototypical correlated material systems



V^{3+} or Ni^{3+}

Vanadates RVO_3 ($3d^2$)

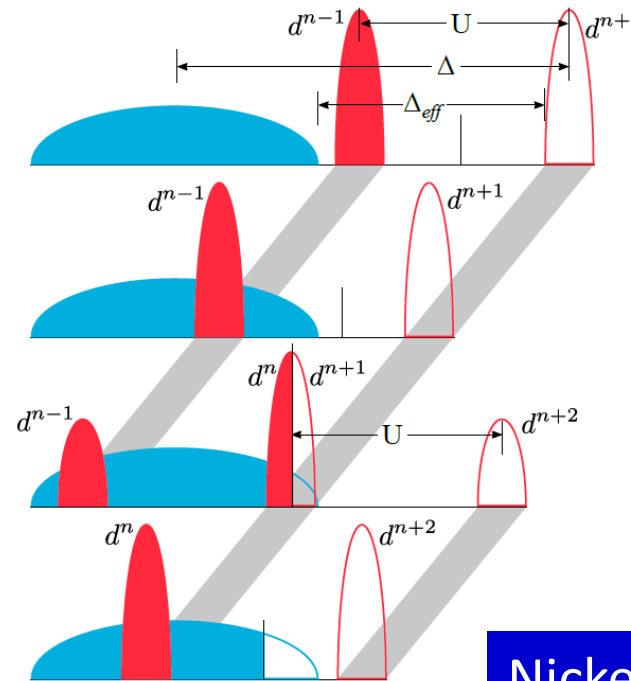


Mott-Hubbard
 $|\psi_0\rangle = |d^n\rangle$

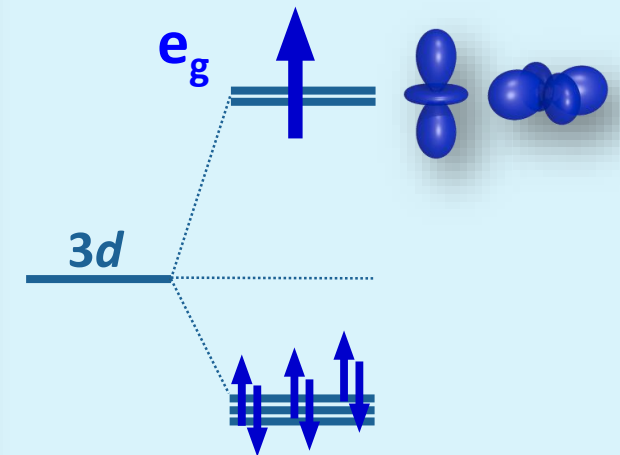
Positive
Charge Transfer
 $|\psi_0\rangle = |d^n\rangle$

Mixed Valence
 $|\psi_0\rangle = ?$

Negative
Charge Transfer
 $|\psi_0\rangle = |d^{n+1}\bar{L}\rangle$



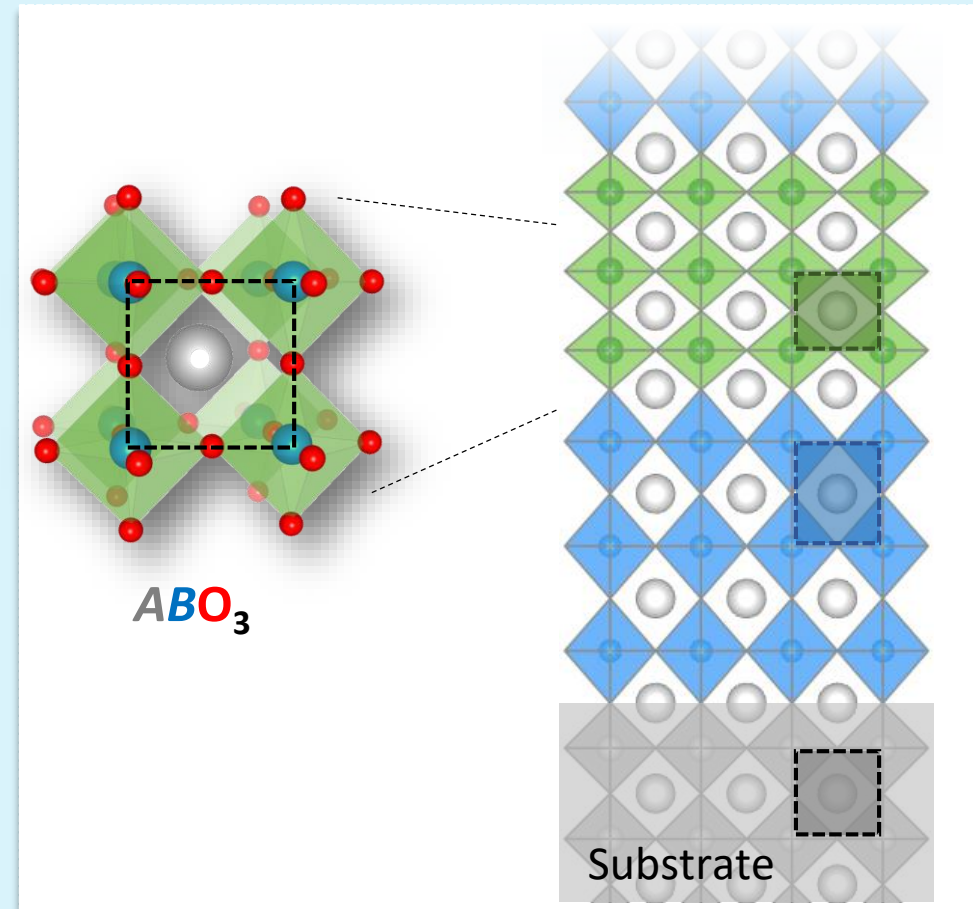
Nickelates $RNiO_3$ ($3d^7$)



Rational design

- (i) Create **unique model systems** to study the materials and understand their interfaces
- (ii) **Stabilization of interesting phases** under more easily accessible conditions and with less disorder (superconductivity, magnetic phases, ...)

Goal: Modify the properties of ABO_3 compounds through targeted realization of interface reconstructions



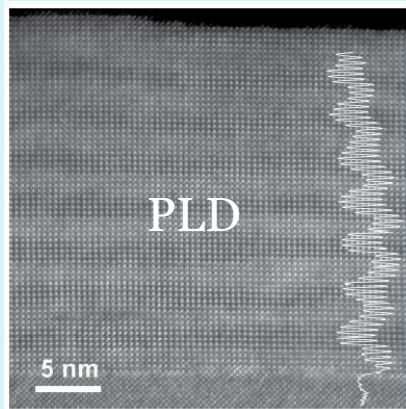
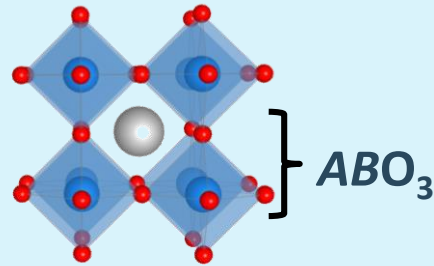
Growth of oxide heterostructures

Pulsed laser deposition

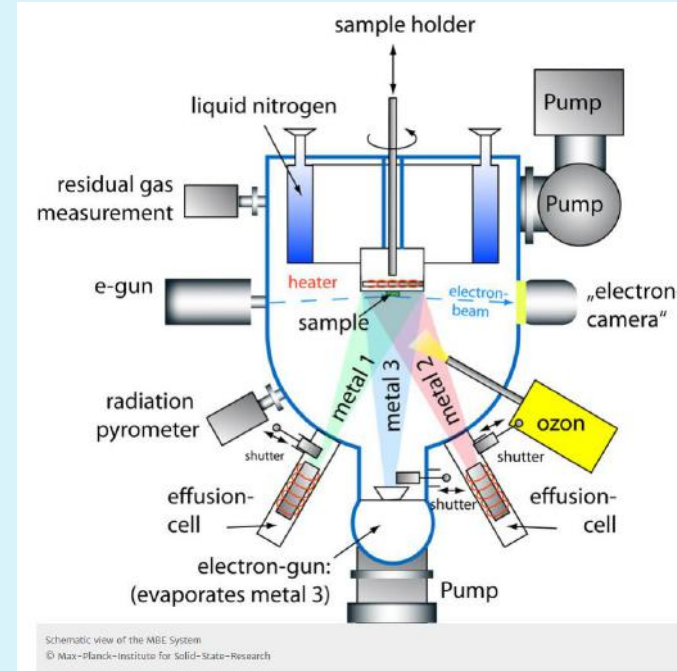


Photograph of the laser plume.
© Max-Planck-Institute for Solid-State-Research

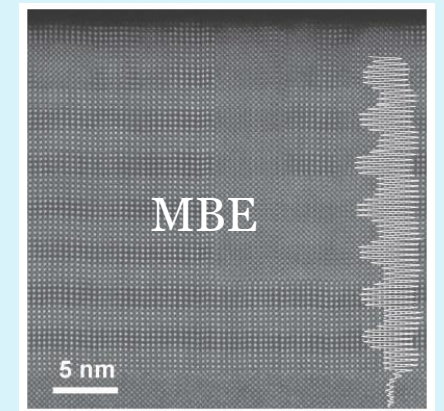
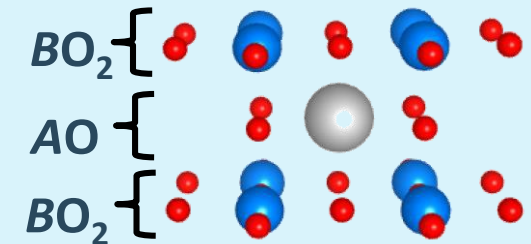
unit cell precision



Molecular beam epitaxy

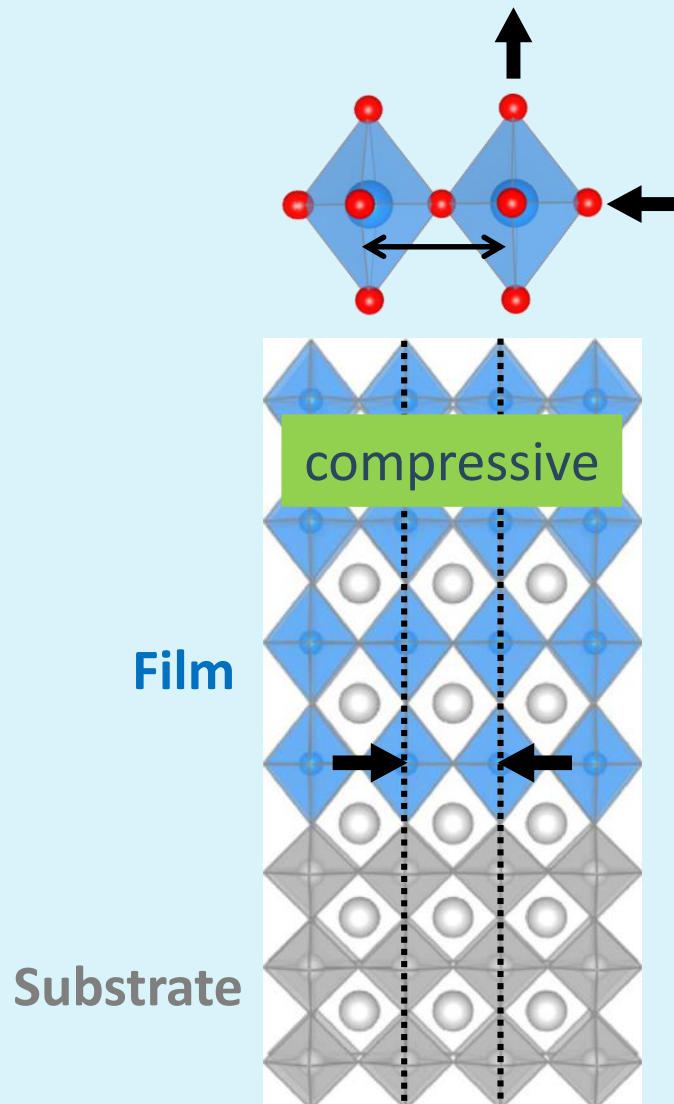


atomic layer precision



In collaboration with G.
Logvenov's group at
MPI-FKF

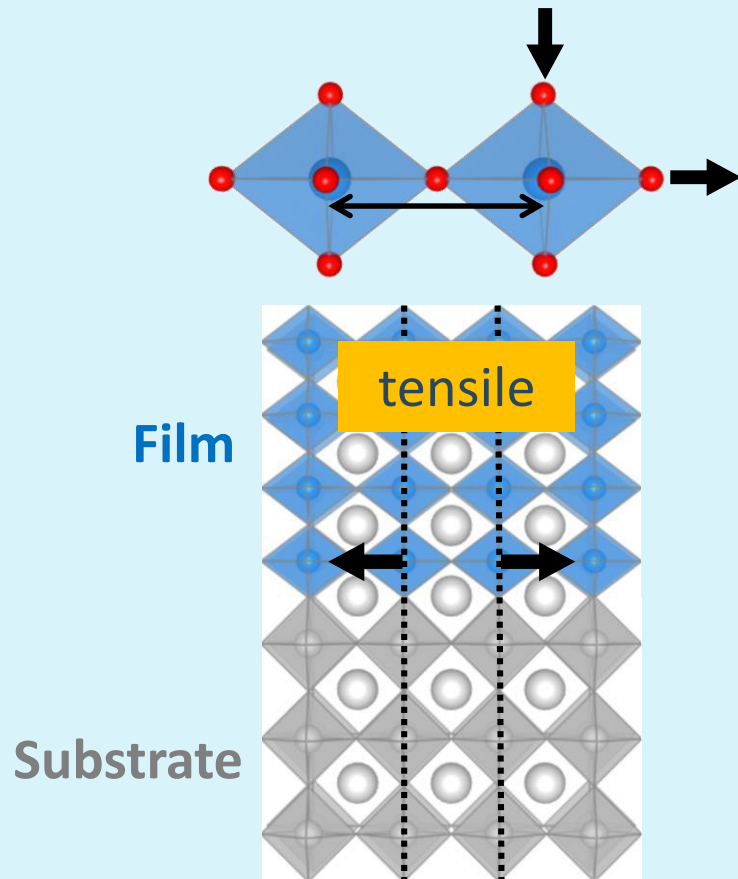
Epitaxial strain – structural modifications



Structural modifications are often crucial

- Lattice mismatch with underlying substrate
→ **compressive or tensile biaxial strain**
- Necessity to connect across the interface:
 - **Deformation** of octahedra
 - **Tilts & rotations** of the octahedra
- **Affect TM-O-TM bond length and bond angles!**

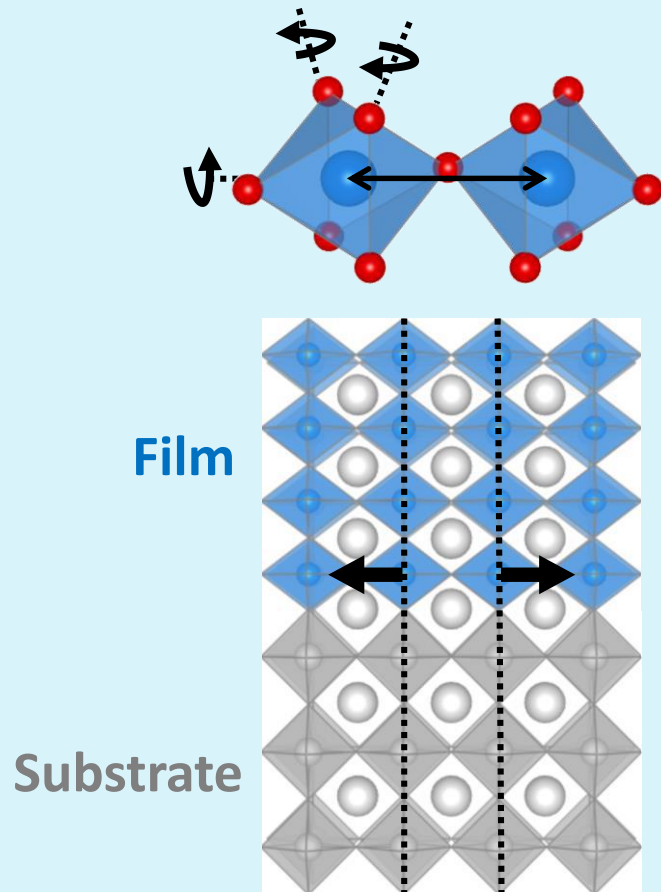
Epitaxial strain – structural modifications



Structural modifications are often crucial

- Lattice mismatch with underlying substrate
→ **compressive or tensile biaxial strain**
- Necessity to connect across the interface:
 - **Deformation** of octahedra
 - **Tilts & rotations** of the octahedra
- **Affect TM-O-TM bond length and bond angles!**

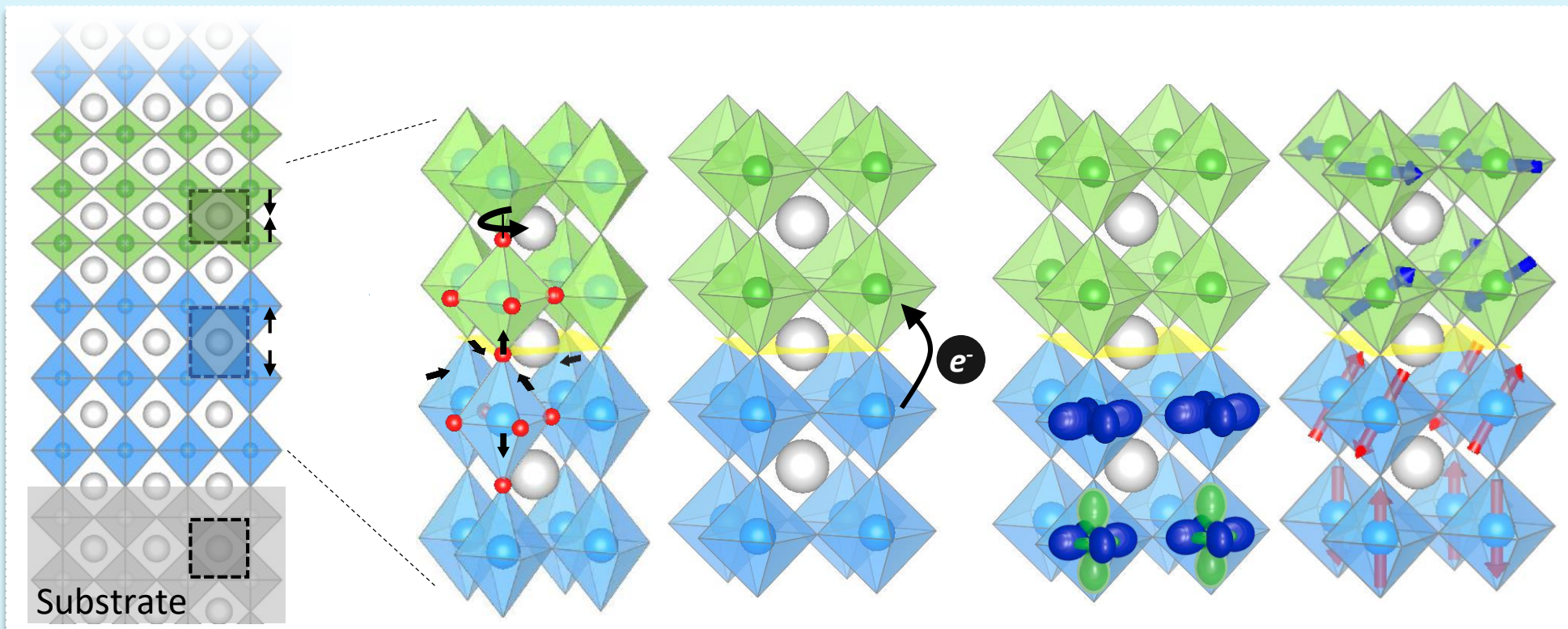
Epitaxial strain – structural modifications



Structural modifications are often crucial

- Lattice mismatch with underlying substrate
→ **compressive or tensile biaxial strain**
- Necessity to connect across the interface:
 - **Deformation** of octahedra
 - **Tilts & rotations** of the octahedra
- **Affect TM-O-TM bond length and bond angles!**

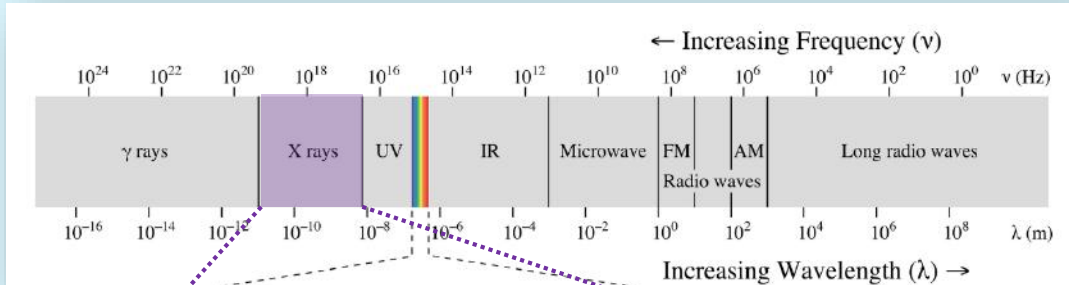
Lattice, charge, orbital, and magnetic reconstructions



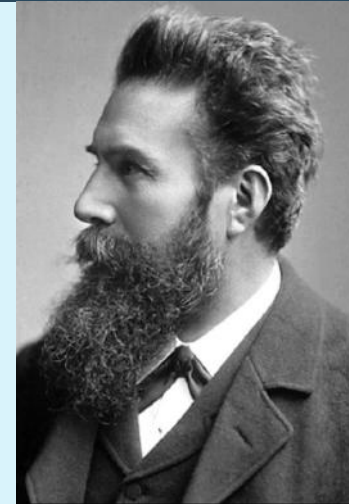
Interfacial charge transfer, orbital reconstructions, and magnetic interactions

How can we probe spin, charge, and orbital degrees of freedom by x-ray spectroscopy?

X-rays



| Range | Energy | Wavelength |
|-------------|---------------------|--------------------|
| Soft | 30 – 1500 eV | 413 – 8.3 Å |
| Tender | 1500 – 7500 eV | 8.3 – 1.7 Å |
| Hard | 8 keV – 60 keV | 1.7 – 0.2 Å |



Wilhelm Conrad Röntgen

*1845 in Lennep
† 1923 in München



... but was buried in the family grave
in the old cemetery in Gießen

X-ray mass absorption coefficient

The measured quantity is the x-ray **mass absorption coefficient** defined by

$$I = I_0 e^{-\mu \rho d}$$

transmitted intensity through a material of density ρ and thickness d .

Absorption cross section:

$$\sigma_{abs}(E) = \frac{\mu(E)}{n}$$

with n : density of targeted particles

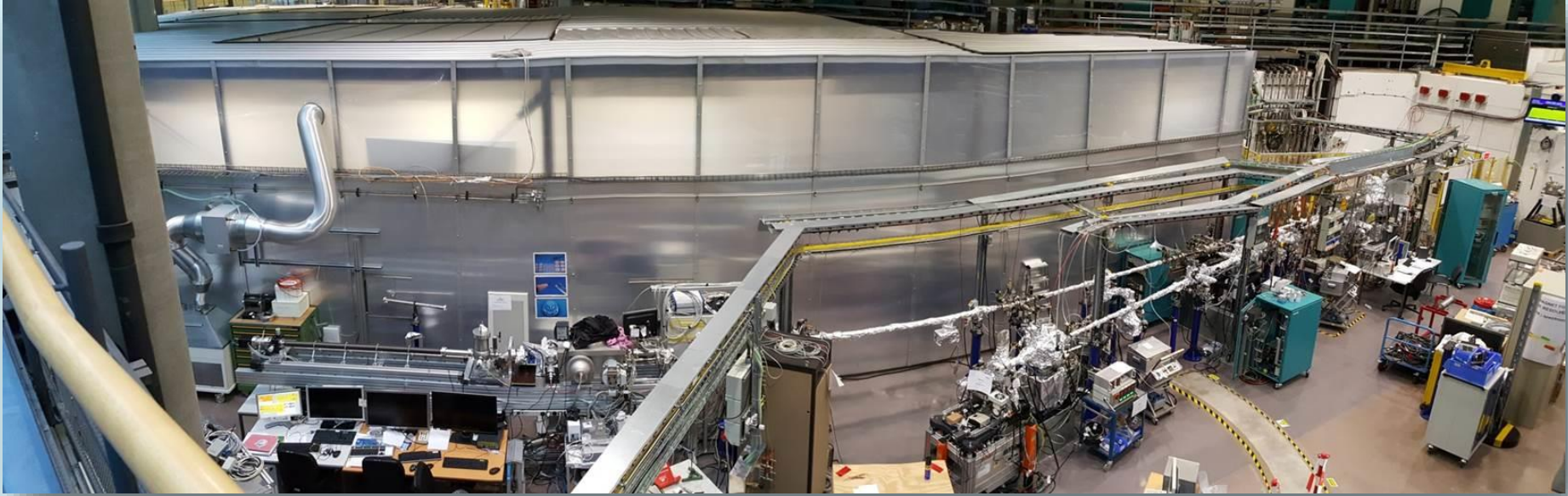
Attenuation Length $1/\mu$: *“penetration depth into the material measured along the surface normal where the intensity of x-rays falls to 1/e of its value at the surface”*

$\mu = \mu(E) \rightarrow$ In x-ray spectroscopy we require highly brilliant, polarized, x-rays with tunable energy

Synchrotrons around the world

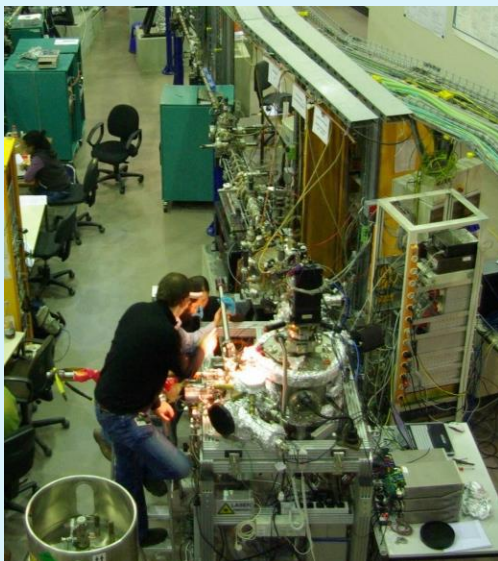


Soft x-ray beamlines

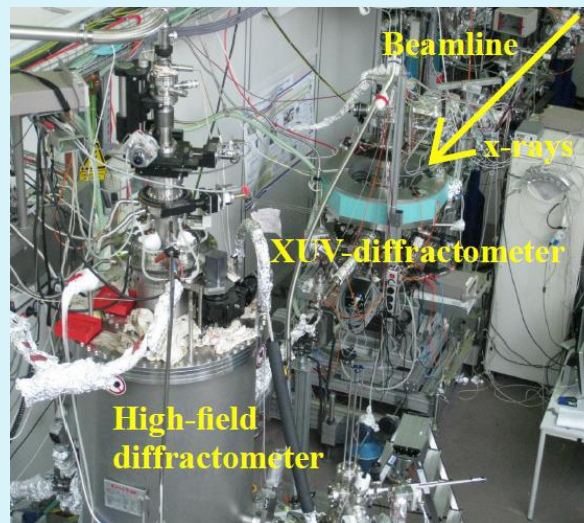


Ultra-high vacuum, Undulator beamline: highly brilliant x-rays, high degree of elliptical polarization which can be varied (linear/circular)

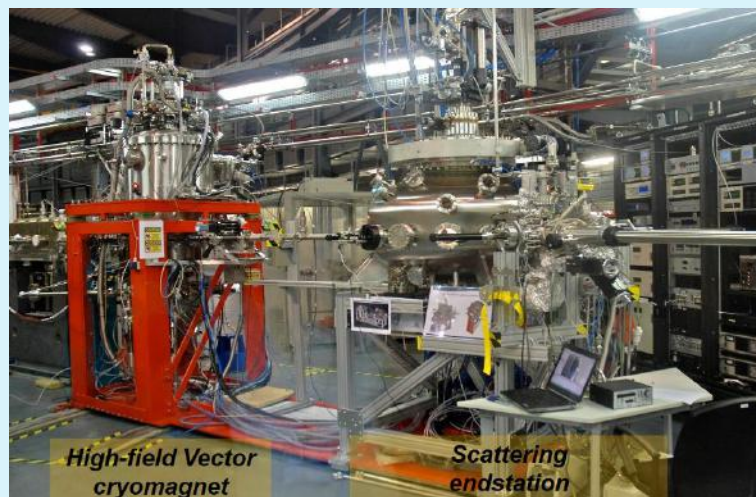
Soft x-ray diffractometers



UE56/2-PGM1
beamline @
BESSY Berlin,
+ MPI UHV
magnetic
reflectometer



UE46-PGM1 beamline @
BESSY Berlin, Germany

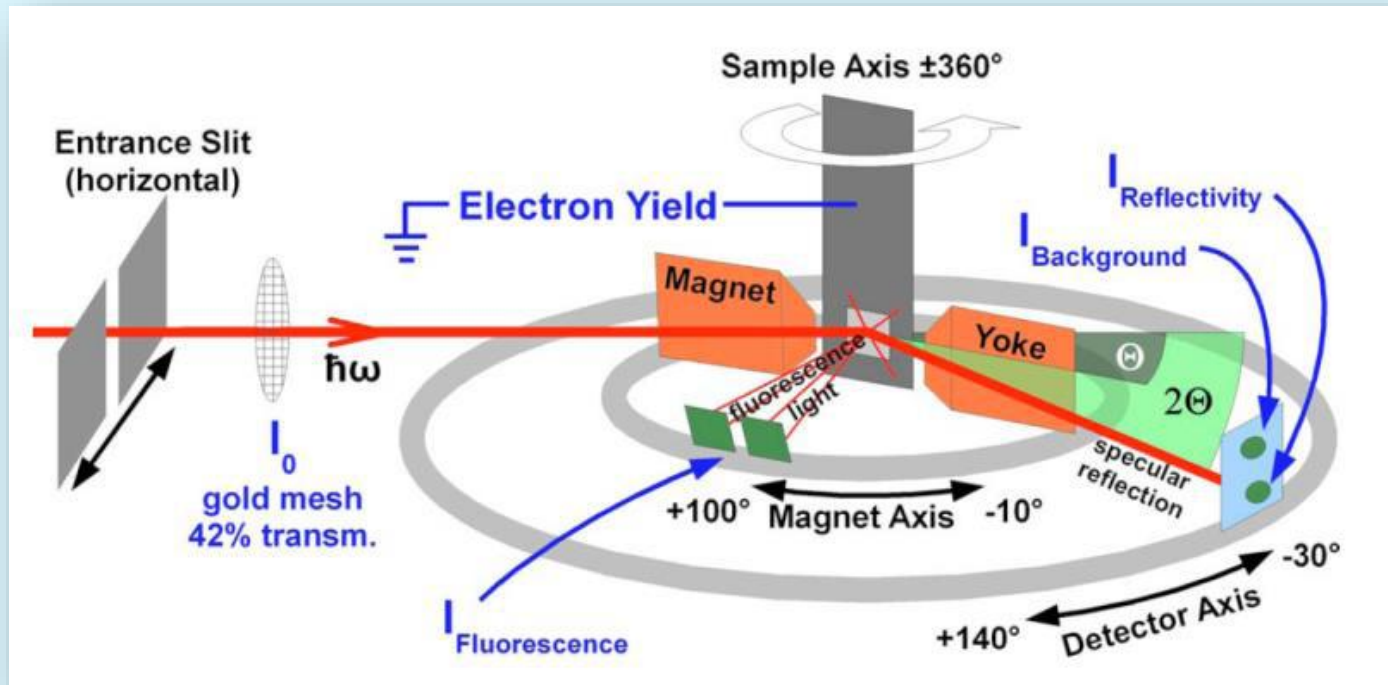


BOREAS beamline
@ ALBA Barcelona,
Spain



REIXS beamline @ CLS
Saskatoon, Canada

UHV reflectometer




- Beamline: linear and circular polarized soft x-rays: $E = 60 - 1300$ eV
- UHV conditions
- Temperature: 30 – 500 K (liquid N₂, He)
- Magnet: max. 640 mT
- In-situ measurement **x-ray absorption** (TEY & FY) and specular **x-ray scattering** (reflectivity)

Absorption and Scattering

Transition probability up to second order perturbation theory (**Fermi's golden rule**)

Total cross section:

$$\sigma = \frac{W}{\phi_0} = \frac{2\pi}{\hbar\phi_0} \left| \langle f | H_{int} | i \rangle + \sum_n \frac{\langle f | H_{int} | n \rangle \langle n | H_{int} | i \rangle}{E_i - E_n} \right| \delta(E_i - E_f)$$


n : intermediate (virtual) state

\sum_n : over all possible intermediate states with E_n

energy conservation; $|n\rangle$ virtual state, i.e. no energy conservation required, i.e. does not appear in $\delta(\dots)$

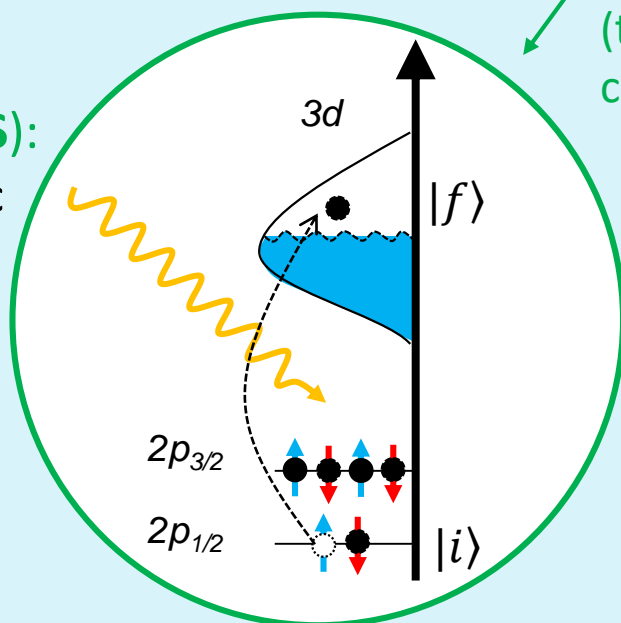
Interaction Hamiltonian

$$H_{int} \propto \mathbf{p} \cdot \hat{\mathbf{A}} + \hat{\mathbf{A}} \cdot \hat{\mathbf{A}}$$

$$\hat{\mathbf{A}}(\mathbf{r}_k, t) \propto \sum_{i,k} \frac{1}{\sqrt{k}} \varepsilon_i (a_{k,i}(t) e^{ikr} + a_{k,i}^\dagger(t) e^{-ikr})$$

Vector potential of radiation field

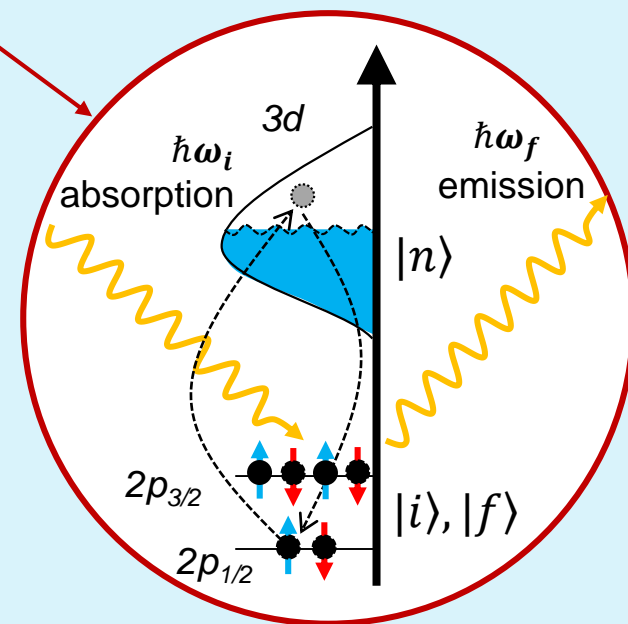
X-ray absorption spectroscopy (**XAS**): average electronic structure



± 1 photon
(term linear in photon creation/annihilation)

Resonant x-ray diffraction ($\hbar\omega_1 = \hbar\omega_2$, **REXS**): ordered electronic/magnetic structure

$0, \pm 2$ photons



Resonant inelastic x-ray scattering ($\hbar\omega_1 \neq \hbar\omega_2$, **RIXS**): dynamics of low energy excitations

Scattering factor

In a crystal, each lattice site acts as a scattering center for the incident x-rays and is described by the atomic scattering factor/tensor

$$F(E, \mathbf{q}) = f_0(\mathbf{q}) + f_{mag}^{non-res} + \underbrace{f'_{res}(E) + if''_{res}(E)}_{\text{energy-dependent anomalous dispersion corrections}}$$

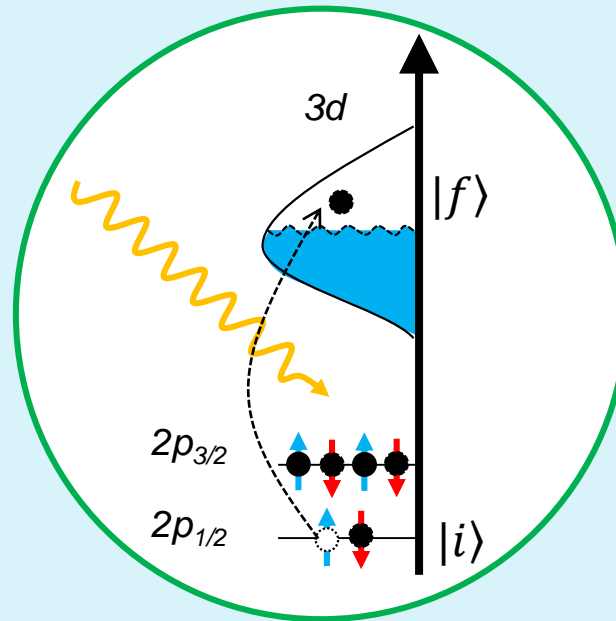
energy-dependent
anomalous dispersion corrections

Optical theorem

$$I_{XAS} \propto -\frac{1}{E} \text{Im}(F(E)) = f''_{res}(E)$$

$$\hat{F} = \begin{pmatrix} F^{xx} & F^{xy} & F^{xz} \\ F^{yx} & F^{yy} & F^{yz} \\ F^{zx} & F^{zy} & F^{zz} \end{pmatrix}$$

X-ray absorption spectroscopy



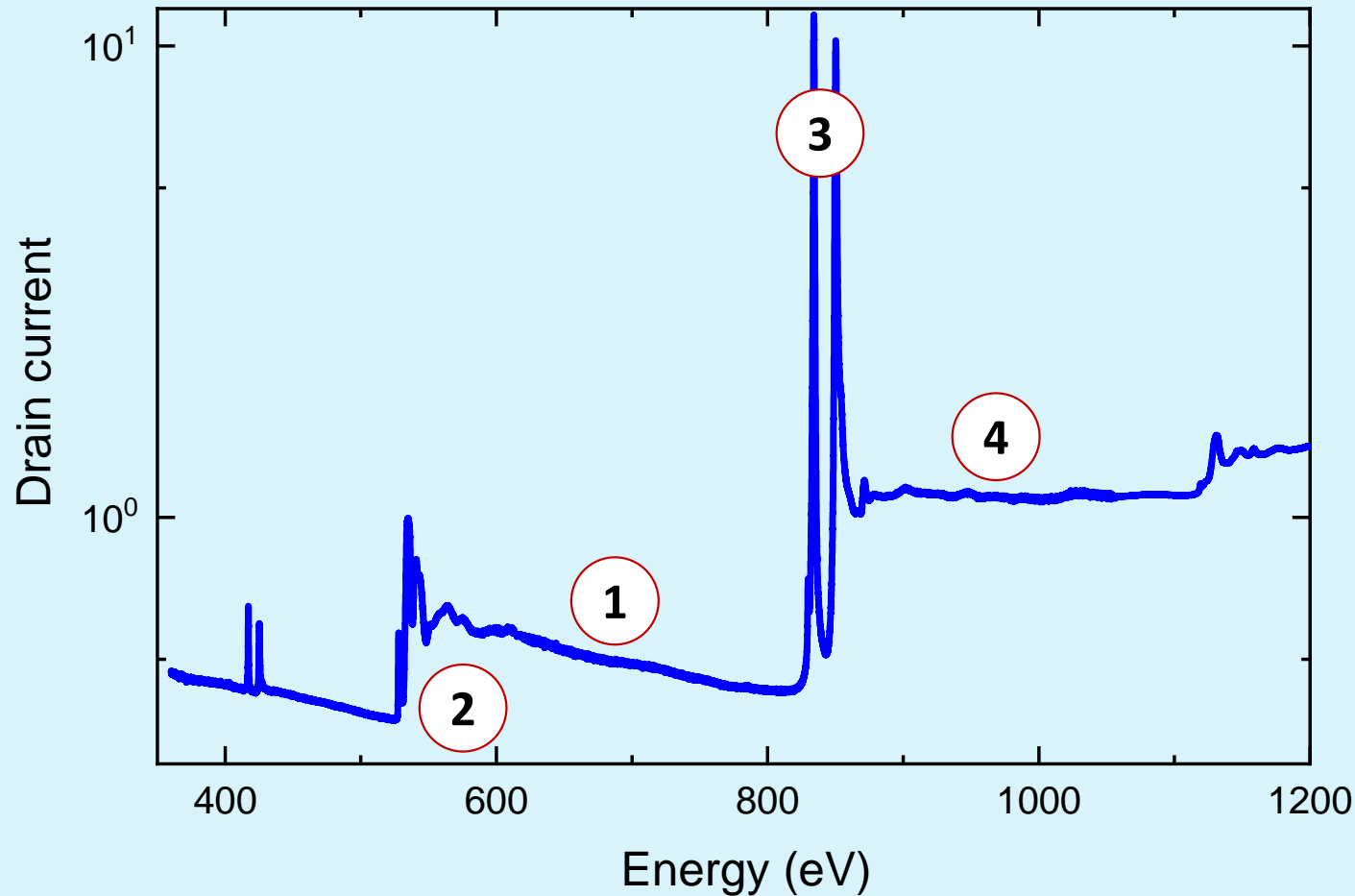
Fermi's golden rule (dipole approximation)

Electric dipole
selection rules:

$$\Delta l = 1, \Delta m = \pm 1$$

$$I_{XAS} = \frac{2\pi}{\hbar} \sum_f |\langle f | \hat{\epsilon} \cdot \mathbf{r} | i \rangle|^2 \cdot \delta(E_i - E_f - \hbar\omega)$$

A measured spectrum over a wide energy range



General features of the spectrum:

- 1 Overall decrease of $\mu(E)$ with $\sim 1/E^3$
- 2 Absorption edges: Element sensitivity & valence state
- 3 Near Edge X-ray Absorption Fine Structure (NEXAFS) also X-ray Absorption Near-Edge Structure (XANES): crystal field, spin & orbital
- 4 Extended X-ray Absorption Fine Structure: local atomic distances (not in this lecture)

Soft XAS

Periodic Table of the Elements

| | | | | | | | | | | | | | | | | | | | | | |
|--------------------|--------------------|--------------------|--------------------|--------------------|--------------------|--------------------|--------------------|--------------------|--------------------|--------------------|--------------------|--------------------|--------------------|--------------------|--------------------|--------------------|--------------------|------------------|------------------|-------------------|-------------------|
| 1 H 1.01 | | | | | | | | | | | | | | | | | 2 He 4.00 | | | | |
| 3 Li 6.94 | 4 Be 9.01 | | | | | | | | | | | | | | | 5 B 10.81 | 6 C 12.01 | 7 N 14.01 | 8 O 16.00 | 9 F 19.00 | 10 Ne 20.18 |
| 11 Na 22.99 | 12 Mg 24.31 | | | | | | | | | | | | | | | 13 Al 26.98 | 14 Si 28.09 | 15 P 30.97 | 16 S 32.07 | 17 Cl 35.45 | 18 Ar 39.95 |
| 19 K 39.10 | 20 Ca 40.08 | 21 Sc 44.96 | 22 Ti 47.87 | 23 V 50.94 | 24 Cr 52.00 | 25 Mn 54.94 | 26 Fe 55.85 | 27 Co 58.93 | 28 Ni 58.69 | 29 Cu 63.55 | 30 Zn 65.39 | 31 Ga 69.72 | 32 Ge 72.61 | 33 As 74.92 | 34 Se 78.96 | 35 Br 79.90 | 36 Kr 83.80 | | | | |
| 37 Rb 85.47 | 38 Sr 87.62 | 39 Y 88.91 | 40 Zr 91.22 | 41 Nb 92.91 | 42 Mo 95.94 | 43 Tc (98) | 44 Ru 101.07 | 45 Rh 102.91 | 46 Pd 106.42 | 47 Ag 107.87 | 48 Cd 112.41 | 49 In 114.82 | 50 Sn 118.71 | 51 Sb 121.76 | 52 Te 127.60 | 53 I 126.90 | 54 Xe 131.29 | | | | |
| 55 Cs 132.91 | 56 Ba 137.33 | 57 La 138.91 | 72 Hf 178.49 | 73 Ta 180.95 | 74 W 183.84 | 75 Re 186.21 | 76 Os 190.23 | 77 Ir 192.22 | 78 Pt 195.08 | 79 Au 196.97 | 80 Hg 200.59 | 81 Tl 204.38 | 82 Pb 207.2 | 83 Bi 208.98 | 84 Po (209) | 85 At (210) | 86 Rn (222) | | | | |
| 87 Fr (223) | 88 Ra (226) | 89 Ac (227) | 104 Rf (261) | 105 Db (262) | 106 Sg (266) | 107 Bh (264) | 108 Hs (269) | 109 Mt (268) | 110 (271) | 111 (272) | 112 (283) | 114 (287) | | | | | | | | | |
| Lanthanide series | | | 58 Ce 140.12 | 59 Pr 140.91 | 60 Nd 144.24 | 61 Pm (145) | 62 Sm 150.36 | 63 Eu 151.96 | 64 Gd 157.25 | 65 Tb 158.93 | 66 Dy 162.50 | 67 Ho 164.93 | 68 Er 167.26 | 69 Tm 168.93 | 70 Yb 173.04 | 71 Lu 174.97 | | | | | |
| Actinide series | | | 90 Th 232.04 | 91 Pa 231.04 | 92 U 238.03 | 93 Np (237) | 94 Pu (244) | 95 Am (243) | 96 Cm (247) | 97 Bk (247) | 98 Cf (251) | 99 Es (252) | 100 Fm (257) | 101 Md (258) | 102 No (259) | 103 Lr (262) | | | | | |

Several important absorption edges in the **soft x-ray** range:

C, N, O, F *K*-edges

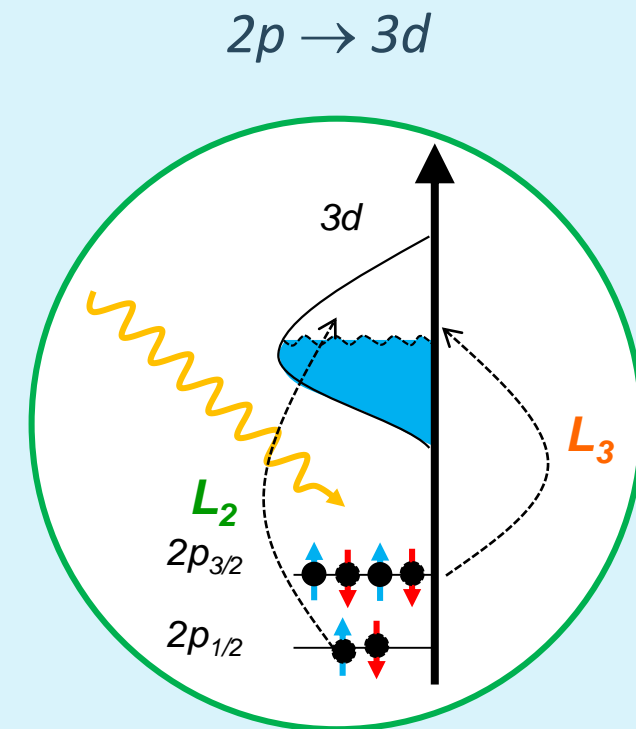
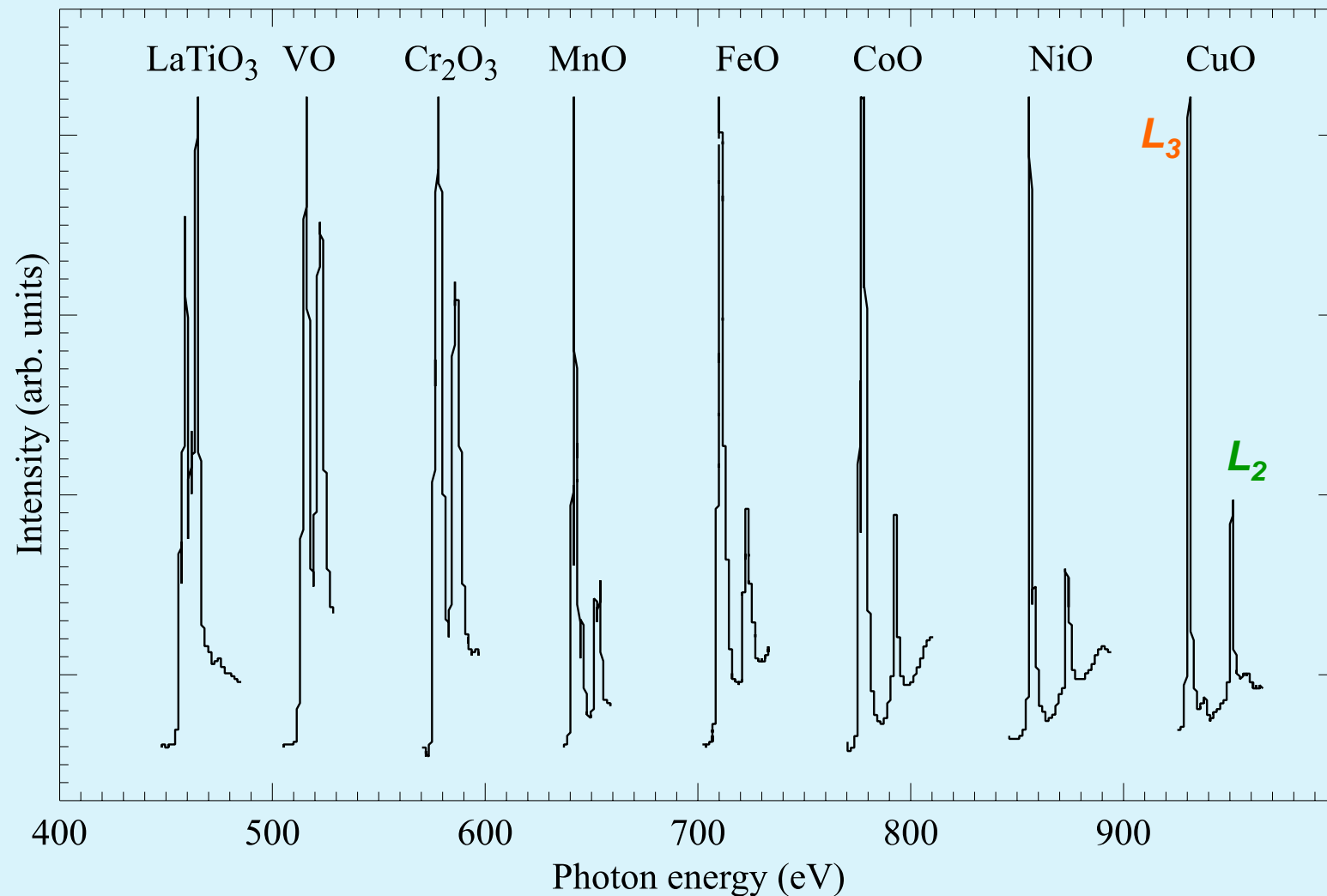
3*d* metal *L*_{2,3}-edges

4*f* rare-earth *M*_{4,5}-edges

Center for X-Ray Optics
and
Advanced Light Source

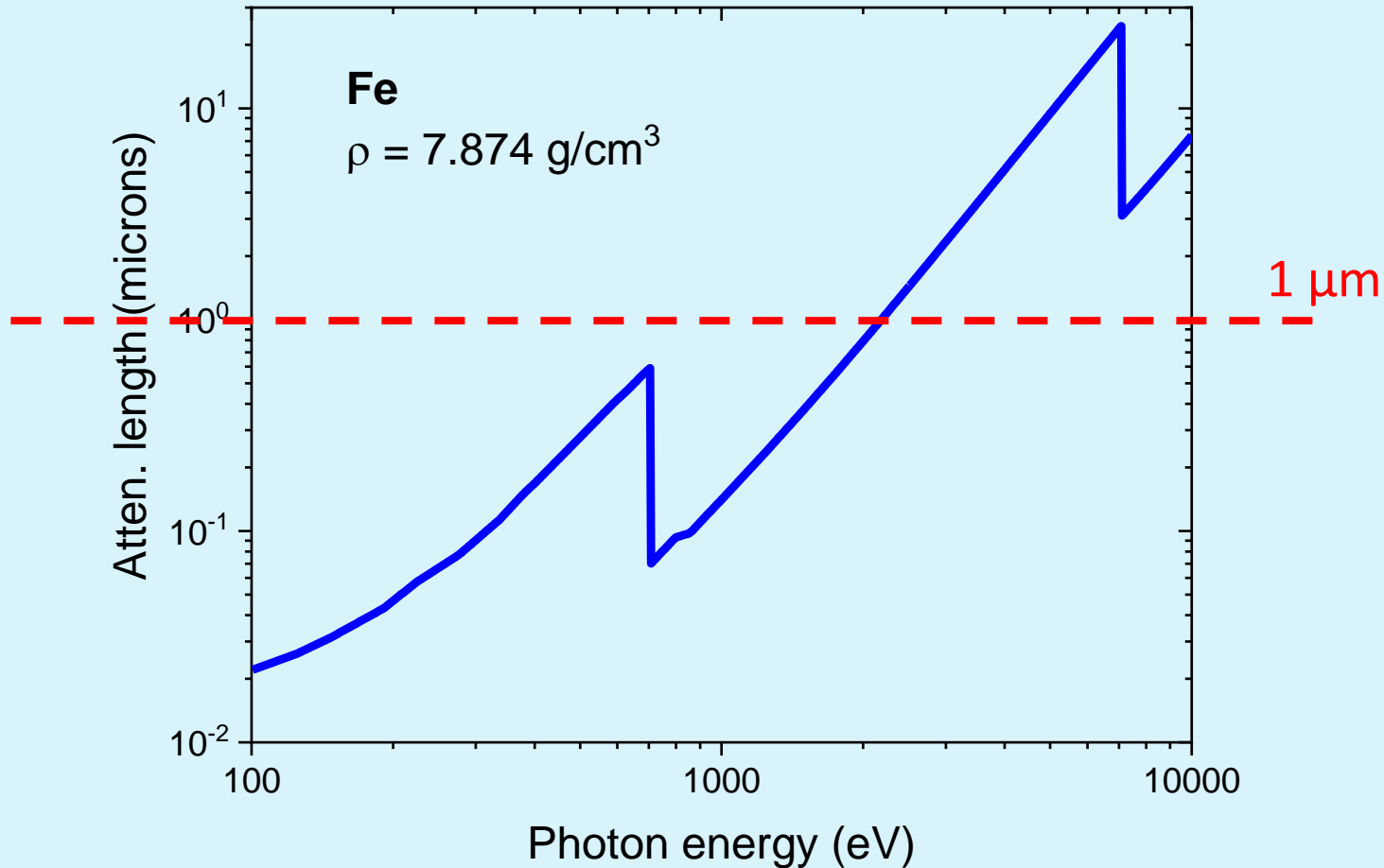
**X-RAY DATA
BOOKLET**

XAS fine structure of 3d transition metal oxides



$L_3 - L_2$ splitting increases with increasing spin-orbit splitting in the 2p core level

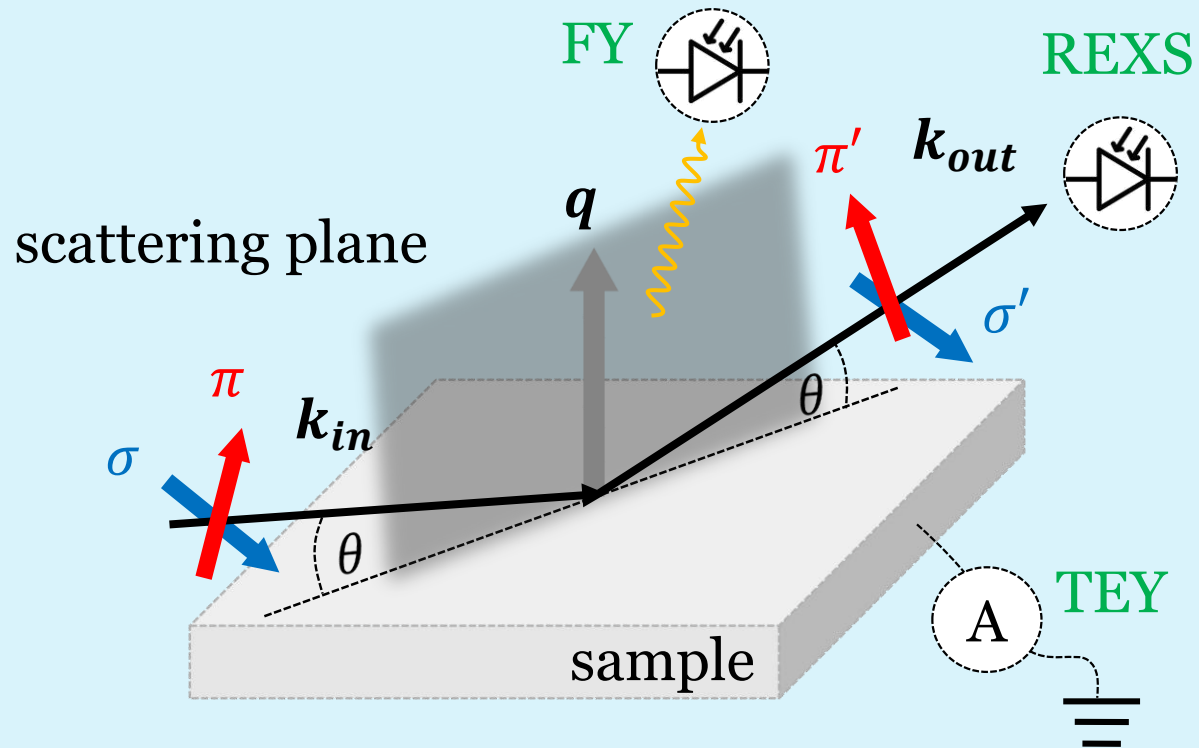
XAS measurement on solid state materials



Attenuation length in soft x-ray range below $\sim 1\ \mu\text{m}$

Transmission measurements only possible on ultrathin films / powders on transparent membranes, but for many bulk samples transmission measurements are not possible

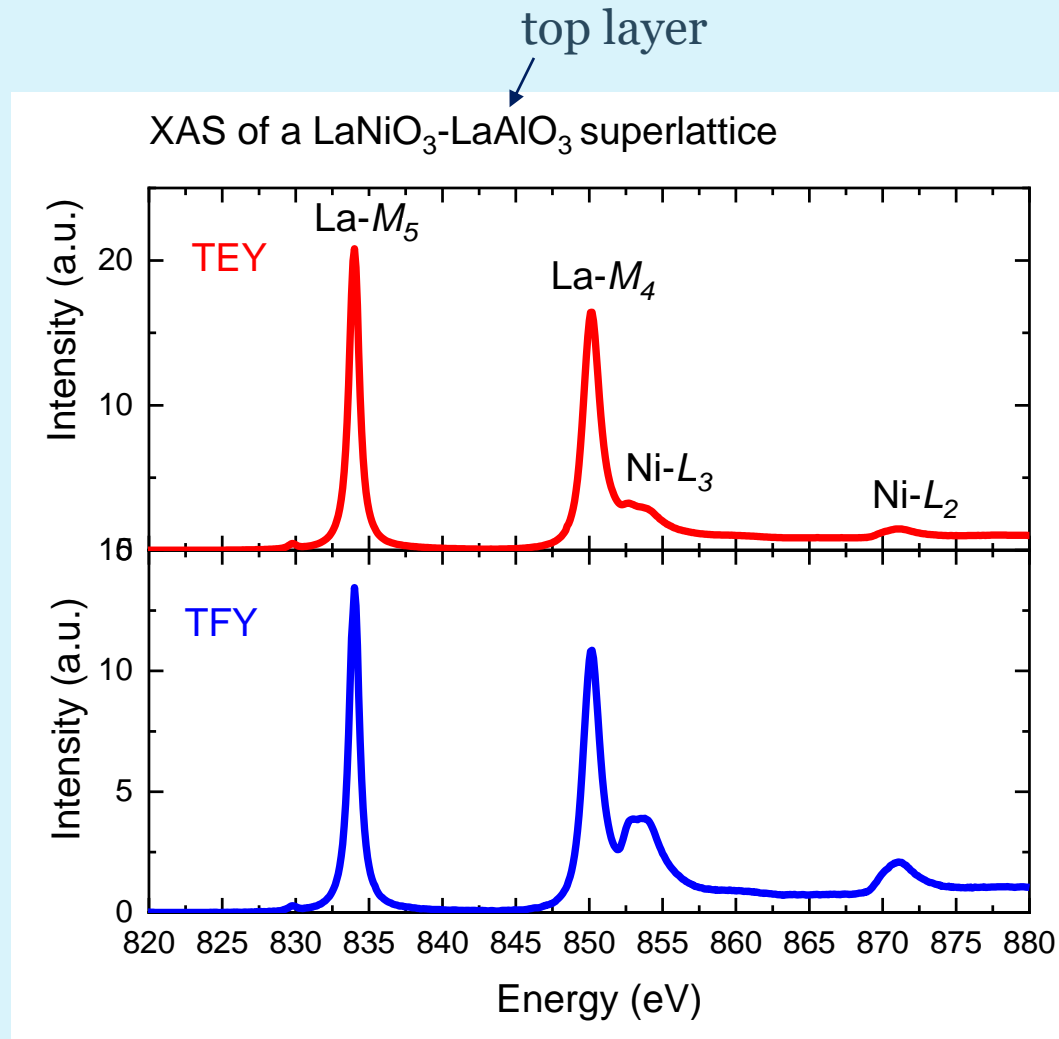
How to measure XAS on bulk samples?



The decay products of the absorption process are used to estimate the absorption!

- I. Emission of a **fluorescence photons**
 \Rightarrow **Fluorescence yield (FY)**
- II. Auger decay, followed by secondary processes that emit electrons, measure **drain current**
 \Rightarrow **Total electron yield (TEY)**

Total electron yield versus fluorescence yield

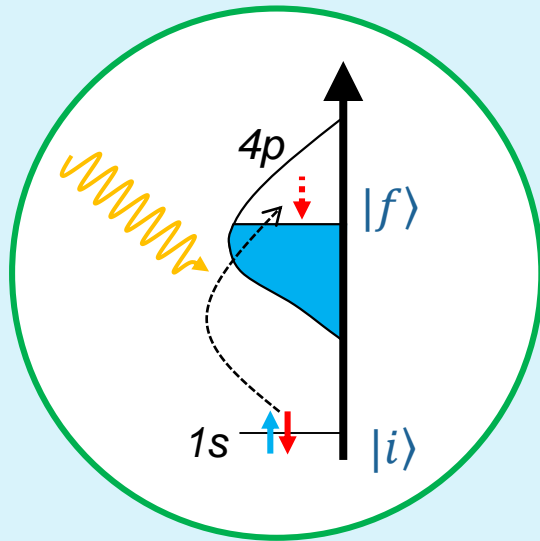


FY: saturation effects in the vicinity of strong absorption lines can falsify the relative intensities in the fine structure.

TEY: Problem of saturation is less relevant, but this type of detection is rather surface sensitive, because it depends on the effective escape depth of the photoelectrons, which is often less than 5 nm, but can vary strongly.

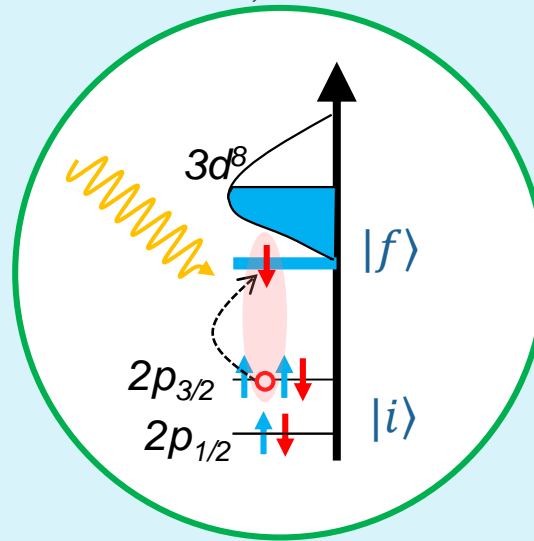
Description of the spectra depends on $|f\rangle$

K-edges



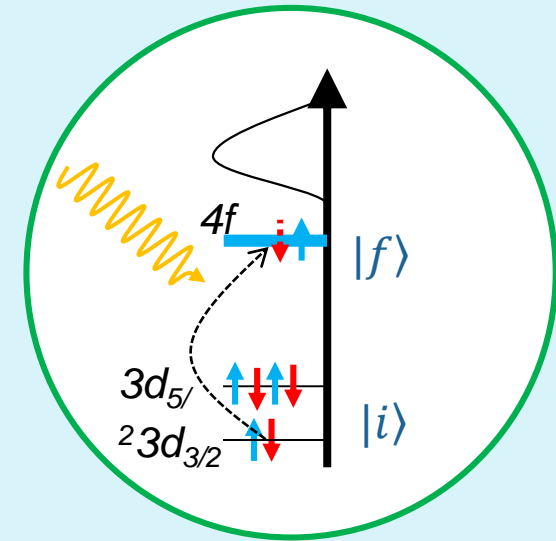
Band excitations

TM $L_{3,2}$ -edges



Resonances

Rare-earth M-edges



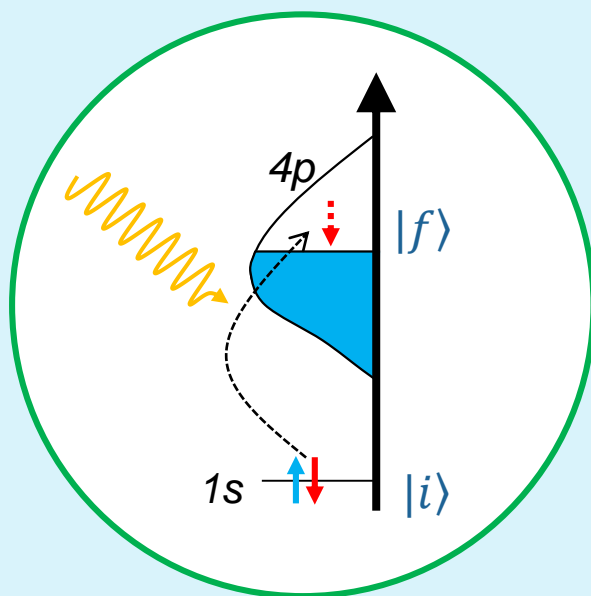
Excitons

... depends on

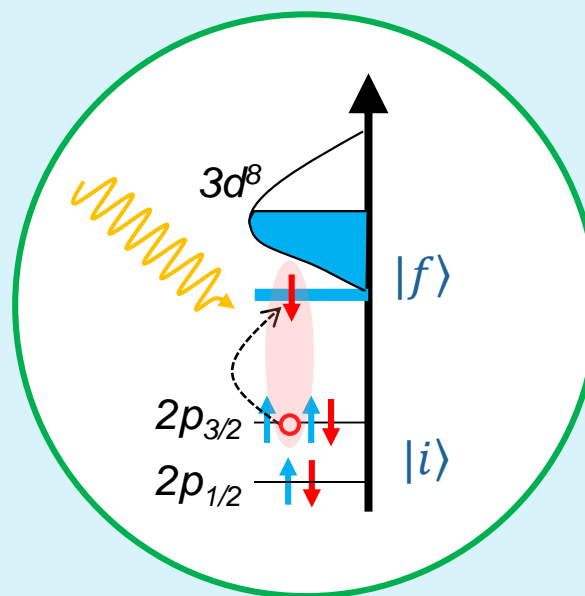
- localized (like f states) or delocalized (like p states) final states are; d states are neither of both really
- Multiplets, significant overlap of core and valence wave functions in the ground state (*Lecture by R. Eder*)
- crystal field
- covalent/ionic character ...

Description of the spectra

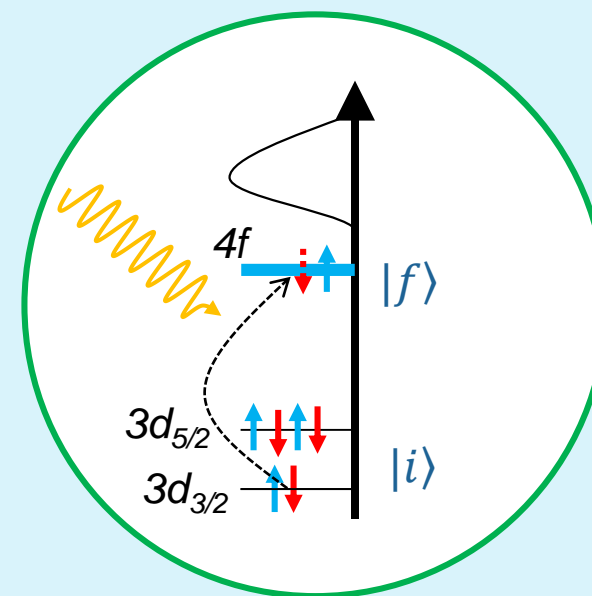
K-edges



TM $L_{3,2}$ -edges



Rare-earth M-edges



Methods used to describe spectra

- LDA(+ U)
- Configuration interaction cluster calculations /double cluster
- Ligand-field parameters from DFT+ U
- ...

Zaanen *et al.* PRB **40** (1989)

Thole *et al.*, PRB **32**, 5107 (1985)

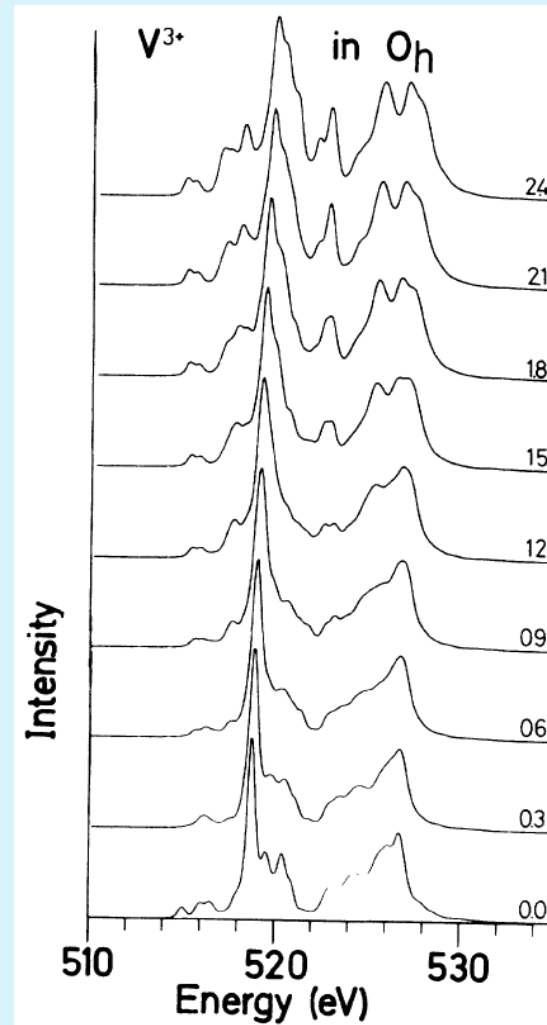
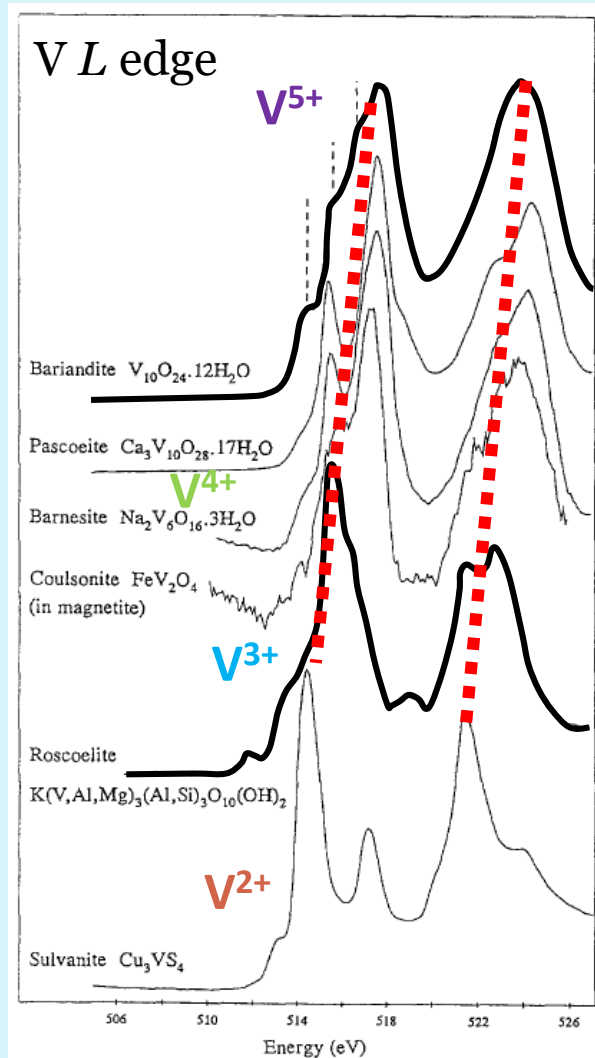
F. de Groot, Coord. Chem. Rev. **249**, 31-63 (2005)

G. van der Laan PRB **33**, 4253 (1986)

M. Haverkort *et al.*, PRB **85**, 165113 (2012)

R. Green *et al.*, PRB **94**, 195127 (2016)

XAS fine structure – Valence state & crystal field parameter

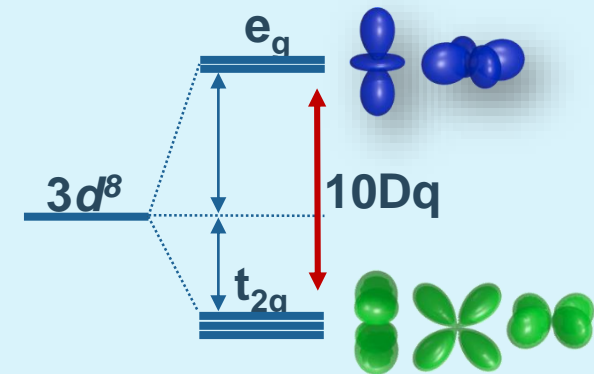


Valence state

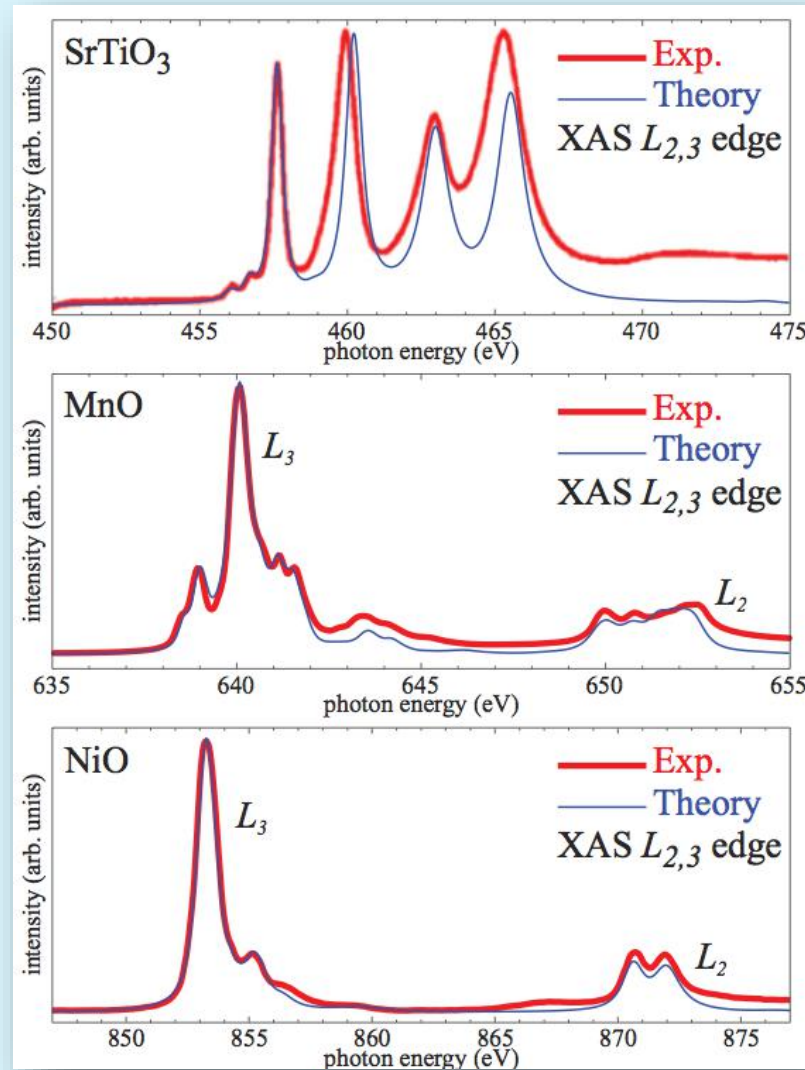
For anions (cations) with different valence state the absorption edge is shifted to lower (higher) photon energies because of the lower (higher) ionization potential

Fine structure

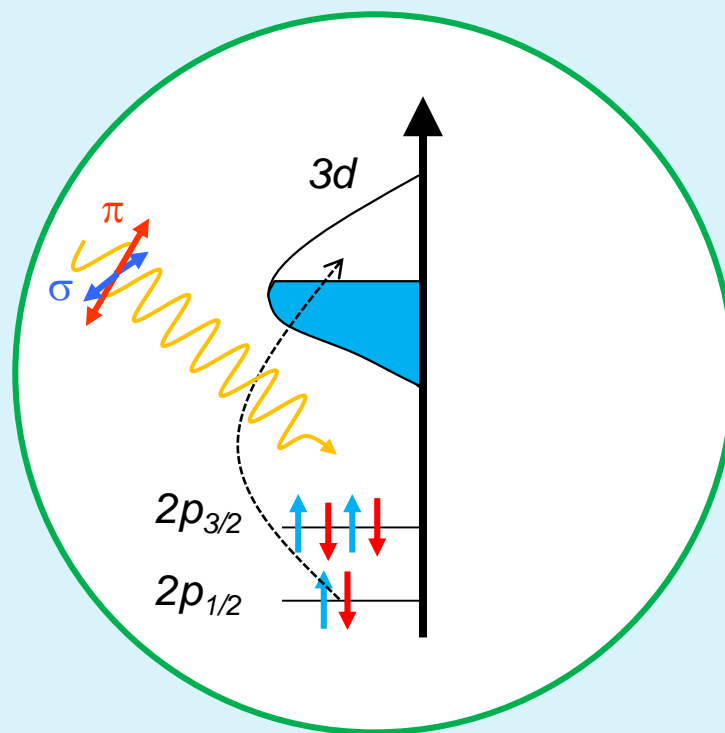
Comparison of fine structure with multiplet calculations for *localized* materials → **crystal field splitting**



Ligand-field cluster calculations of transition metal $L_{3,2}$ edges



X-ray dichroism

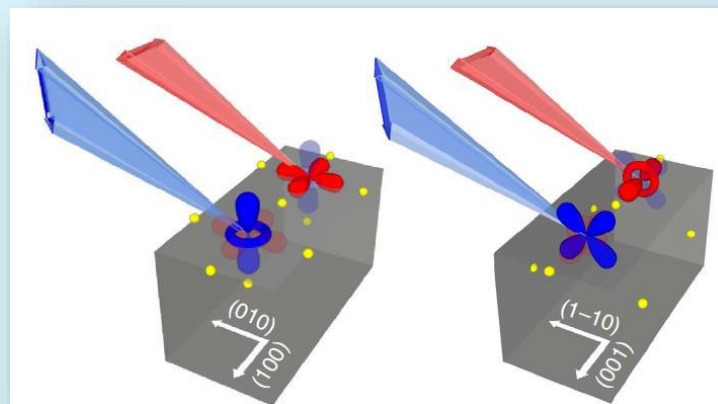


X-ray dichroism

Occurs when the spherical symmetry of the free atom is broken due to a magnetic or (crystalline) electric field

Optical theorem:

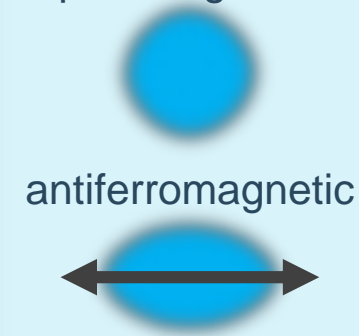
$$I_{\text{XAS}}(E) \propto -\frac{1}{E} \text{Im}(F(E))$$



Crystal field

$$F(E)^{\text{tetragonal}} = \begin{pmatrix} F_{xx} & 0 & 0 \\ 0 & F_{xx} & 0 \\ 0 & 0 & F_{zz} \end{pmatrix}$$

paramagnetic



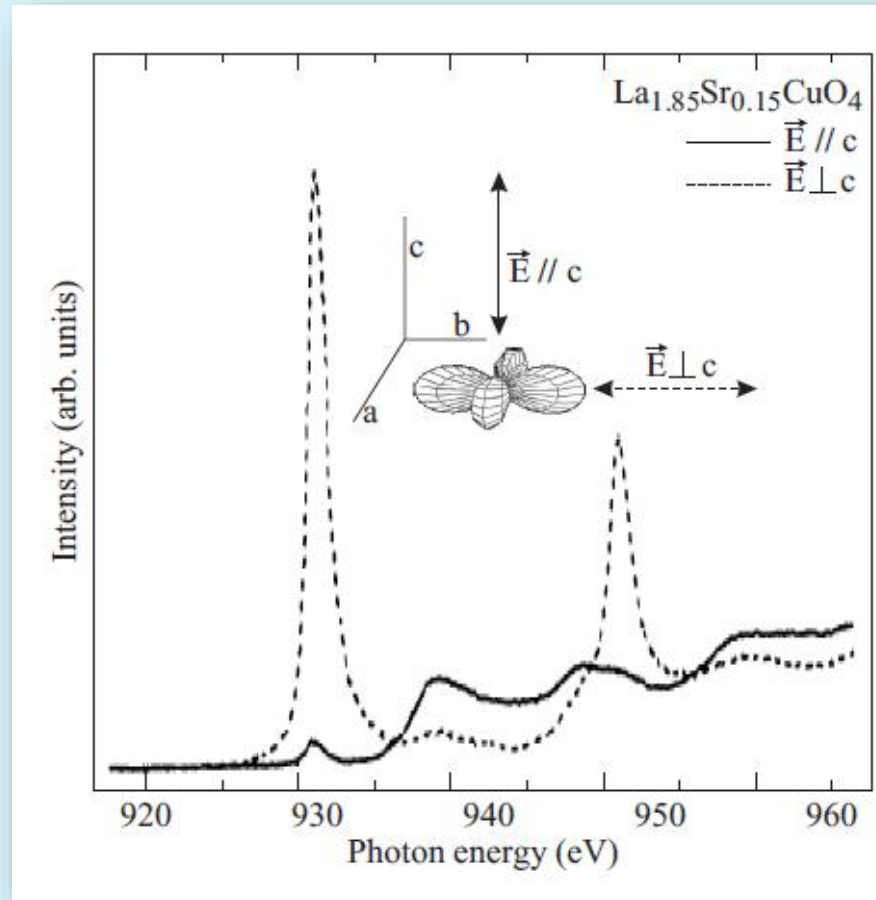
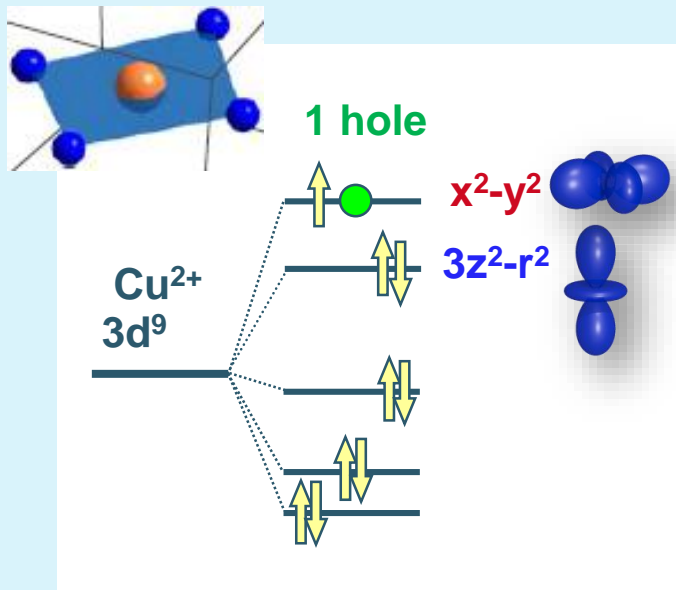
antiferromagnetic

Ferromagnet

$$F(E)^{\text{magnetic}} = \begin{pmatrix} F_{xx} & iF_{xy} & 0 \\ -iF_{xy} & F_{xx} & 0 \\ 0 & 0 & F_{xx} \end{pmatrix}$$

X-ray linear dichroism (XLD)

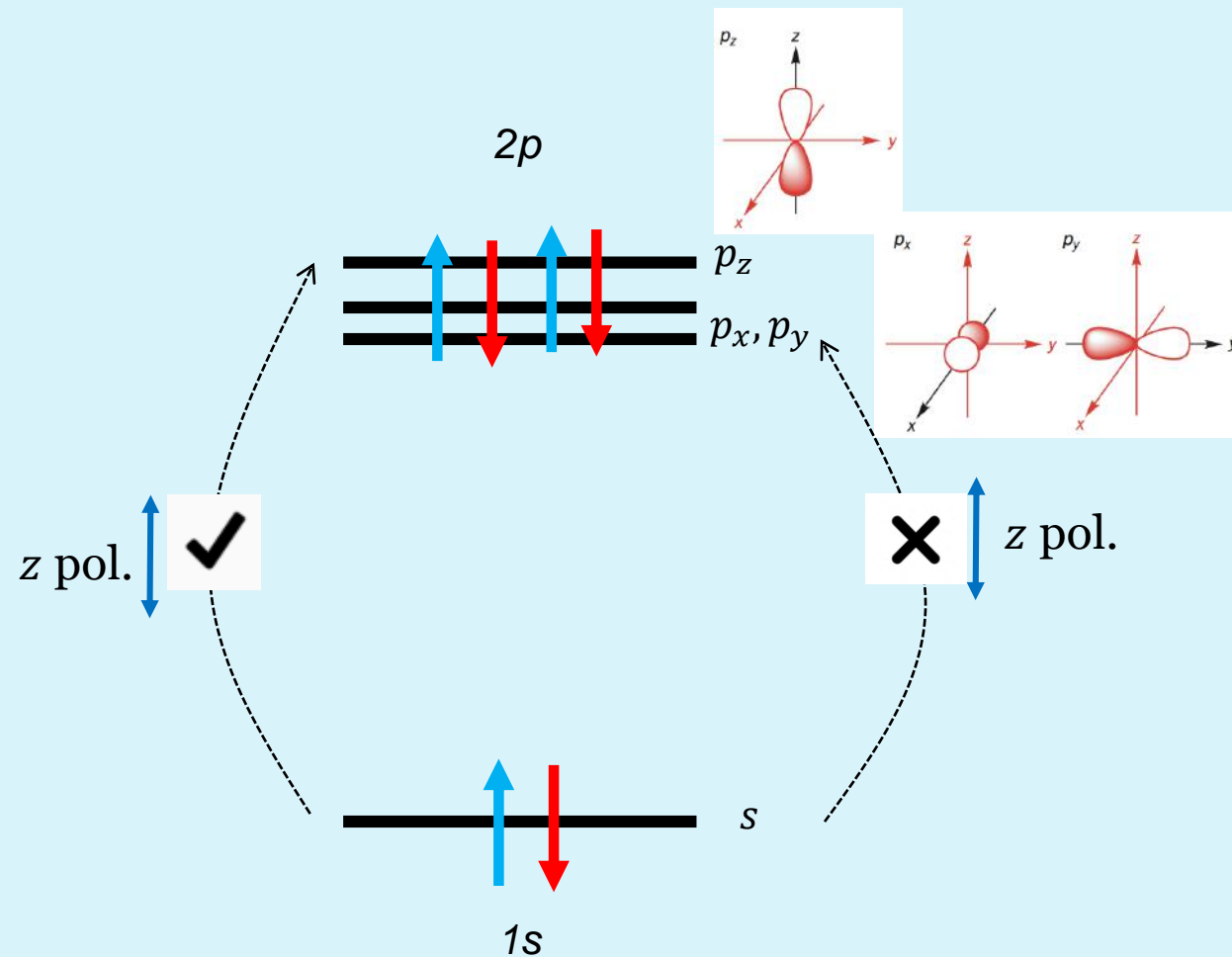
Natural linear dichroism (crystal field)



Linear dichroism

- Excitation from a s orbital to a p orbital.
- Three different p orbitals (p_x , p_y , and p_z) as final states.
- If we use z polarized light then the intensity for an excitation to an p_x orbital is proportional to the square $\langle s | z | p_x \rangle$
- Since s is even in z , z is odd in z and p_x is again even in z , the total integrand is odd in z
- The integral over an odd function is zero

→ With z polarized light one can only excite an s orbital to the p_z orbital.

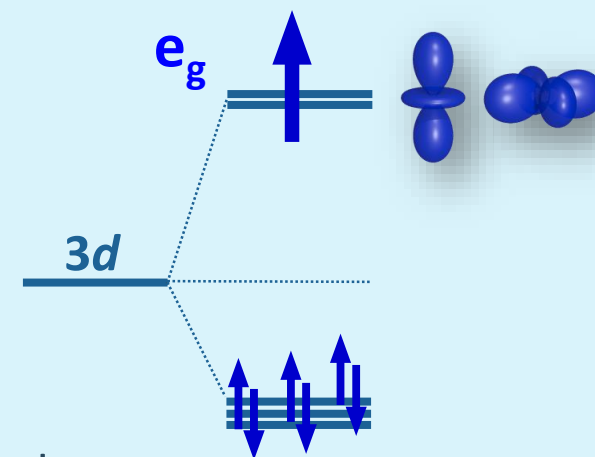
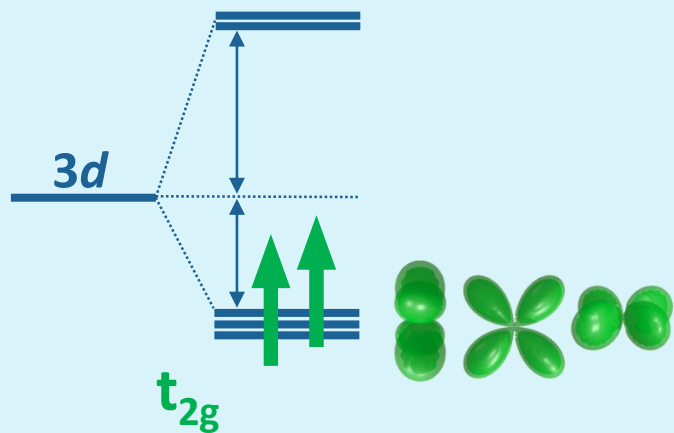


Sum rules for linear dichroism

$$\begin{aligned} I_x &= \frac{1}{2}h_{xy} + \frac{1}{2}h_{xz} + \frac{2}{3}h_{x^2} \\ I_y &= \frac{1}{2}h_{xy} + \frac{1}{2}h_{yz} + \frac{2}{3}h_{y^2} \\ I_z &= \frac{1}{2}h_{xz} + \frac{1}{2}h_{yz} + \frac{2}{3}h_{z^2}. \end{aligned}$$

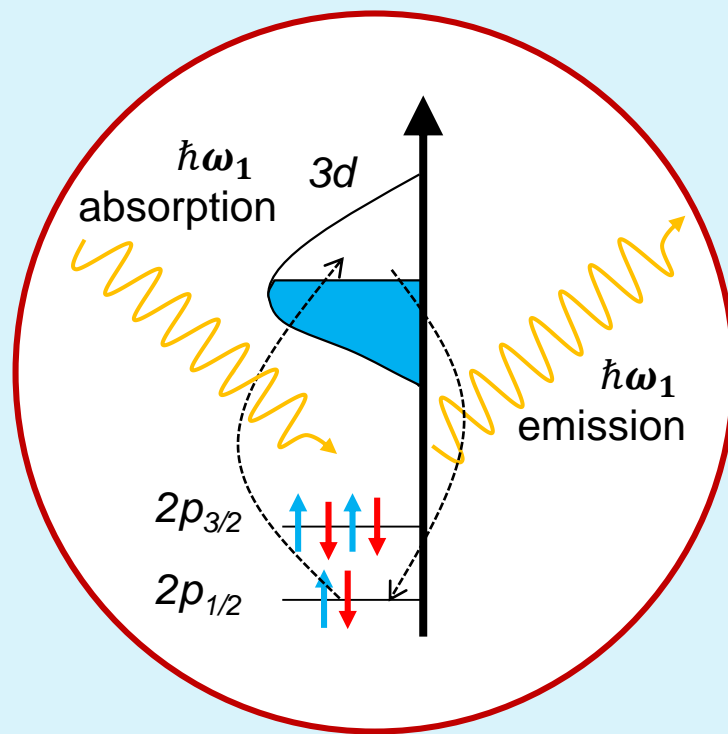
For **3d electron systems** with fully filled t_{2g} and partially filled e_g orbitals, the sum rules simplify, and we can directly relate the ratio of e_g holes to the integrated XAS intensities for in-plane ($I_{x,y}$) and out-of-plane (I_z) polarization:

$$X = \frac{h_{3z^2-r^2}}{h_{x^2-y^2}} = \frac{3I_z}{4I_x - I_z}$$



Since for t_{2g} -systems the e_g -orbitals have finite hole occupations, the orbital occupations cannot be determined directly from the measured spectra, but cluster calculations

Resonant elastic x-ray scattering



Resonant x-ray diffraction

X-ray scattering factor/tensor

$$F(E, \mathbf{q}) = f_0(\mathbf{q}) + f_{mag}^{non-res} + f'_{res}(E) + if''_{res}(E)$$

Optical theorem

$$I_{XAS} \propto -\frac{1}{E} \text{Im}(F(E)) = f''_{res}(E)$$

Fermi's golden rule (second order perturbation)

$$I_{scat}^{res} \propto |F(E)|^2 \propto \left| k^2 \sum_n \frac{\langle i | \hat{\epsilon} \cdot \mathbf{r} | n \rangle \langle n | \hat{\epsilon}' \cdot \mathbf{r} | i \rangle}{E_n - E_i - \hbar\omega - i\Gamma_n/2} \right|^2$$

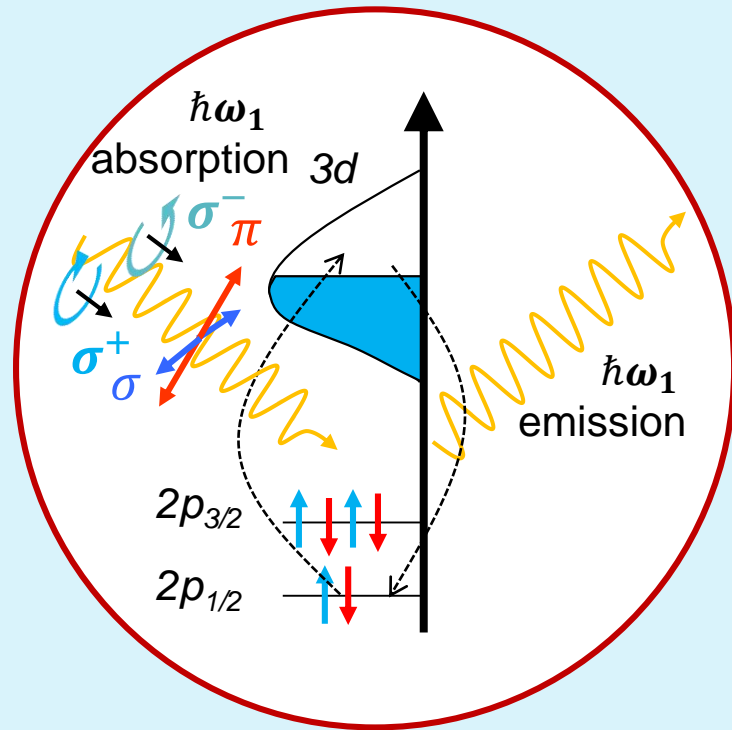
sum over all (virtual) intermediate states

Polarisation dependence

$$I_{scat} = \left| \sum_i e^{i(k_{in} - k_{out})r_i} \epsilon_{out} \cdot \hat{F}_i \cdot \epsilon_{in} \right|$$

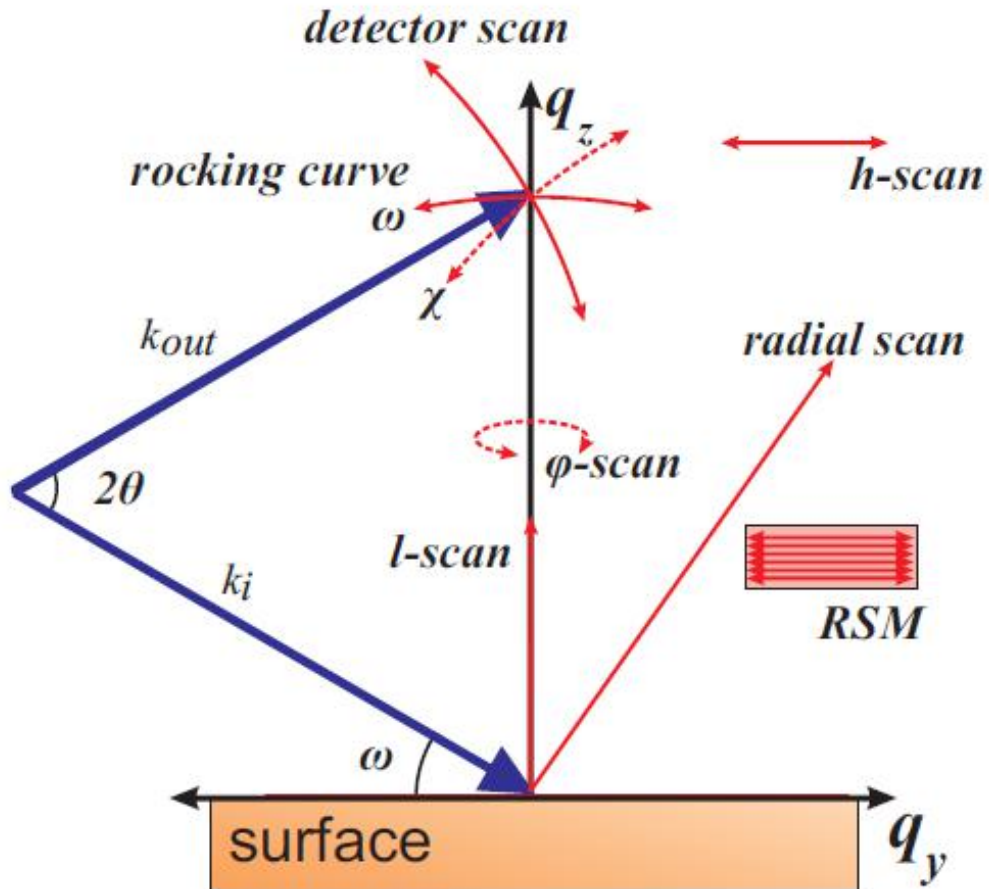
$$\hat{F} = \begin{pmatrix} F^{xx} & F^{xy} & F^{xz} \\ F^{yx} & F^{yy} & F^{yz} \\ F^{zx} & F^{zy} & F^{zz} \end{pmatrix}$$

Resonant x-ray scattering/reflectometry



- Combine diffraction (information on **spatial modulation**) with x-ray absorption (**spectroscopic information**) in a single experiment.
- **Elastic scattering** ($\hbar\omega_1 = \hbar\omega_2$)
- **Element sensitivity** & strong **enhancement** of the cross section.
- Defined **polarization** state of incoming x-rays / analyse outgoing polarization
- Transitions depend on the **spin, orbital and charge** configuration (XAS final state) of the resonant scatter centres

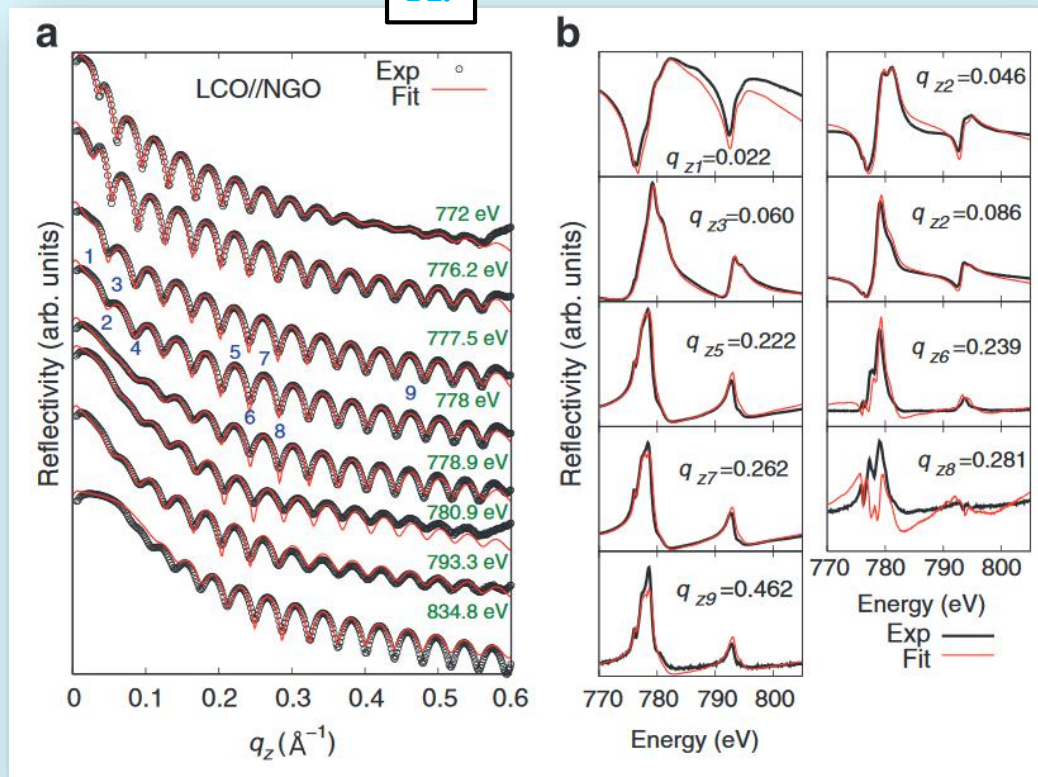
Scan types



- A. **$\theta/2\theta$ (l) scan**: scan along fixed direction defined by q
- B. **θ scan** (ω scan; rocking curve): scan perpendicular to q
- C. **azimuth (ϕ) scan**: turning the sample around \rightarrow vary projection onto polarization vectors
- D. **constant- q energy scan**: scanning E across the resonance while keeping q -transfer constant.

$\theta/2\theta$ scan at low angles (x-ray reflectivity)

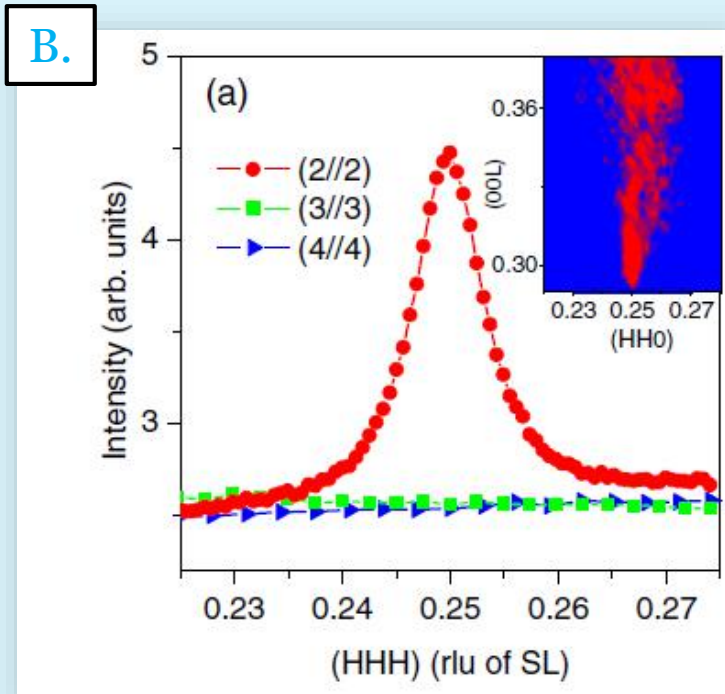
A.



- A. $\theta/2\theta$ scan: scan along fixed direction defined by \mathbf{q}
- B. θ scan (rocking curve): scan perpendicular to \mathbf{q}
- C. azimuth scan: turning the sample around \rightarrow vary projection onto polarization vectors
- D. constant- \mathbf{q} energy scan: scanning E across the resonance while keeping \mathbf{q} -transfer constant.

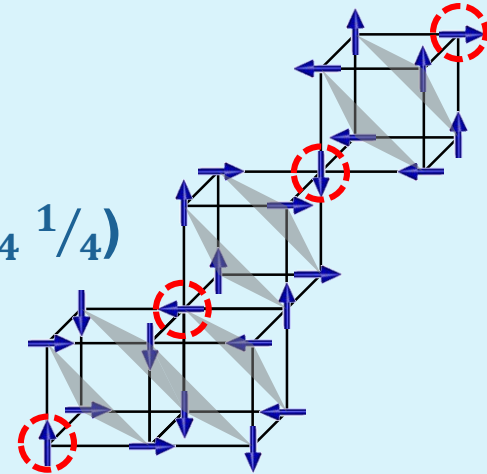
\Rightarrow Charge, elemental, magnetic profile

Rocking scan, for example of the AFM Bragg peak in $RNiO_3$



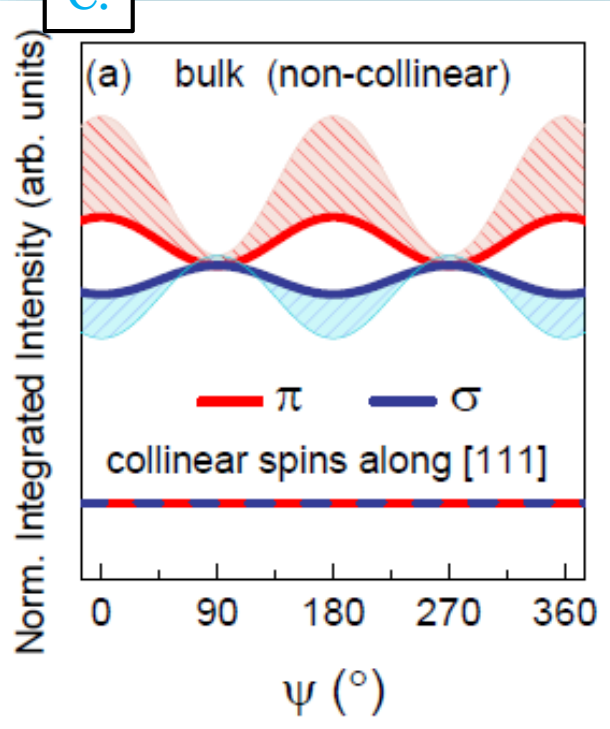
- A. $\theta/2\theta$ scan: scan along fixed direction defined by \mathbf{q}
 - B. θ scan (rocking curve): scan perpendicular to \mathbf{q}
 - C. azimuth scan: turning the sample around \rightarrow vary projection onto polarization vectors
 - D. constant- \mathbf{q} energy scan: scanning E across the resonance while keeping \mathbf{q} -transfer constant.
- \Rightarrow Information on ordering vector

$$\mathbf{q}_{mag} = \left(\frac{1}{4} \frac{1}{4} \frac{1}{4}\right)$$

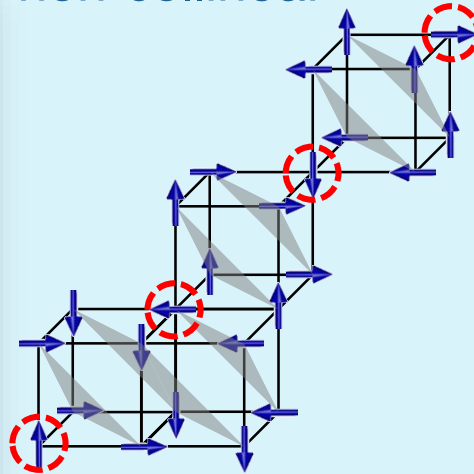


Azimuthal scan, around the magnetic Bragg peak

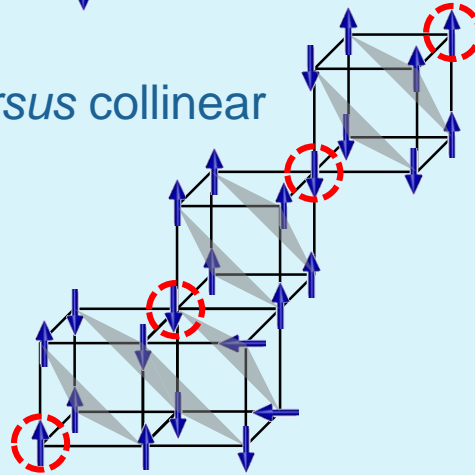
C.



non-collinear



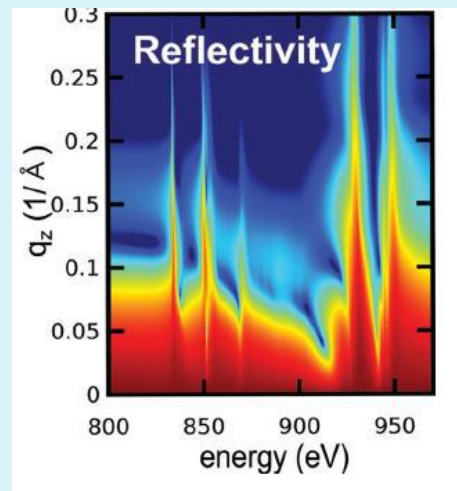
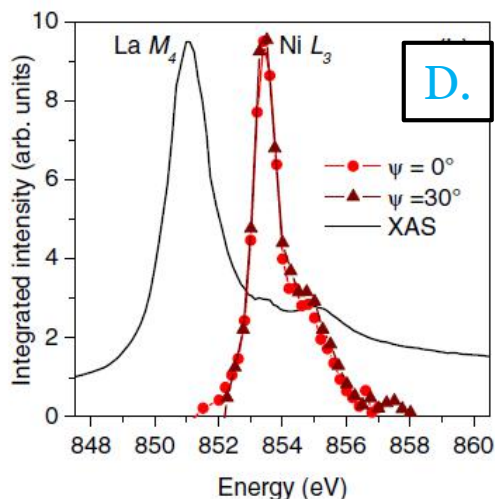
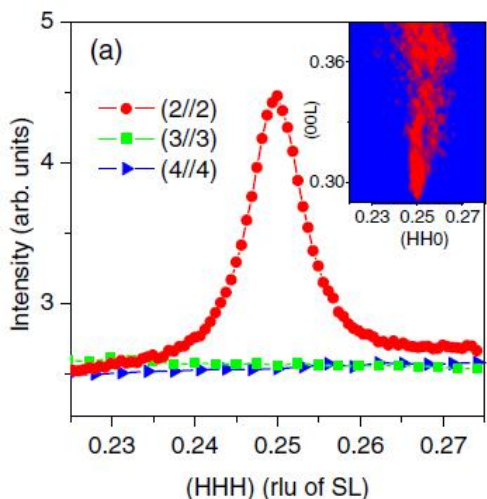
versus collinear



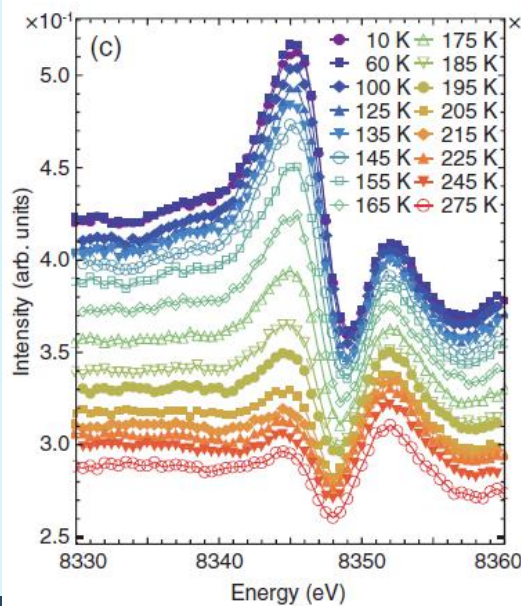
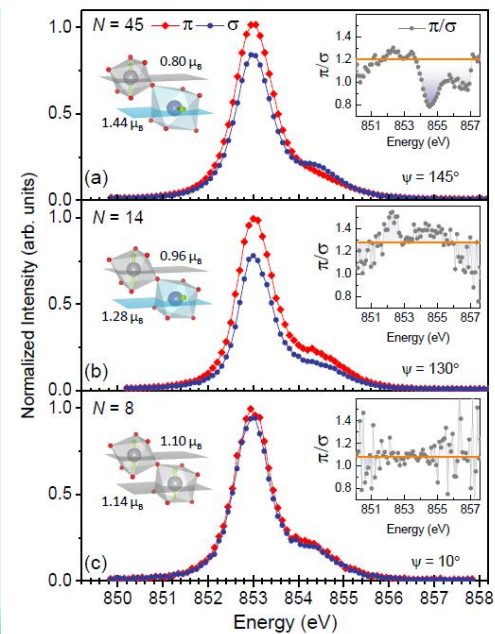
- A. $\theta/2\theta$ scan: scan along fixed direction defined by q
- B. θ scan (rocking curve): scan perpendicular to q
- C. **azimuth scan**: turning the sample around \rightarrow vary projection onto polarization vectors
- D. **constant- q energy scan**: scanning E across the resonance while keeping q -transfer constant.

\Rightarrow Moment directions and amplitudes

Energy scan



- A. $\theta/2\theta$ scan: scan along fixed direction defined by \mathbf{q}
- B. θ scan (rocking curve): scan perpendicular to \mathbf{q}
- C. azimuth scan: turning the sample around \rightarrow vary projection onto polarization vectors
- D. **constant- \mathbf{q} energy scan**: scanning E across the resonance while keeping \mathbf{q} -transfer constant.



\Rightarrow Information of contributions from different elements and sites

Resonant reflectivity (“low-angle” specular scattering)

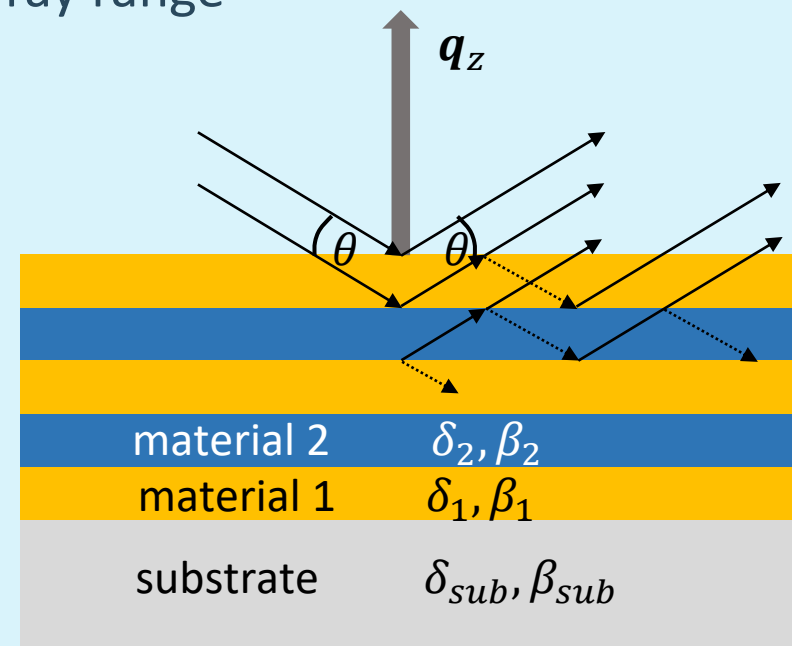
Homogenous medium approach: Refractive index in the x-ray range

$$n = 1 - \delta + i\beta$$

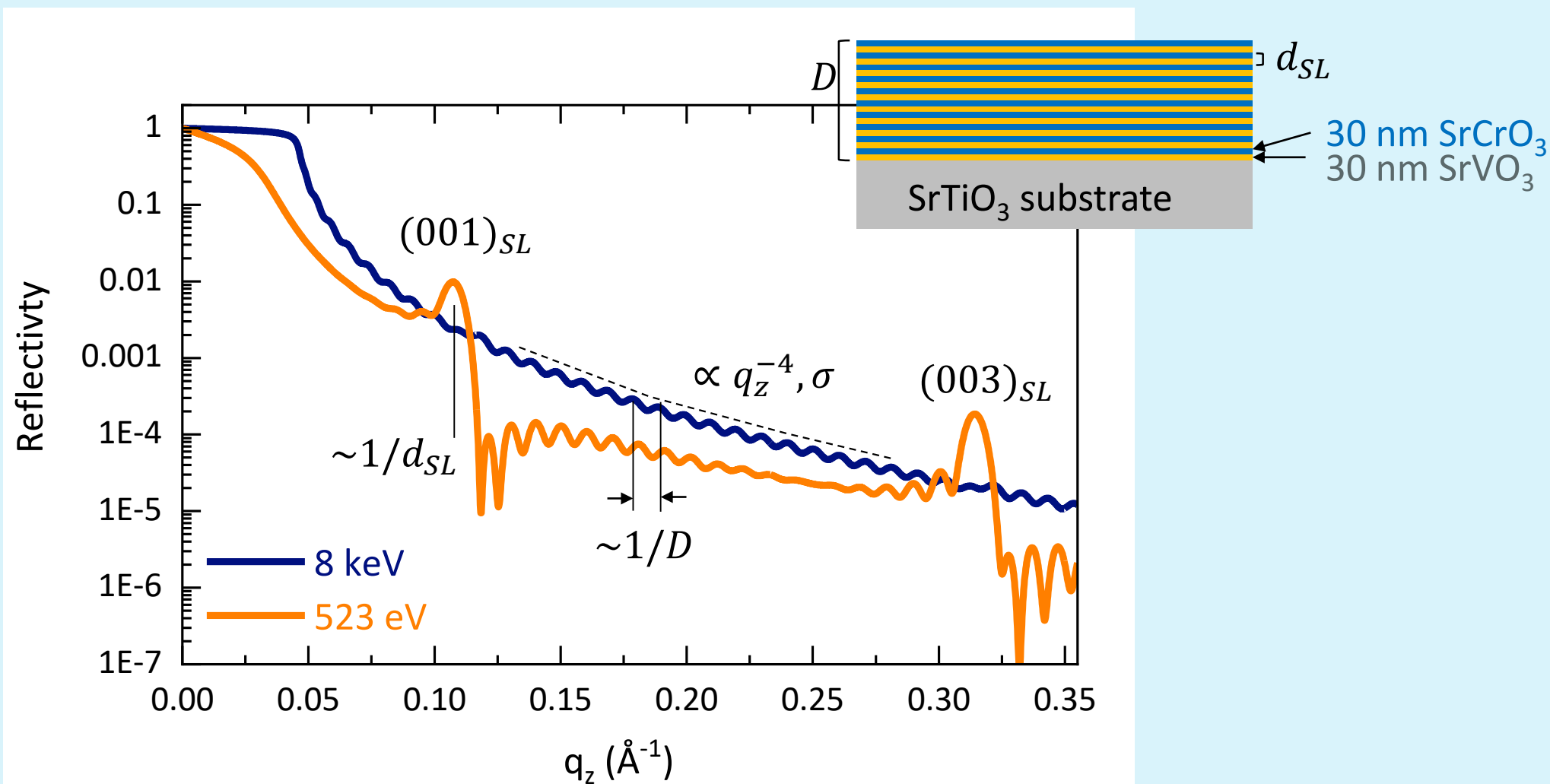
with optical constants δ and β

$$\delta(E) = \frac{2\pi\rho r_0 (c\hbar)^2}{E^2} (Z^* + f'(E))$$
$$\beta(E) = \frac{2\pi\rho r_0 (c\hbar)^2}{E^2} (f''(E)),$$

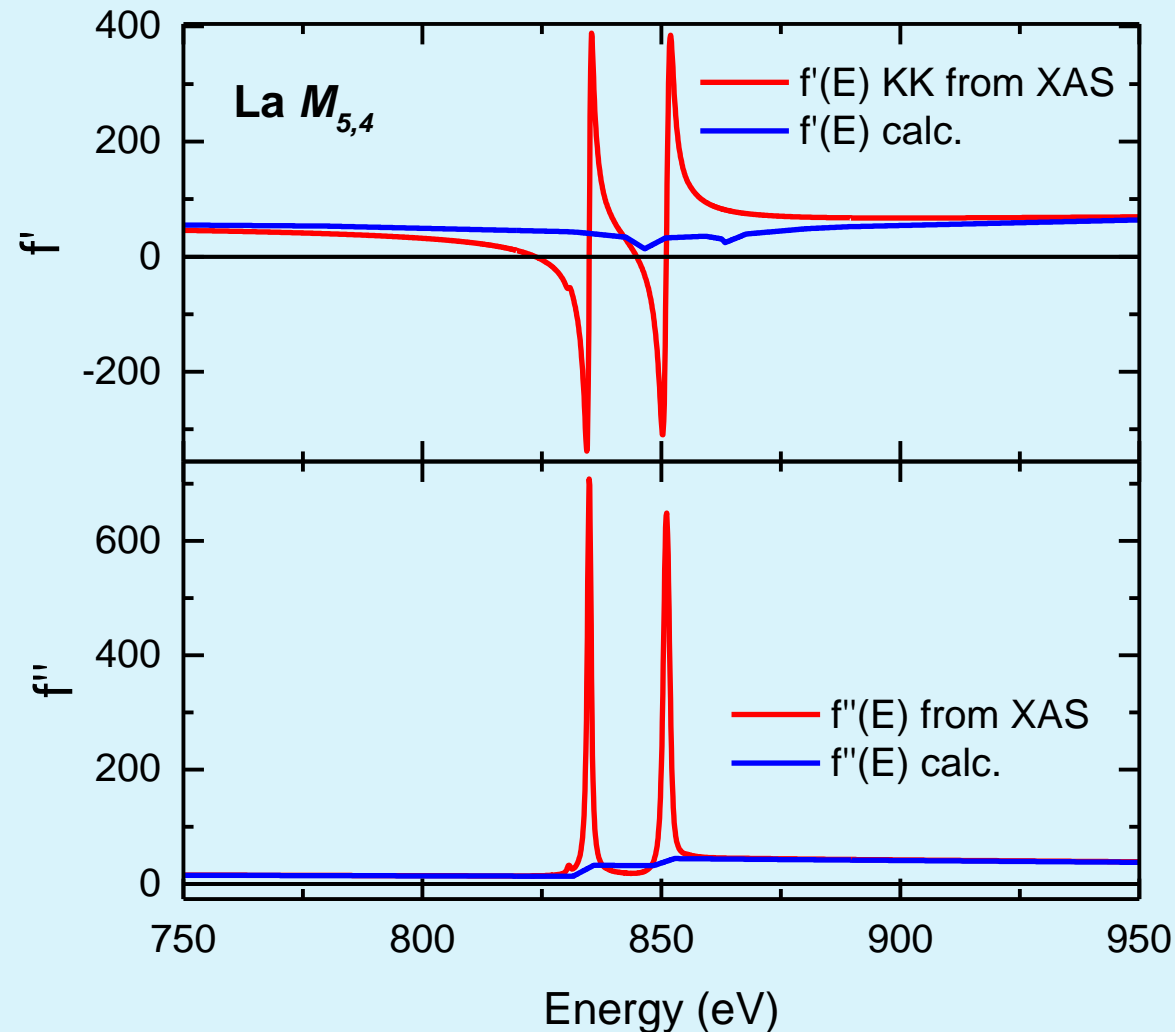
with the real and imaginary part f' , f'' of the scattering factor (forward scattering $\mathbf{q} \approx 0$) and ρ the electron density and r_0 the Thompson scattering amplitude.



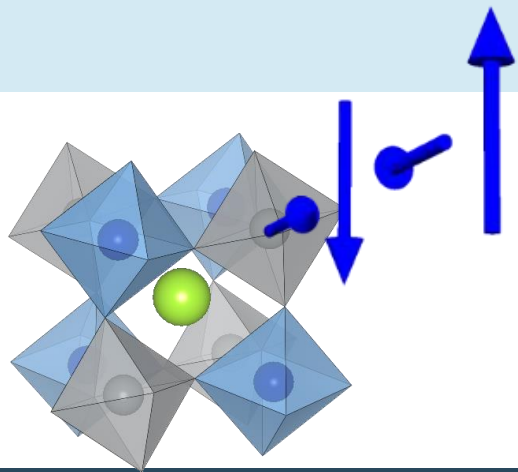
Structural parameters



Energy dependent anomalous dispersion corrections



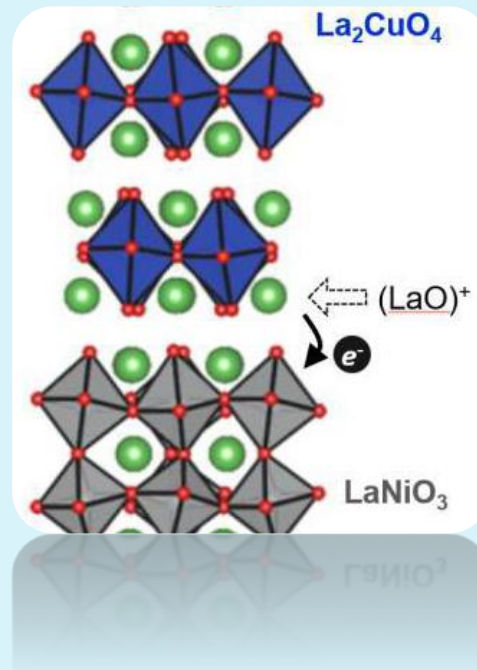
- Very strong intensity variations across the resonances not captured by theoretical values
- Usually the **resonance lines are measured by XAS**, then scaled to tabulated values of f''
- In the real part f' is then obtained via the Kramer-Kronig relation
- The anomalies across the resonances in f' extend over a wider energy range.



Case studies

- **Interfacial doping** in cuprate-nickelate hybrid structures
- **Orbital reflectometry** of nickelate and vanadate superlattices
- Noncollinear **magnetic order** in nickel oxide heterostructures

Interfacial doping in cuprate-nickelate hybrid structures



Friederike Wrobel

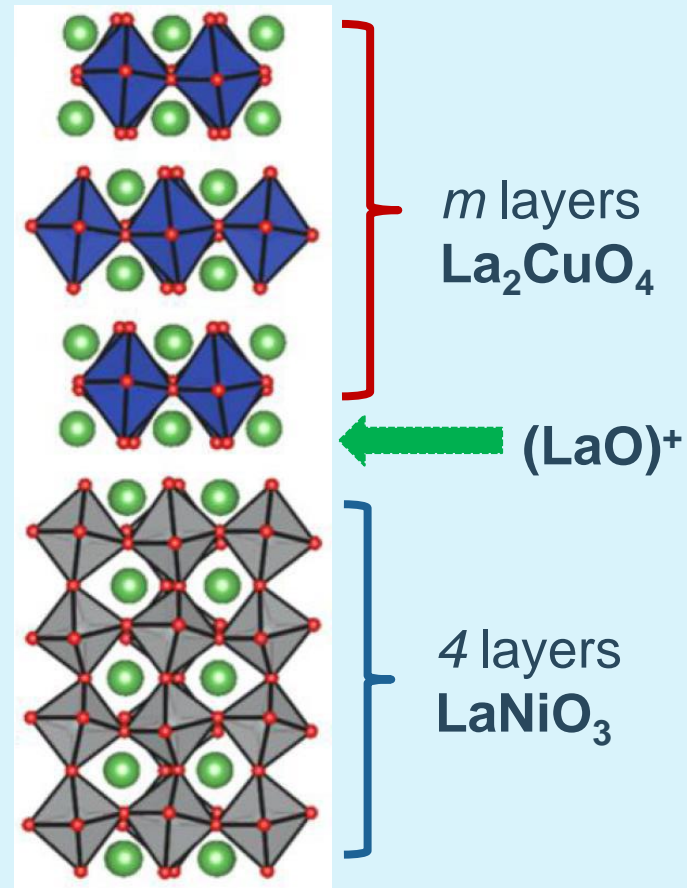
Motivation

Charge carrier doping in correlated transition metal oxides:

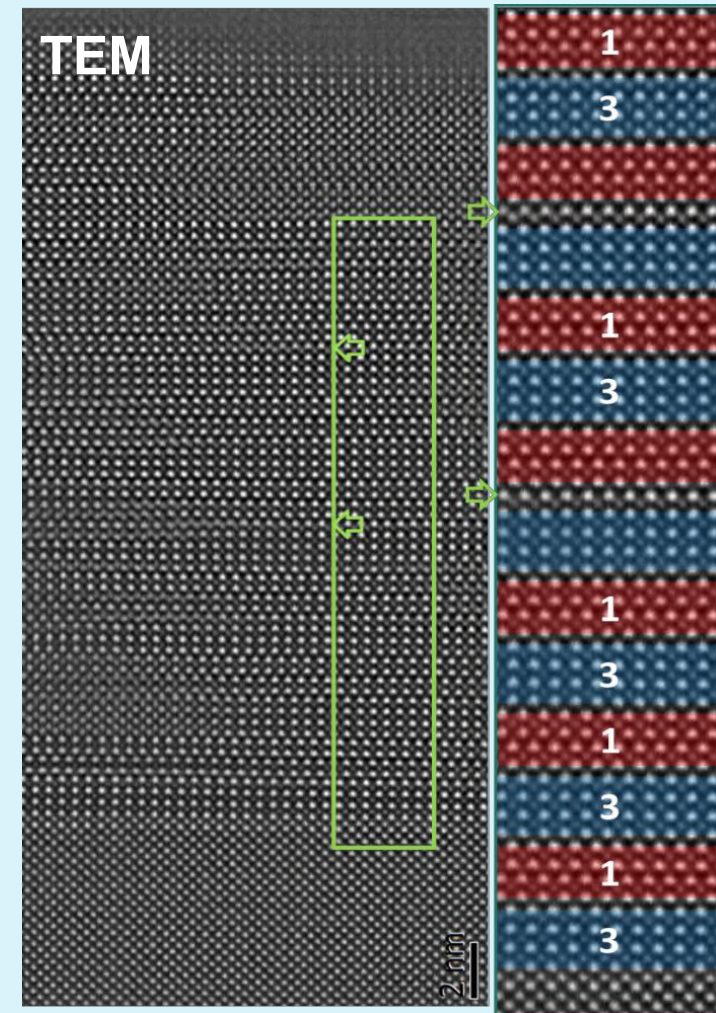
- **Bulk:** Chemical substitution often generates strong structural and chemical disorder can drastically modify the electronic behaviour
- **Oxide interfaces:** thermal diffusion of dopant atoms limits the ability to create sharp interfaces between different dopant and doped layers.

Atomic layer-by-layer molecular beam epitaxy

$(\text{La}_2\text{CuO}_4)_m/\text{LaO}/(\text{LaNiO}_3)_n$ hybrid structures

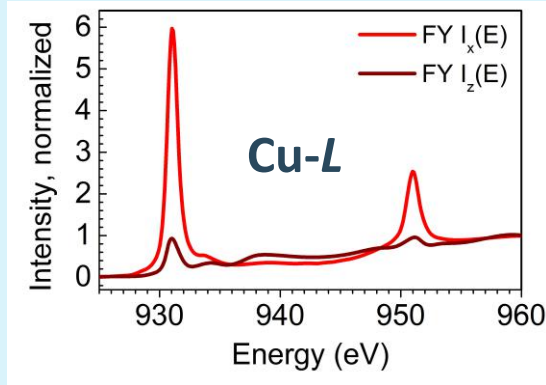


“B cation ordered Ruddlesden-Popper”

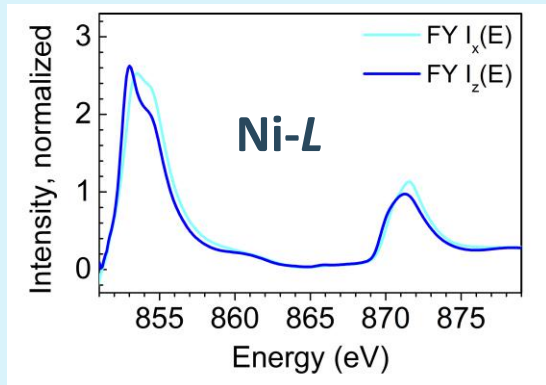


Nickel valence state modulation

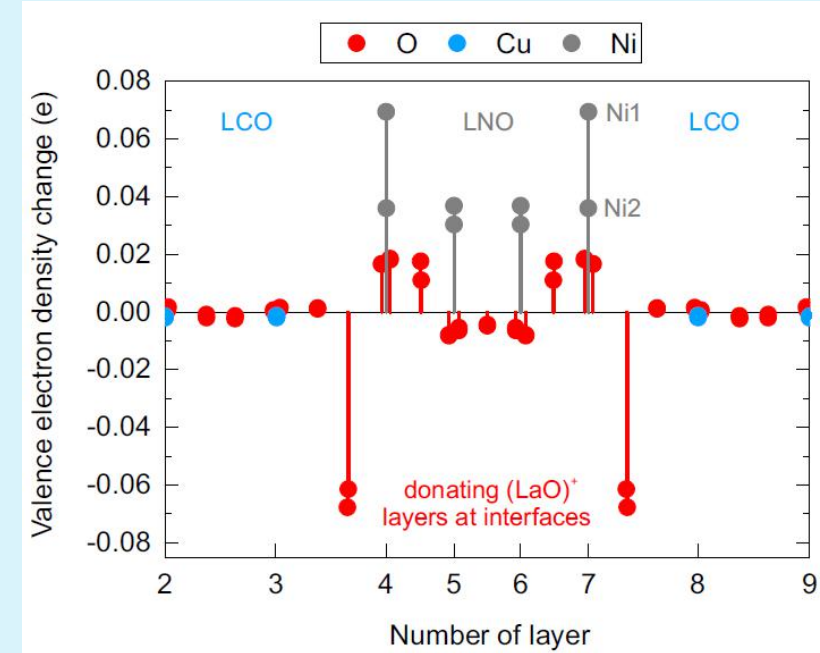
X-ray absorption



Characteristic of Cu^{2+}



Signatures of a Ni^{2+} and Ni^{3+} mixture



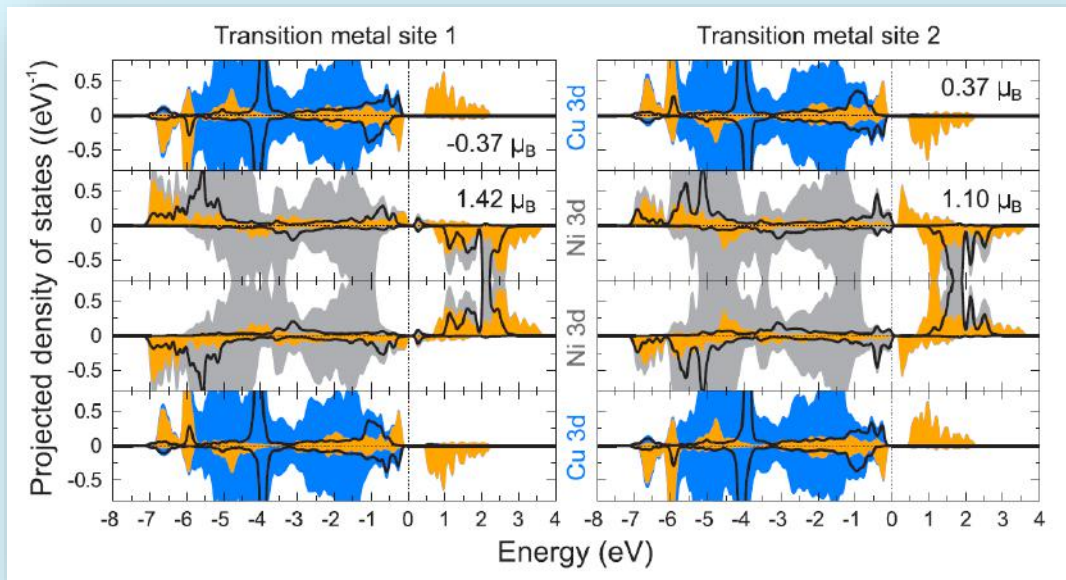
DFT+U

(Pentcheva & Geisler, University of Duisburg):

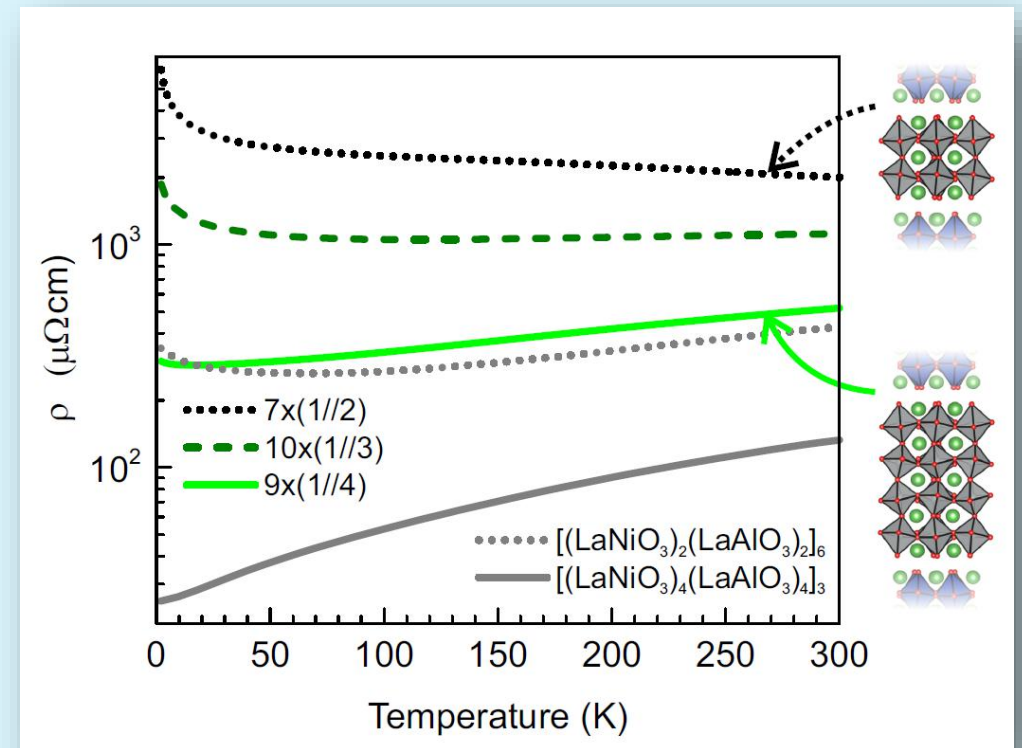
Additional charge is predominantly accommodated in the interfacial nickelate layers

Metal-insulator transition

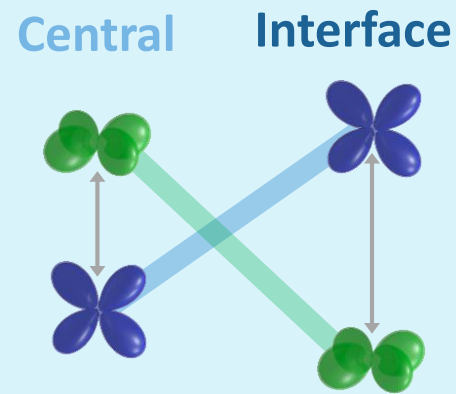
DFT+ U : charge disproportionation in the interfacial nickelate layers



Experiment: LaNiO_3 layer thickness dependent in-plane electronic transport



Orbital reflectometry of nickelate and vanadate superlattices



Meng Wu



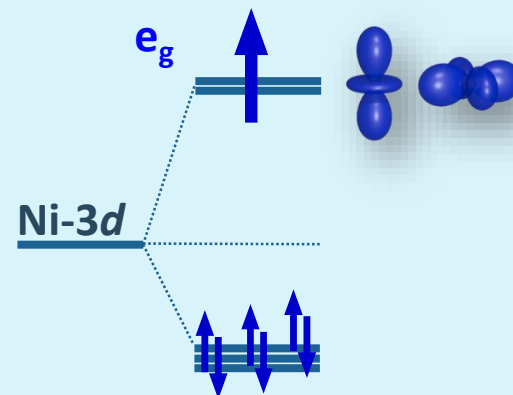
Padma
Radhakrishnan

How to measure layer-resolved orbital occupations?

nature materials LETTERS
PUBLISHED ONLINE: 6 FEBRUARY 2011 | DOI:10.1038/NMAT2958

Orbital reflectometry of oxide heterostructures

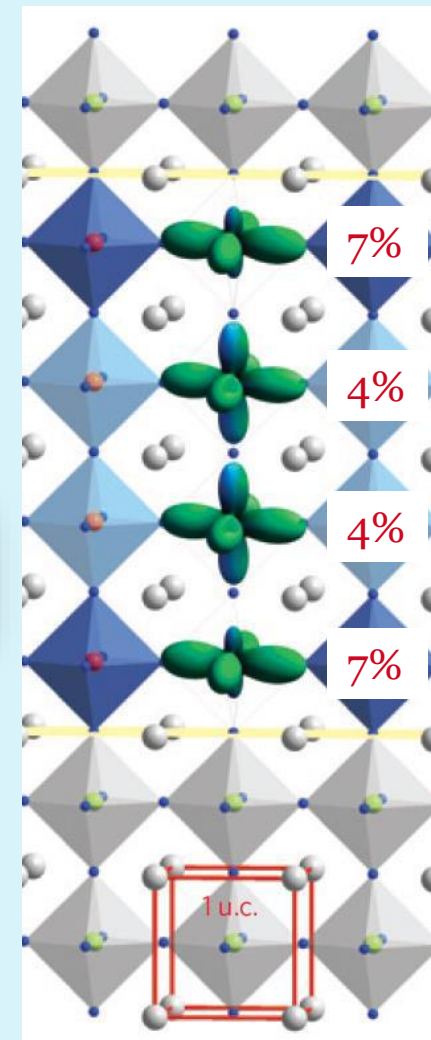
Eva Benckiser¹, Maurits W. Haverkort¹, Sebastian Brück^{2,3}, Eberhard Goering², Sebastian Macke², Alex Frañó¹, Xiaoping Yang^{1,4}, Ole K. Andersen¹, Georg Cristiani¹, Hanns-Ulrich Habermeier¹, Alexander V. Boris¹, Ioannis Zegkinoglou¹, Peter Wochner², Heon-Jung Kim^{1,5}, Vladimir Hinkov^{1*} and Bernhard Keimer^{1*}



$$X = \frac{h_{3z^2-r^2}}{h_{x^2-y^2}} = \frac{3I_z}{4I_x - I_z}$$

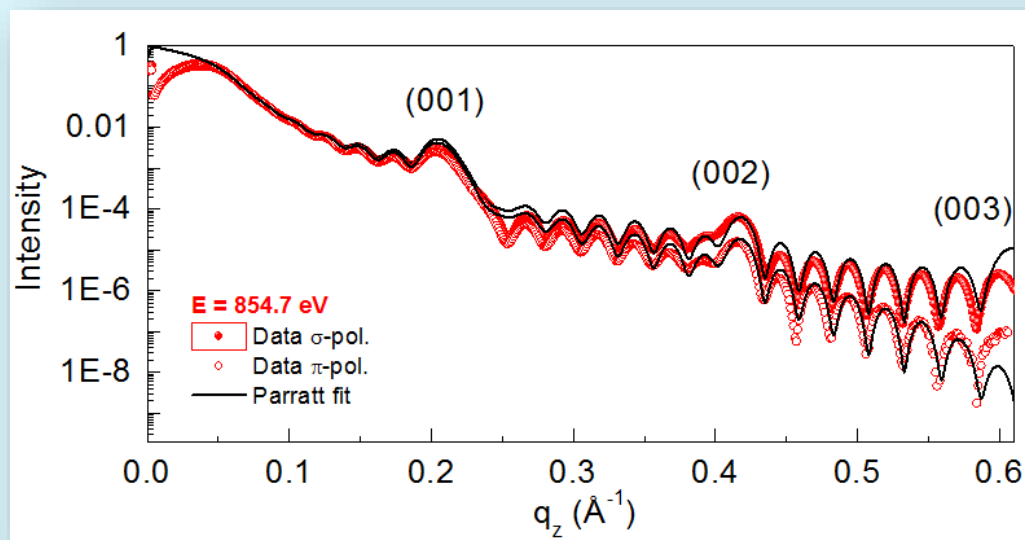
Resonant X-ray reflectivity with linearly polarized soft x-rays tuned to the Ni-L edge:

- **XAS**: quantitative information via the sum rules
- **Reflectivity** allows to determine layer-resolved orbital polarization profiles

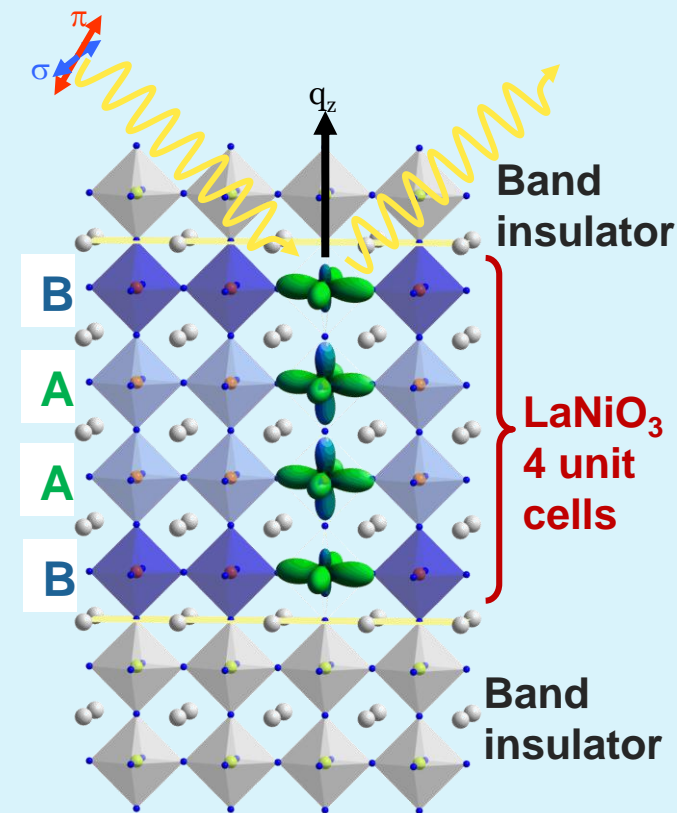


Layer-resolved orbital polarizations in LaNiO_3 superlattices

Resonant x-ray reflectometry of a symmetric superlattice:

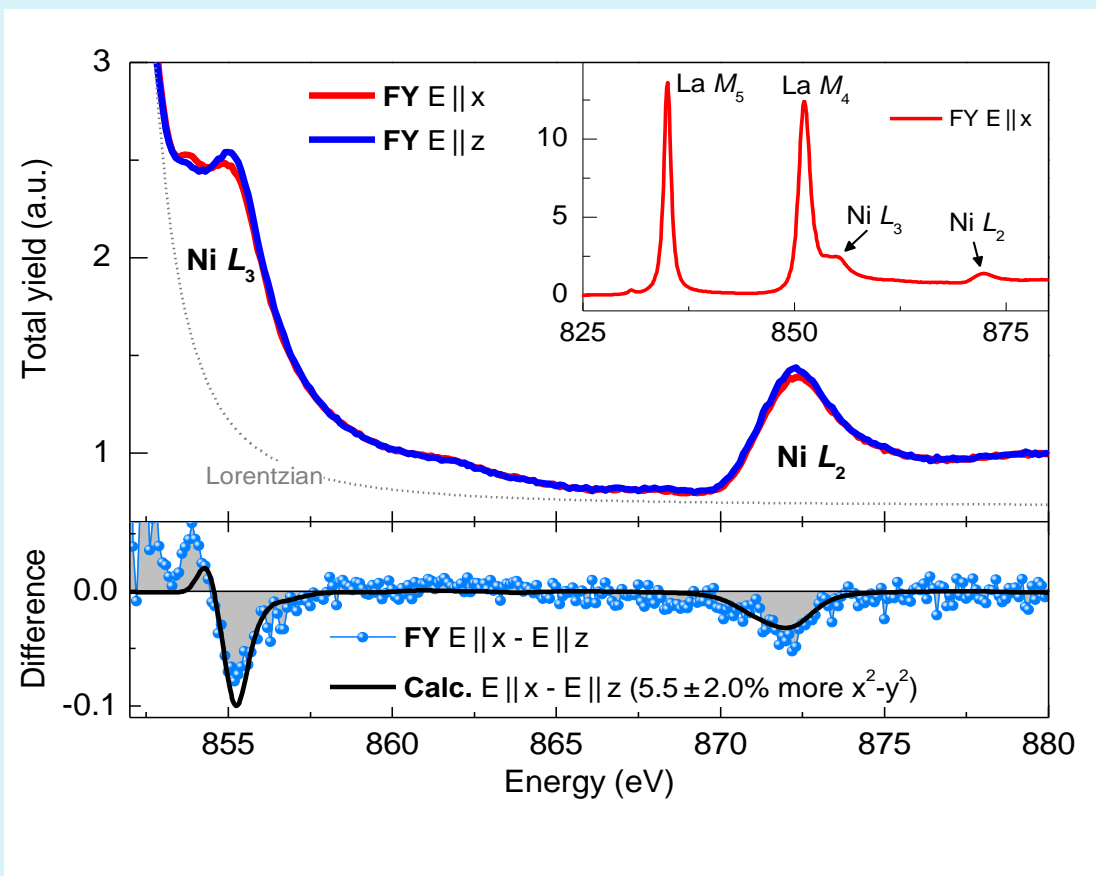


$$F^{(002)} \propto (1 - i)(f_B - f_A)^{LNO}$$

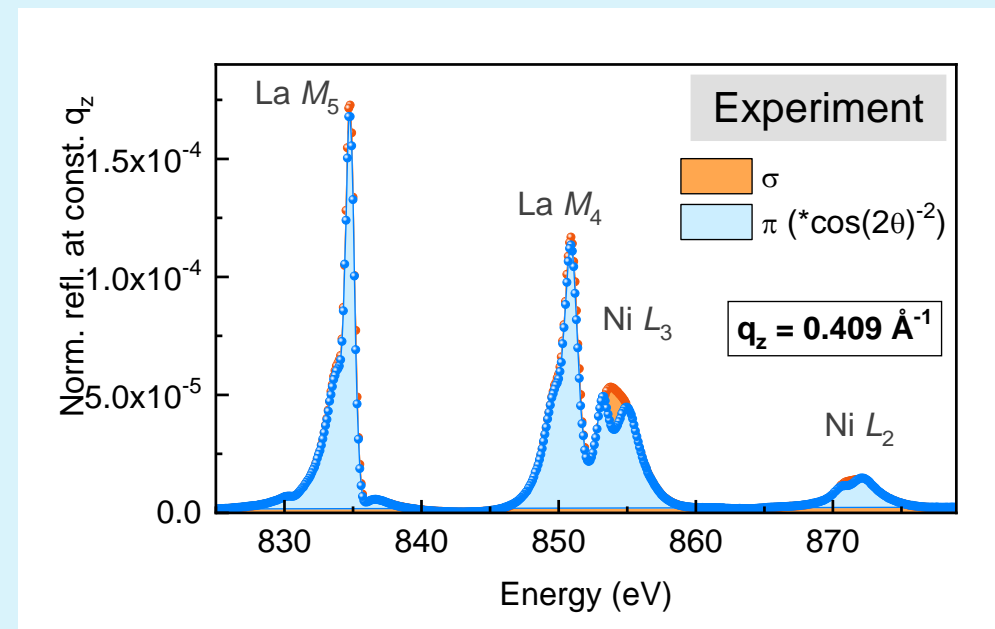


Orbital reflectometry $\text{LaNiO}_3\text{-LaAlO}_3$ SL

XAS



Reflectivity



Strong linear dichroism in reflectivity at (002) \rightarrow modulation in orbital polarization!

Simulation of the constant- q spectra

Multiple scattering important (dynamical theory for Multilayer)
(Parratt, PR 95, 359 (1954))

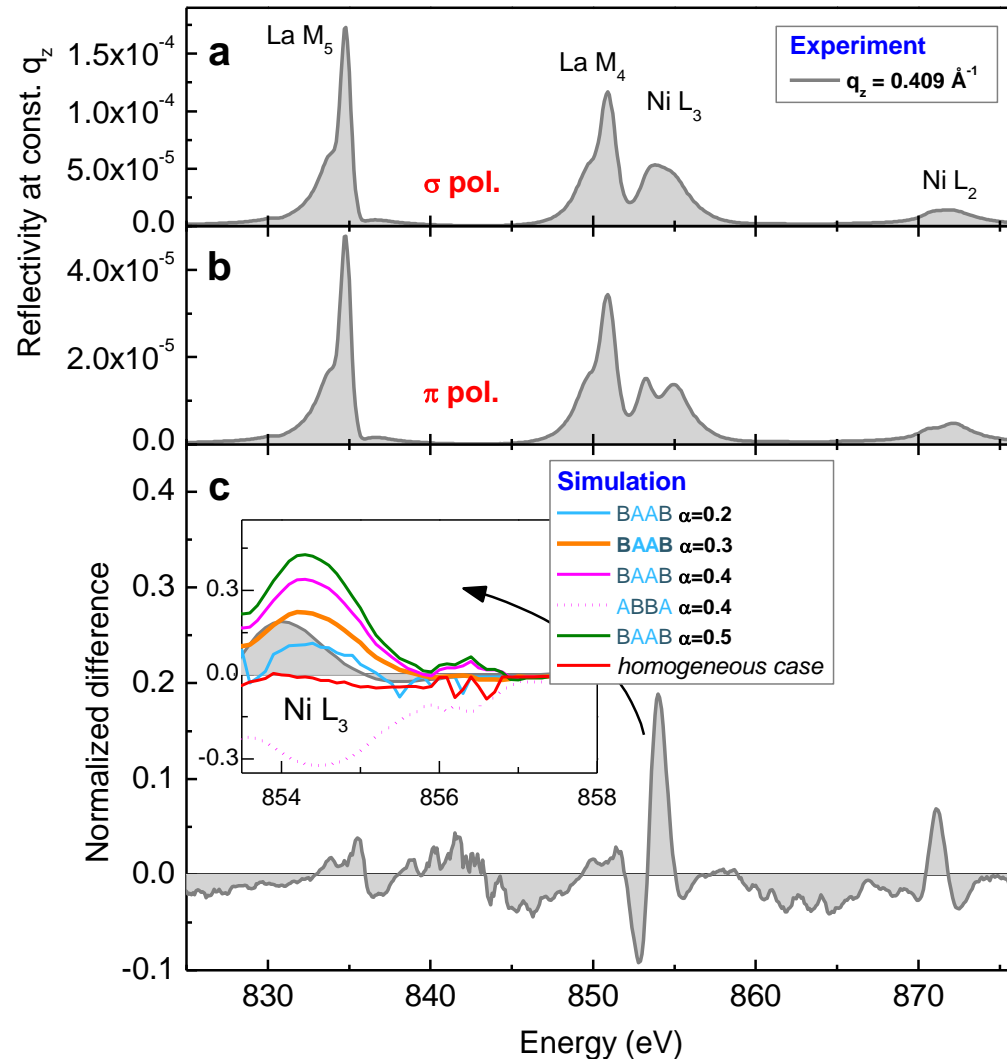


RemagX (by S. Macke):

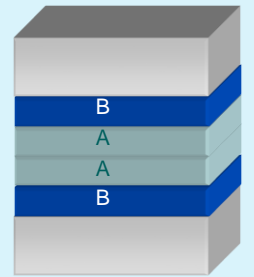
- handle materials with arbitrary, in particular anisotropic, dielectric properties
- 3 different algorithms for isotropic and anisotropic media (Parratt / Matrix(Zak) / Full Matrix)

$$\hat{F}_{\text{tetra}}^{\text{LNO}} = \begin{pmatrix} F^{xx} & 0 & 0 \\ 0 & F^{xx} & 0 \\ 0 & 0 & F^{zz} \end{pmatrix}$$

Quantitative analysis



- Compare normalized difference spectra with simulations
- Vary parameter α that defines the degree to which the orbital polarization of the A and B sub-layers differ (XAS average polarization fixed)

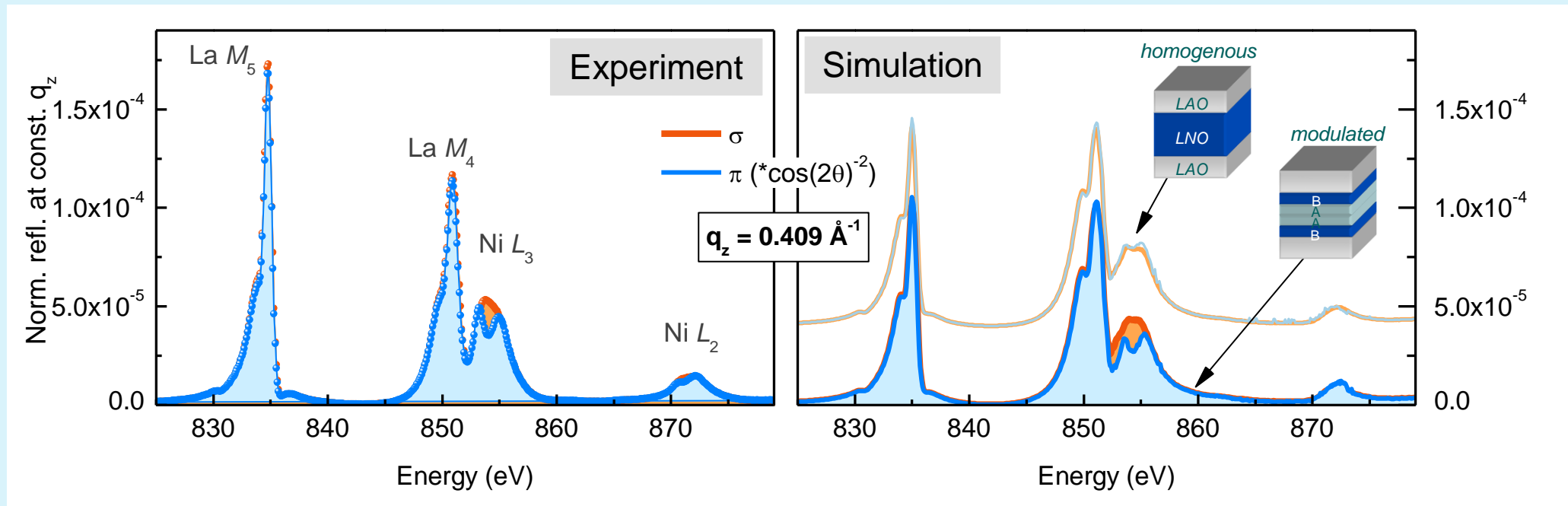


Best fit: $\alpha = 0.3$

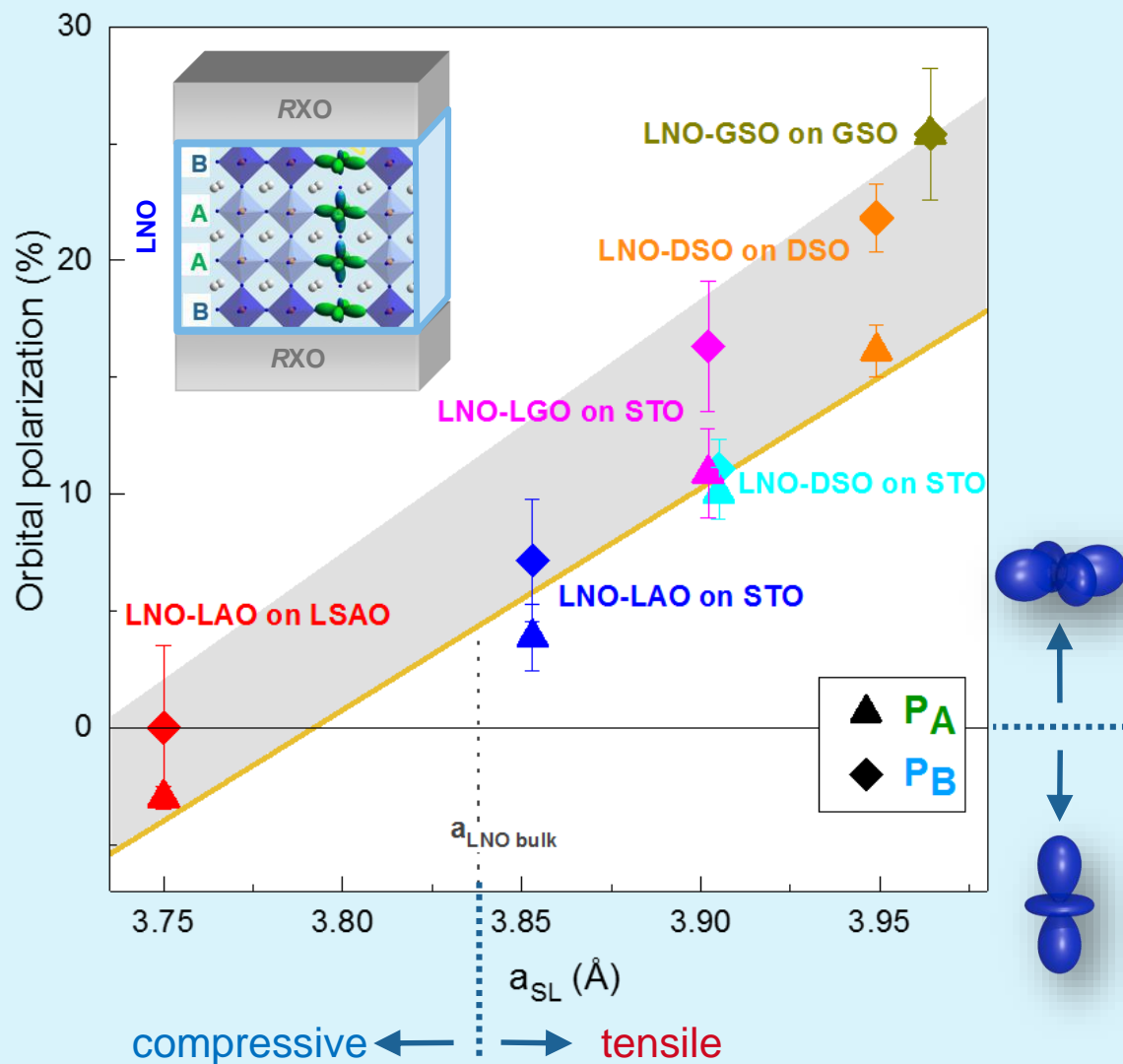
Interface layers B: $(7 \pm 3)\%$ more x^2-y^2 occupation

Central layers A: $(4 \pm 1)\%$ more x^2-y^2 occupation

Simulation of the energy dependent scattering



Orbital polarisation versus in-plane lattice constant



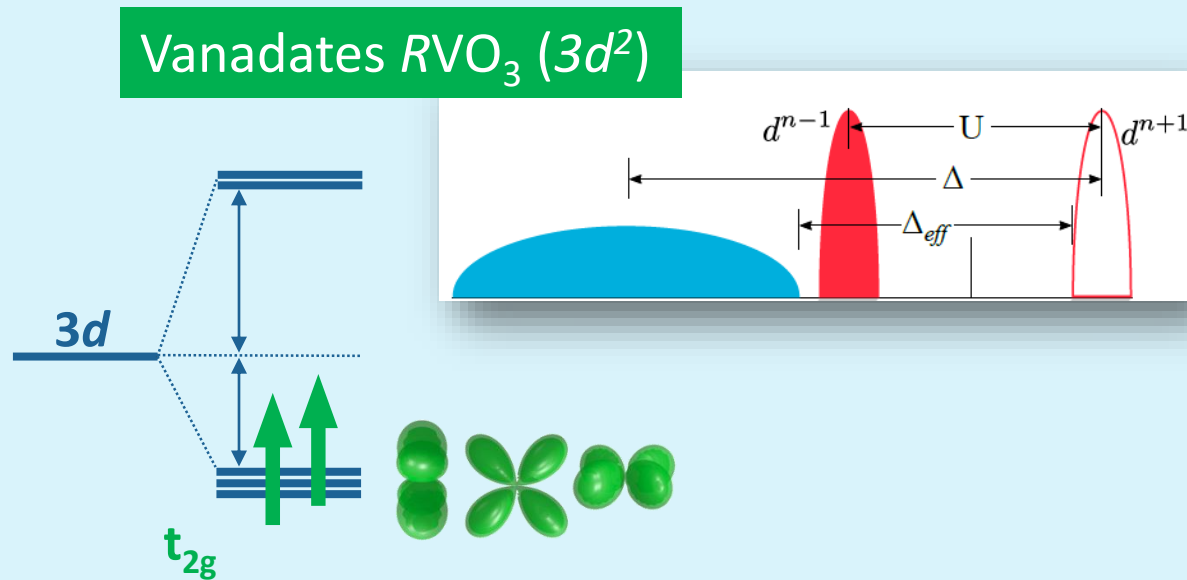
- Strain is the most effective control parameter.
- “Confinement effect” of different band insulators is rather small.
- Up to **25% x^2-y^2 polarisation**, but more is difficult to archive.

Motivation to study YVO_3 superlattices

Orbital occupations determine electronic structure and magnetic superexchange interactions:

- **e_g electron systems:** Several studies on heteroepitaxial modifications (strain, confinement) in nickelates, manganates, cuprates,
- **t_{2g} systems:** Less explored and couple less to the lattice

Rare-earth vanadates (RVO_3 , $R = Y, \text{La-Lu}$)

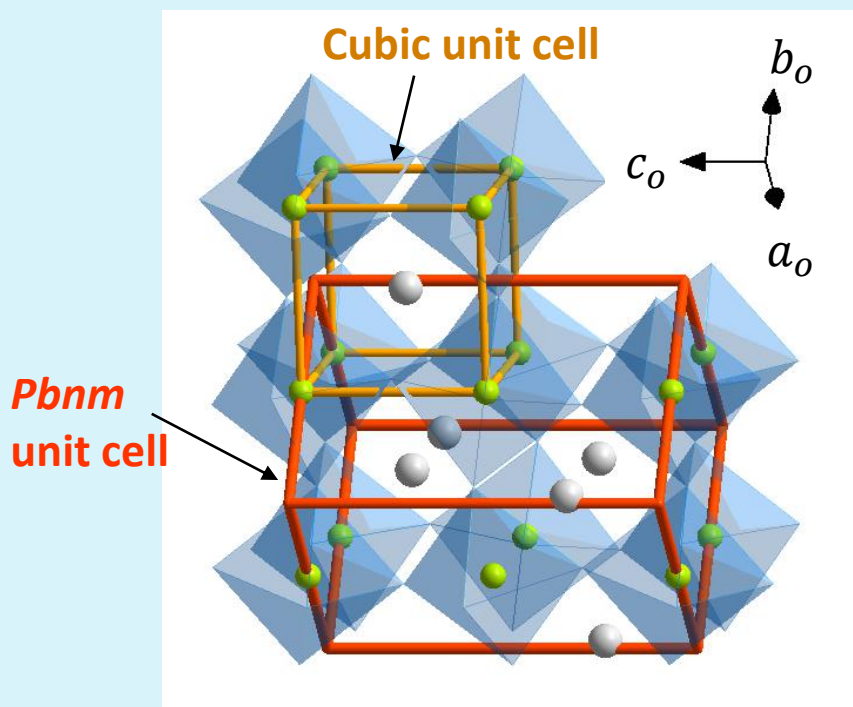


- Strongly correlated **Mott-Hubbard insulator** (no MIT)
- Crystal-field + superexchange dominate

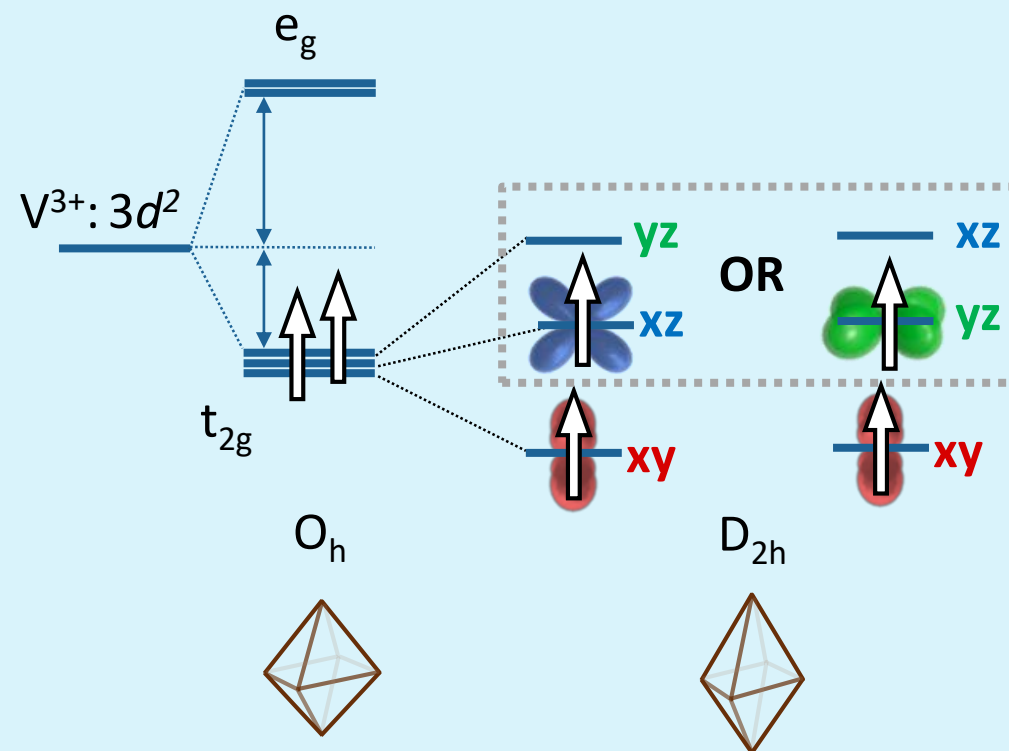
Interplay of spin, orbital and lattice degrees of freedom results in **unique orbital and spin ordering** patterns

Rare-earth vanadates (RVO_3)

Orthorhombic crystal structure



Electronic structure

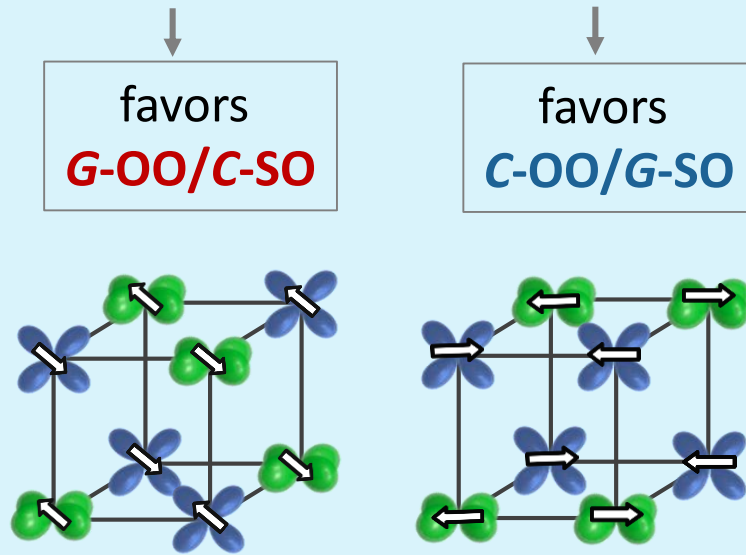


Two **competing** orbital ordered phases

Phase diagram of rare-earth vanadates

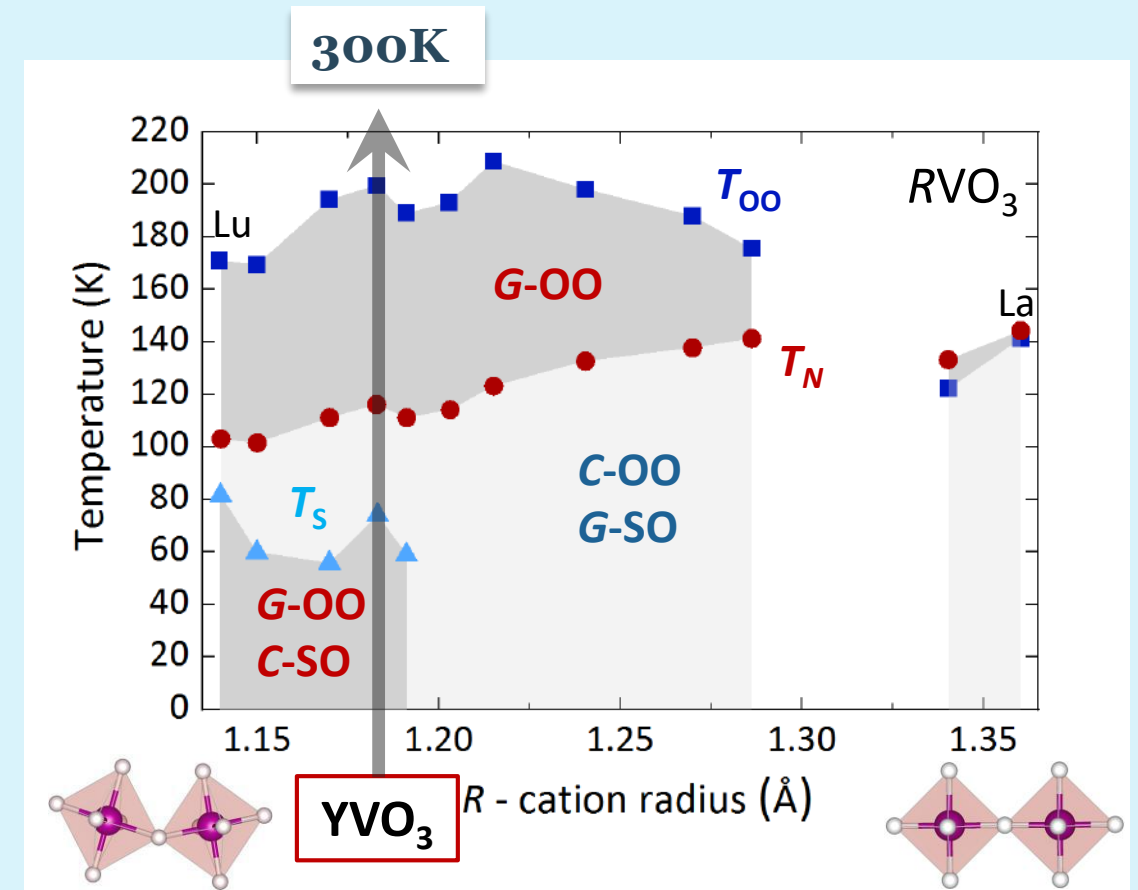
Hamiltonian $\mathcal{H} = \mathcal{H}_J + \mathcal{H}_V$

= Superexchange + Lattice effects



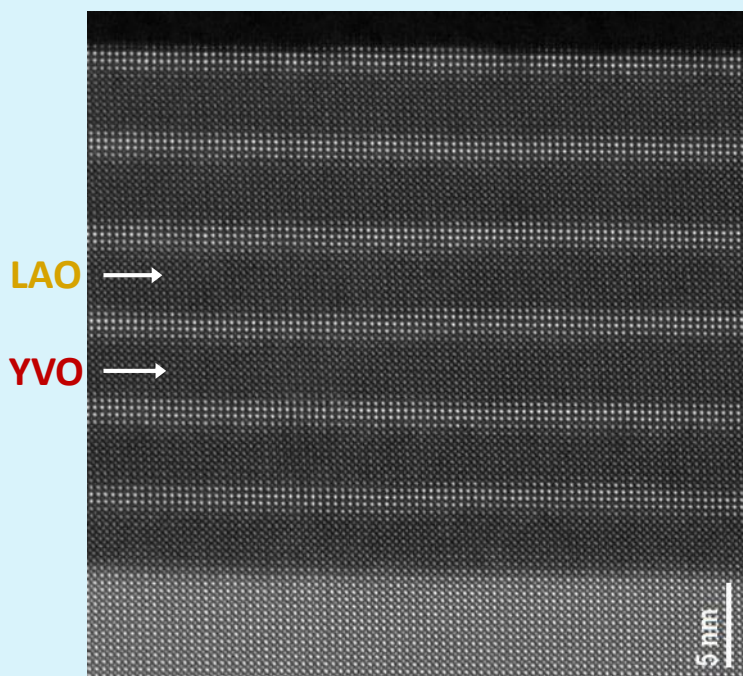
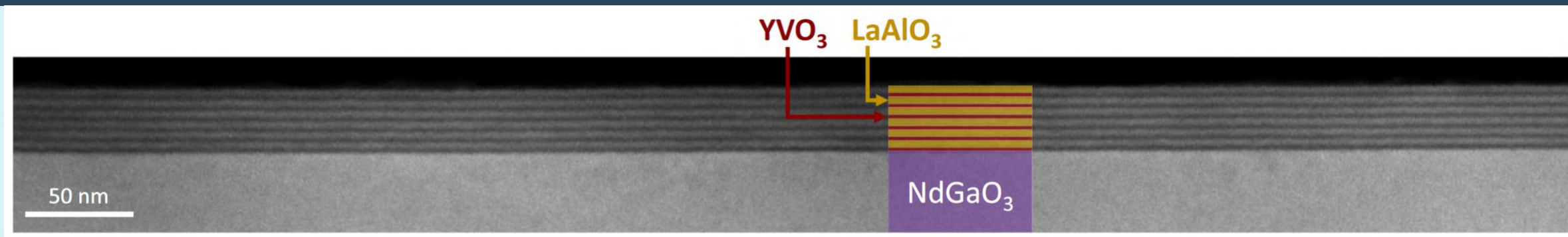
Heterostructures of member at phase boundary: YVO_3

Explore possible changes induced by heteroeptaxy

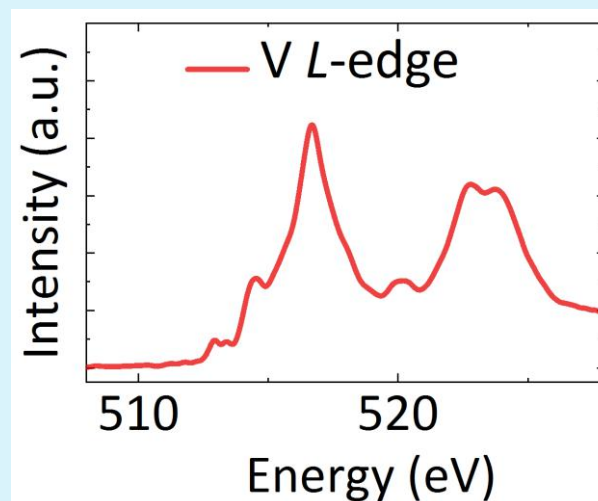


Lecture by A. Oleś

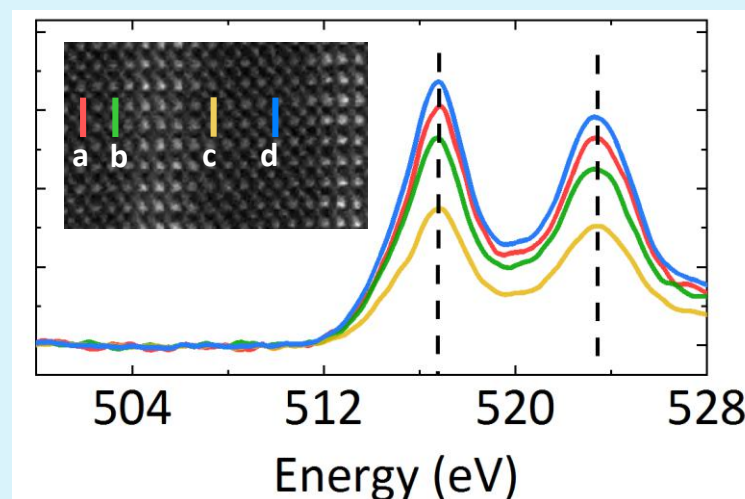
Scanning transmission electron microscopy



XAS V L-edge



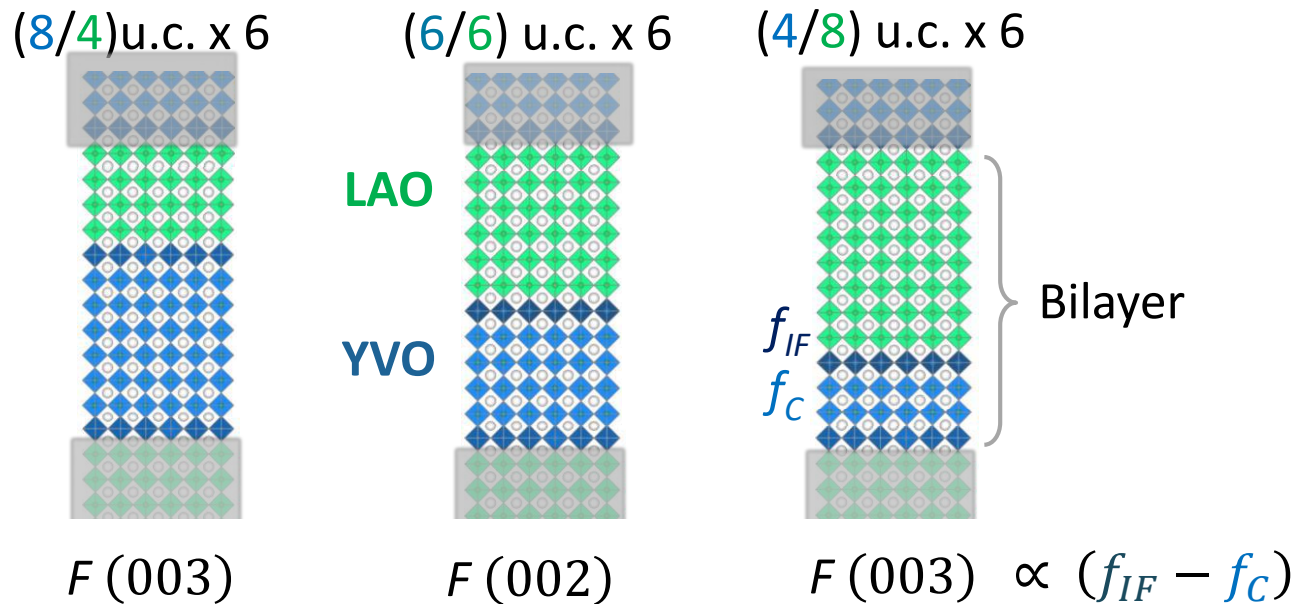
EELS line scans V L-edge



V^{3+} oxidation state throughout the layer stacks

Design of the superlattice geometry

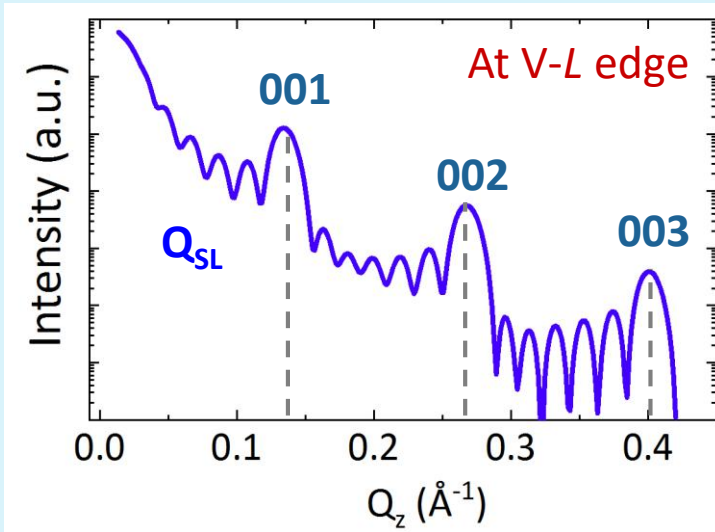
Three $\text{YVO}_3/\text{LaAlO}_3$ Superlattices on NdGaO_3 (110)



Superlattice structure chosen to optimize the analysis of resonant x-ray reflectometry

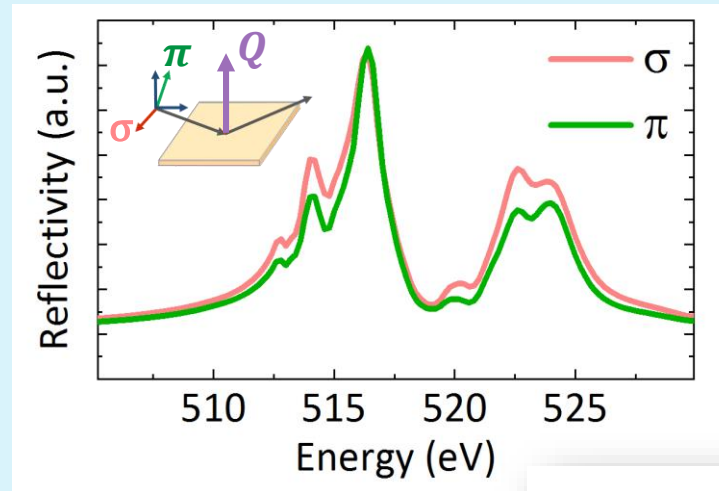
Resonant reflectometry measurements

Q-dependent reflectivity

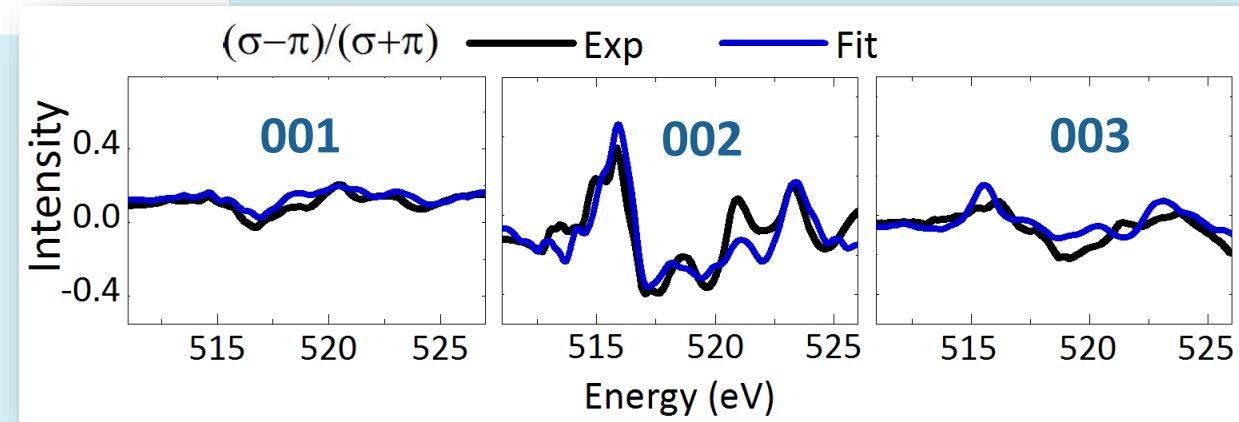


Fit to get depth-dependent structural information

Polarized E-dependent reflectivity



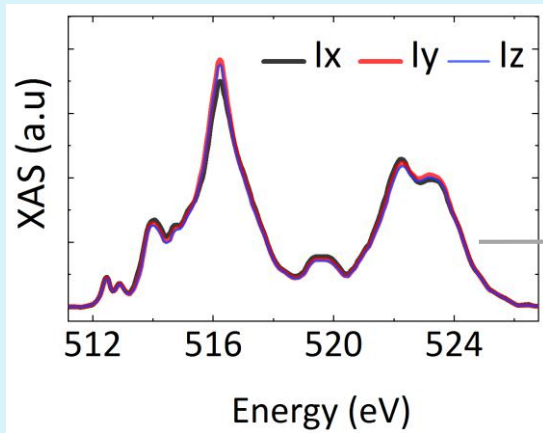
Dichroism



Simulate to get depth-dependent electronic information

Simulating reflectivity – Example 4/8 superlattice

Measured Polarized XAS

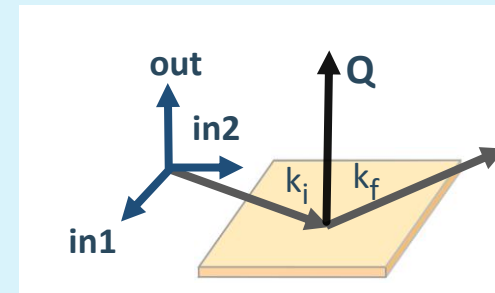


Complex refractive index

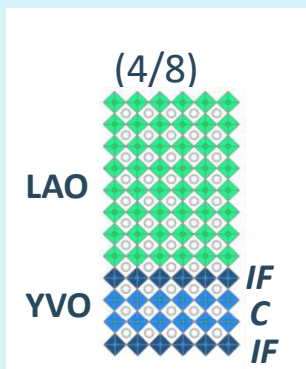
$$N = (1 + \delta) + i\beta = \sqrt{\epsilon}$$

Kramers-Kronig

$$\begin{bmatrix} \epsilon_{in1} & 0 & 0 \\ 0 & \epsilon_{in2} & 0 \\ 0 & 0 & \epsilon_{out} \end{bmatrix}$$



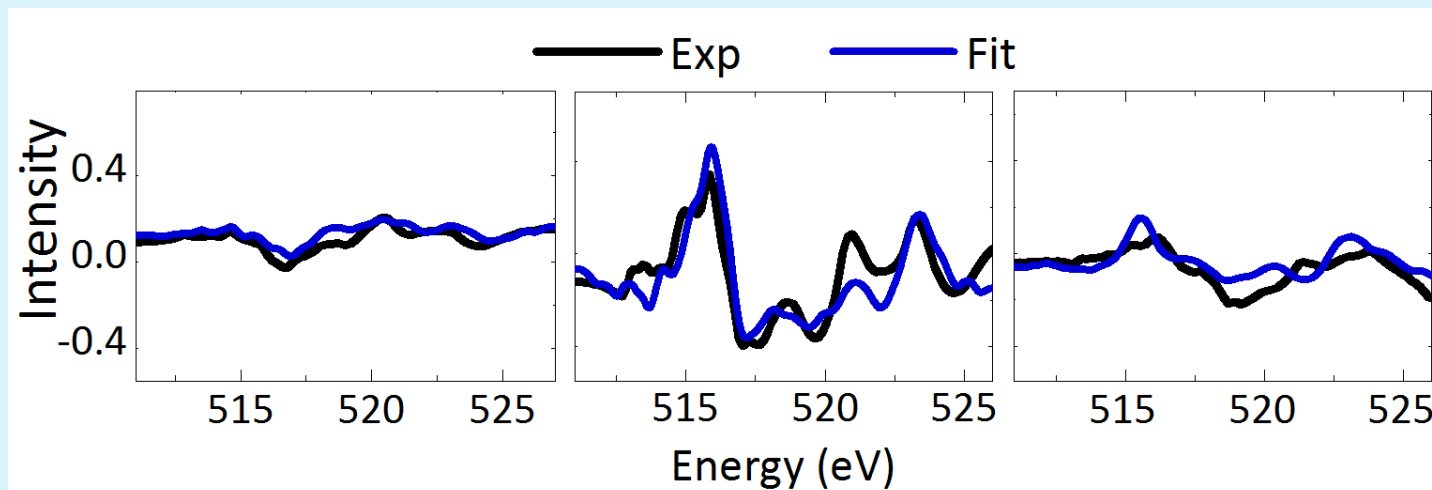
Test different models



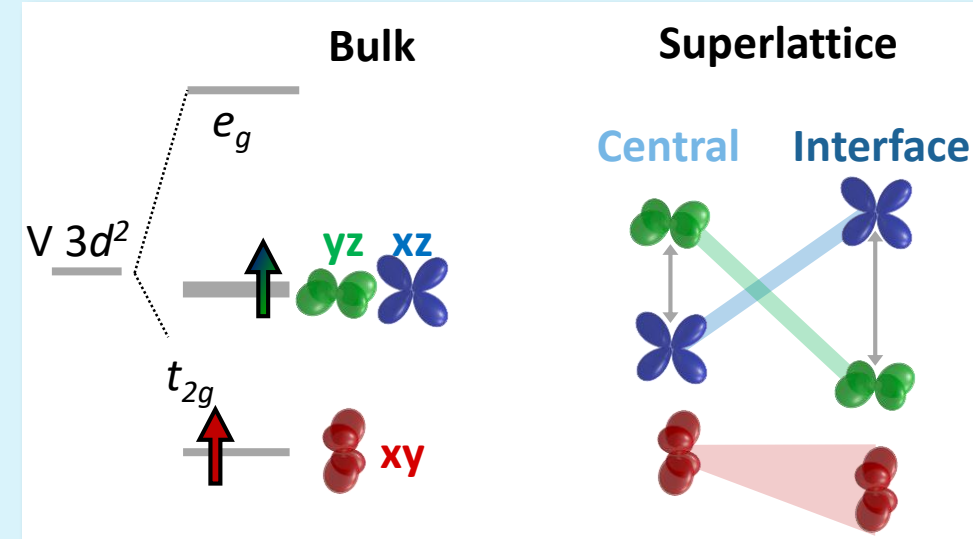
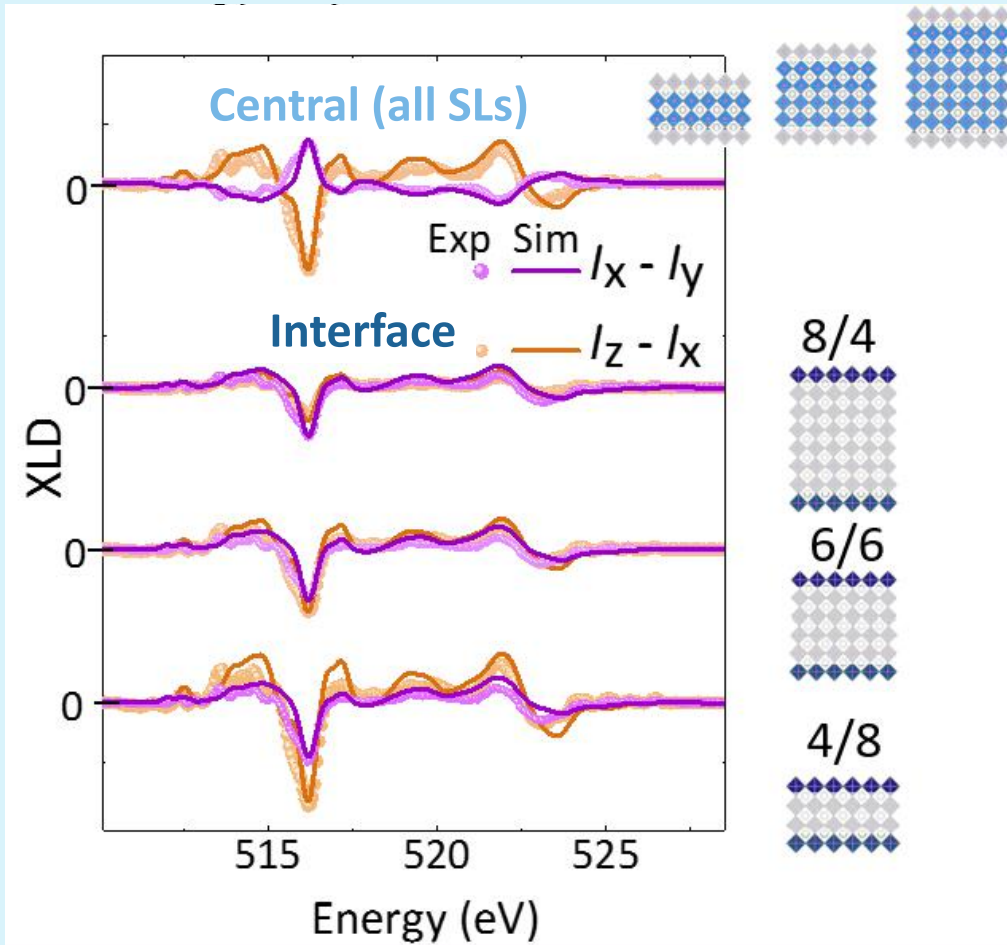
Vary parameters:

$\alpha_x, \alpha_y, \alpha_z$: modulation
and f : total dichroism

$$\text{XLD}_{\text{average}} = \text{XLD}_{\text{Interface}} + \text{XLD}_{\text{central}}$$



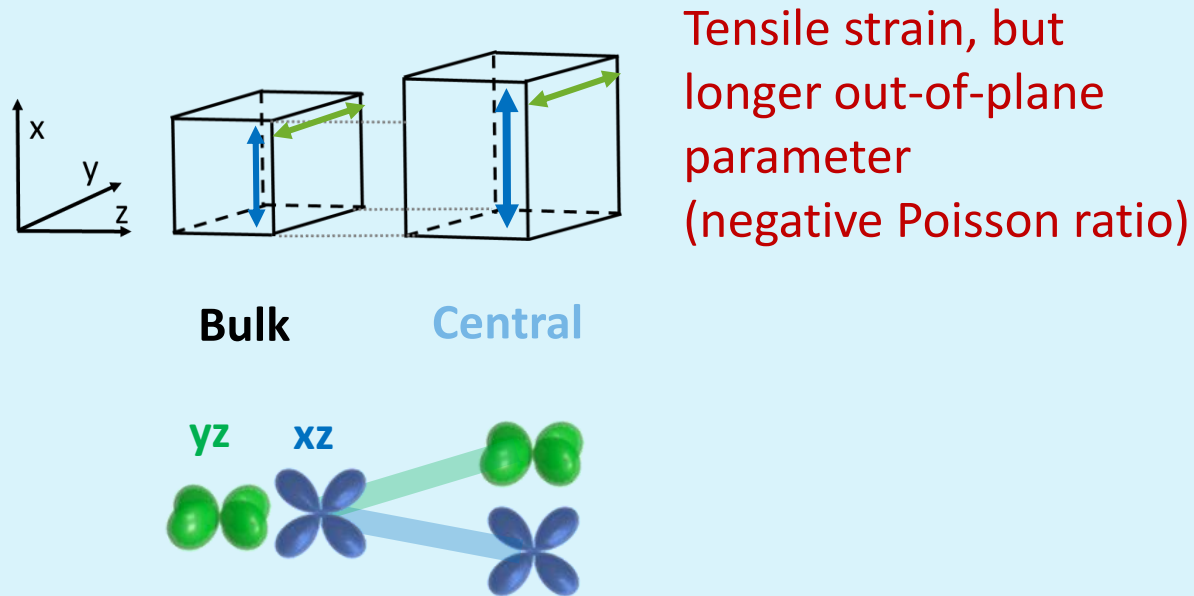
Layer-resolved linear dichroism



- xz and yz average degeneracy lifted in SL unlike bulk
- xz - yz polarization is inverted between Central and Interface layers
- xy occupation depends on number of YVO₃ layers

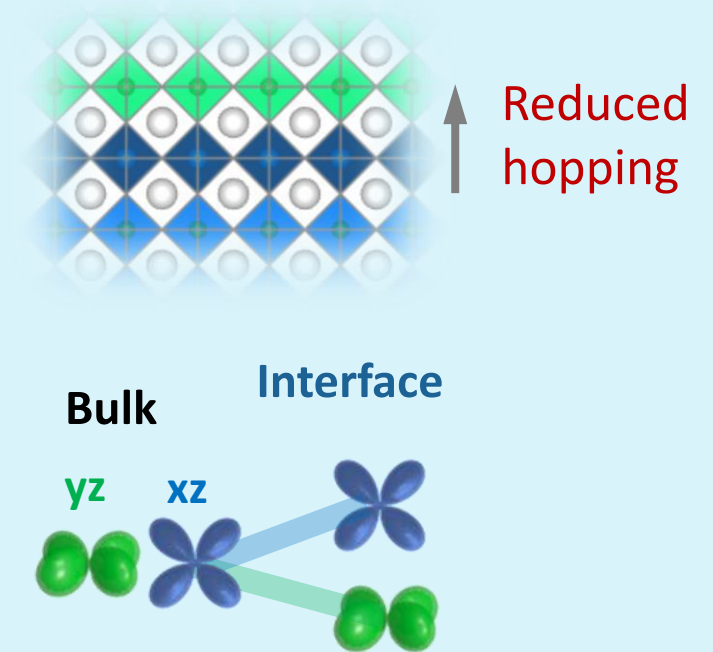
Qualitative understanding

Central layers: Epitaxial strain



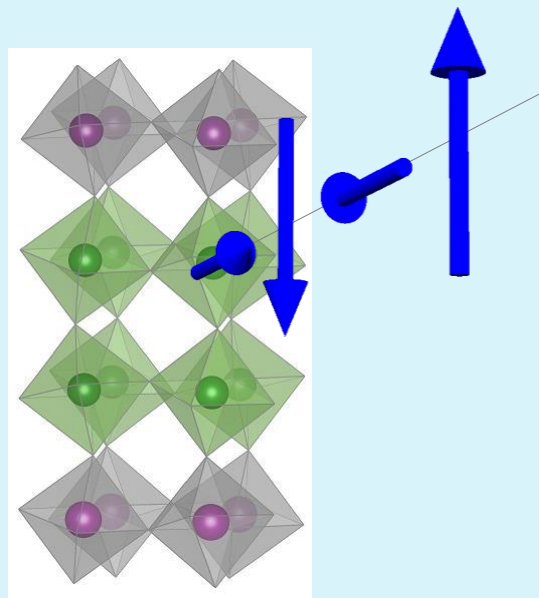
Longer out-of-plane axis \rightarrow increase **xz** occupation

Interface layers : Confinement



Confinement \rightarrow increase **yz** occupation

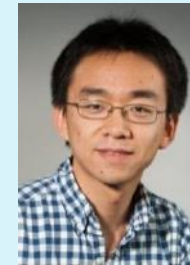
Noncollinear magnetic order in nickel oxide heterostructures



Martin
Bluschke



Alex Frano

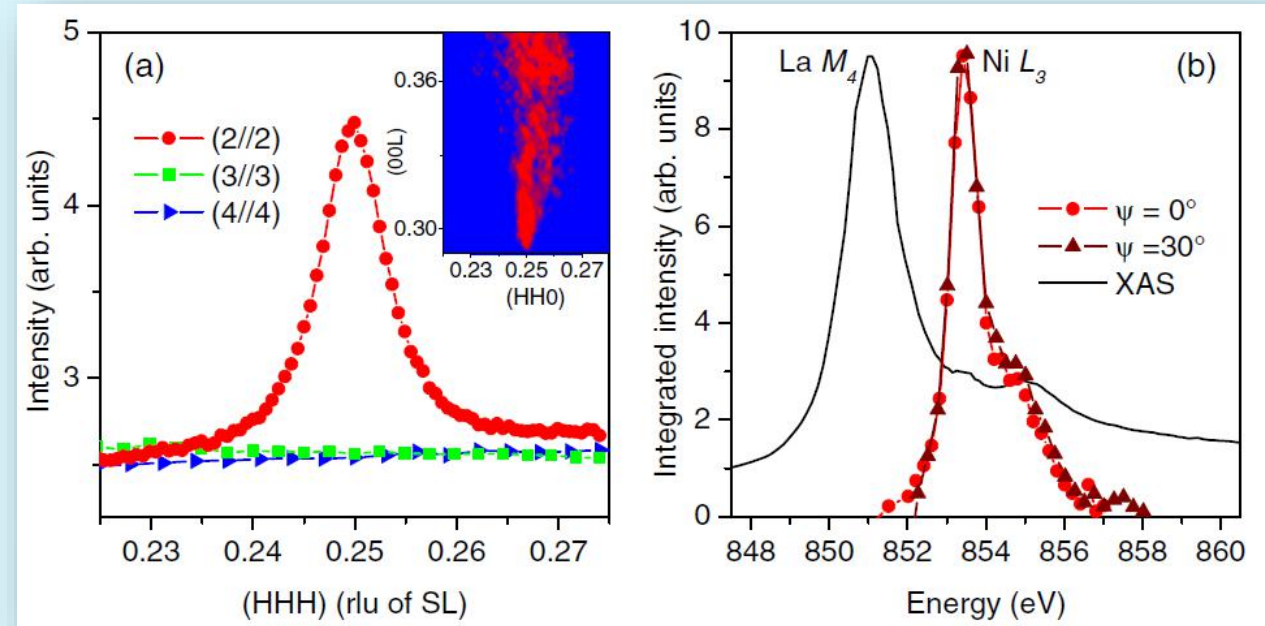
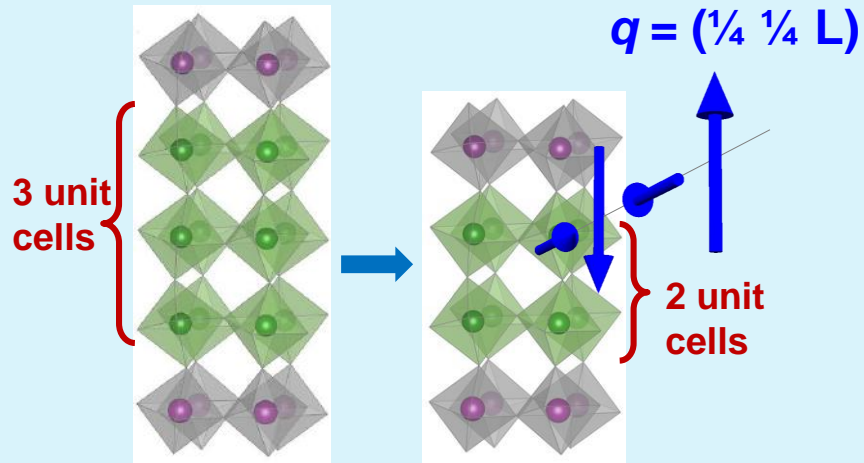


Yi Lu



Matthias
Hepting

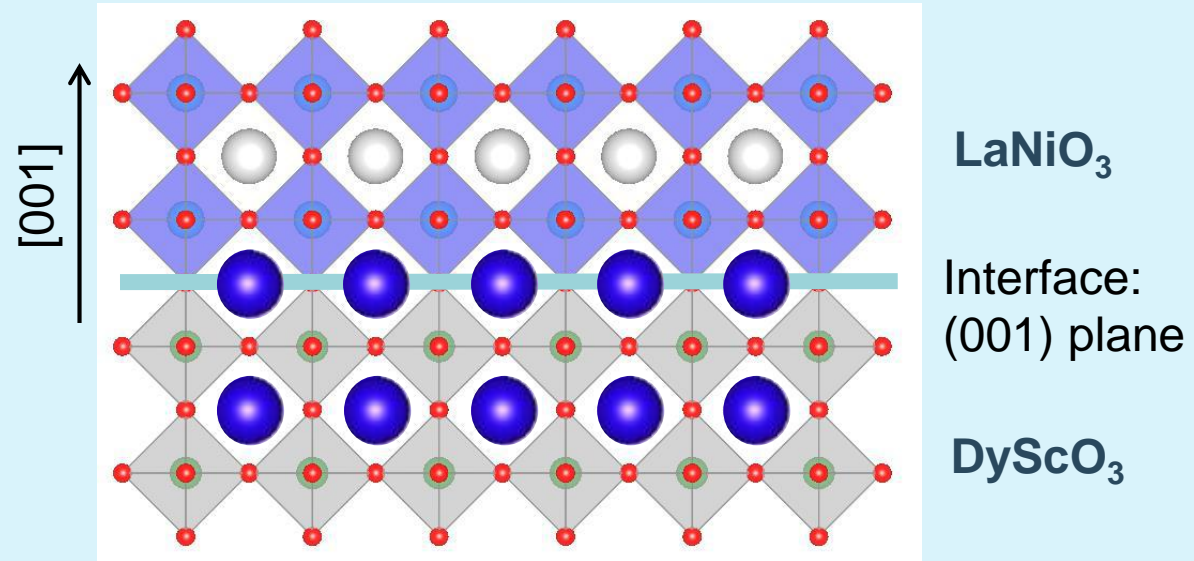
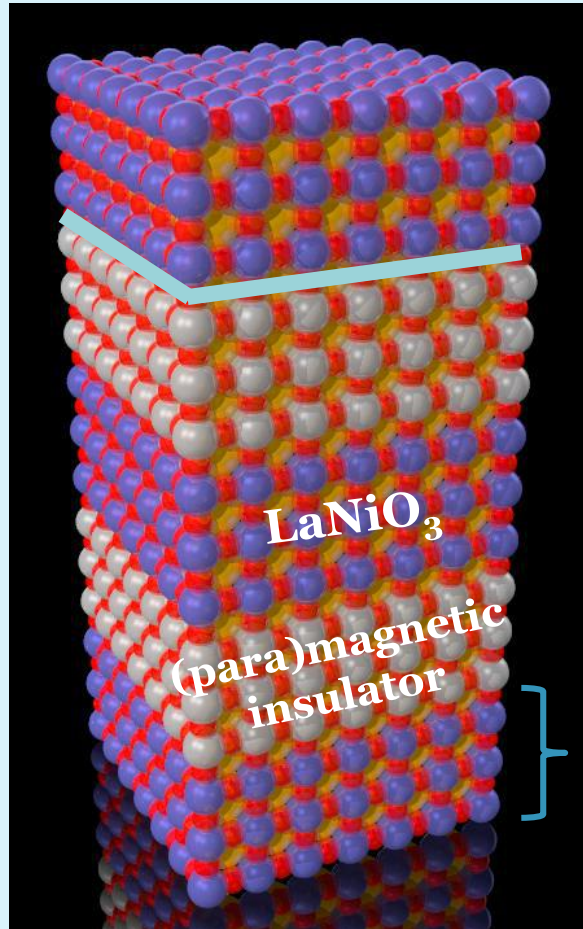
Resonant magnetic scattering of $\text{LaNiO}_3\text{--LaAlO}_3$ superlattices



LaNiO_3 slabs ≤ 2 unit cells: magnetic peak at $q = (\frac{1}{4} \frac{1}{4} L)$, but no bond disproportionation ($\delta_{\text{Ni-O}} \leq 0.01\text{\AA}$)

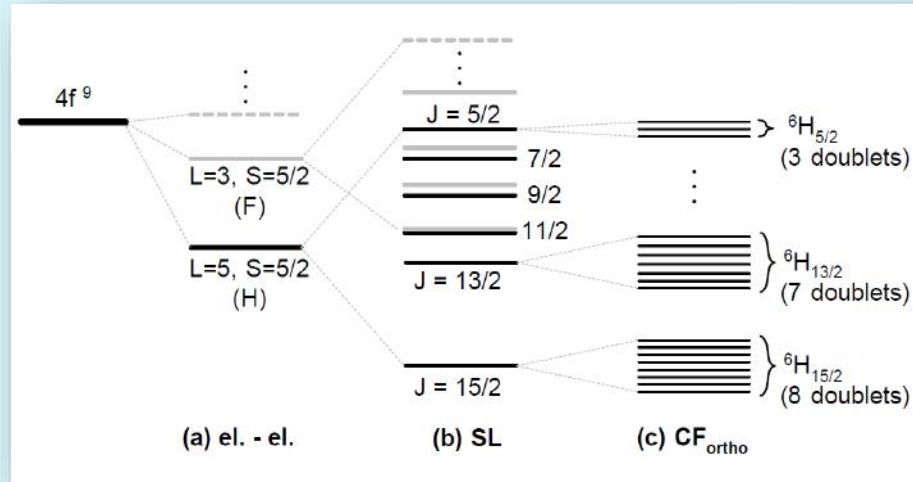
New phase without bulk analog!

II. (001) LaNiO_3 - DyScO_3 superlattices

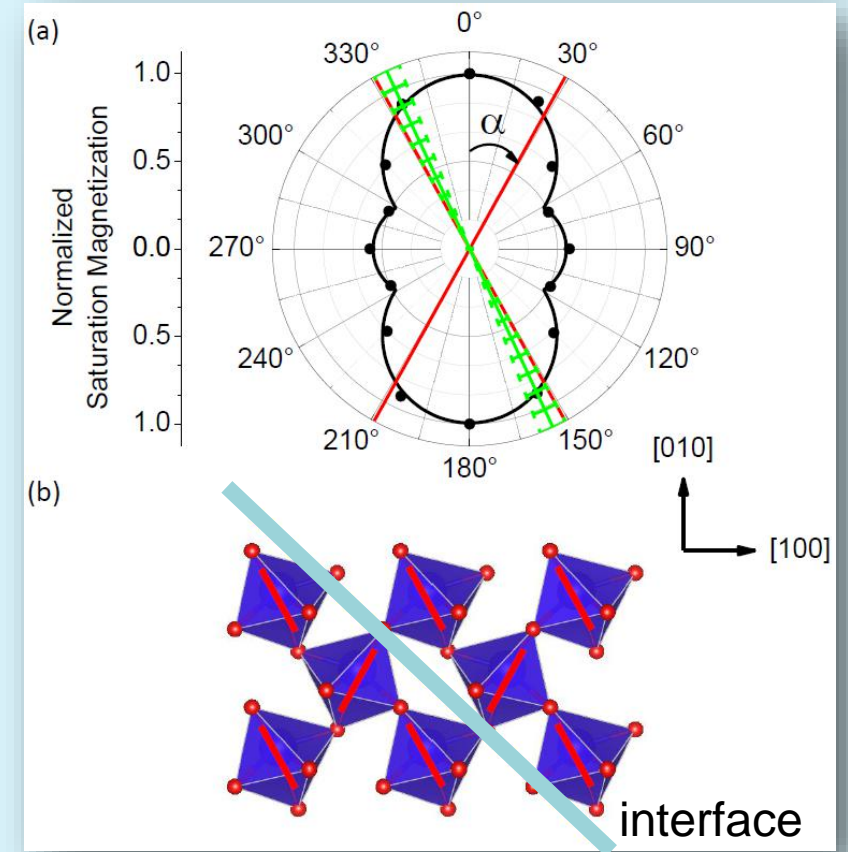


- 2 unit cell thick LaNiO_3 : non-collinear order below $T \sim 100\text{K}$
- DyScO_3 : paramagnetic insulator with Dy-Dy exchange interaction driven magnetic order below $T \sim 3\text{K}$

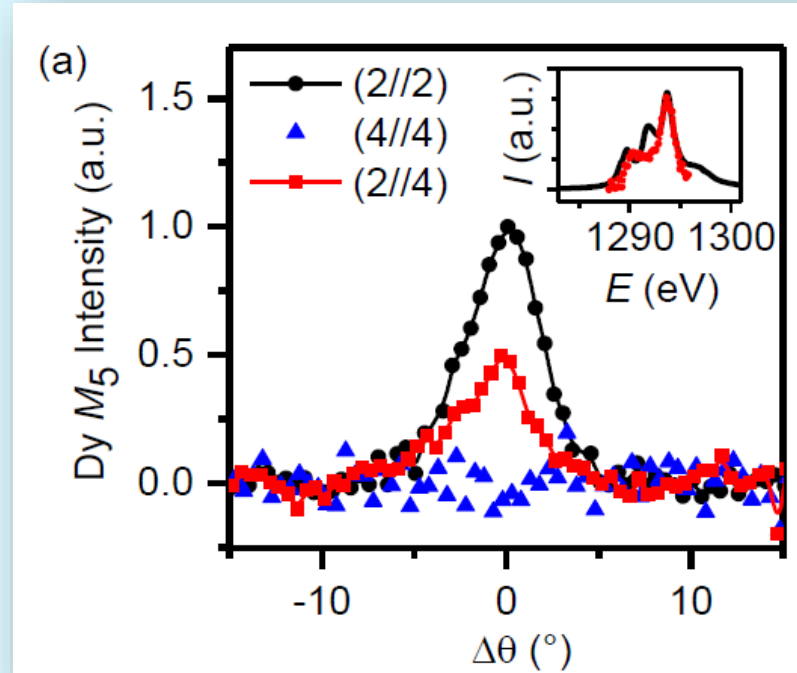
Bulk DyScO₃



- Distorted orthorhombic $Pbnm$ structure
- Magnetic moment of $10 \mu_B$
- Low symmetry crystal field produces a strong Ising anisotropy with two inequivalent Ising axes (bc mirror plane) that alternate from site to site.
- Ising axes lie 29° from the b axis.

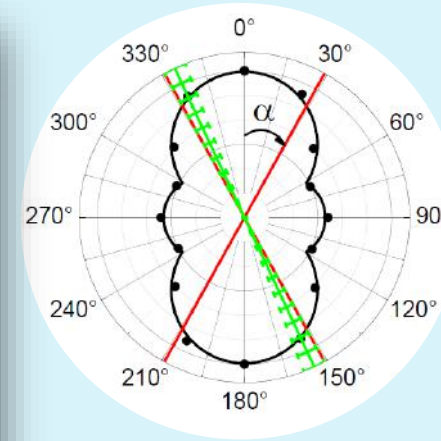
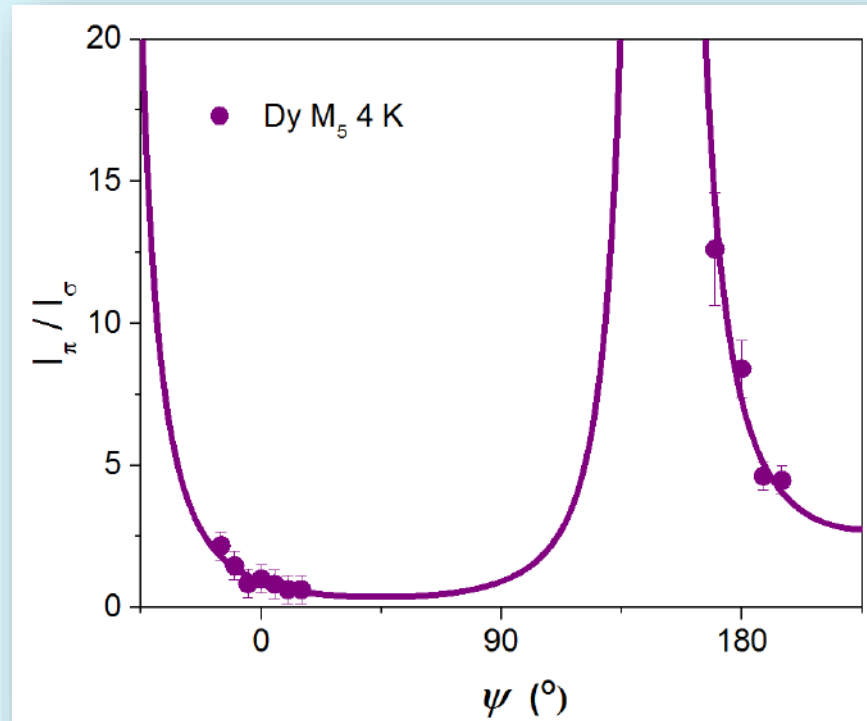


Resonant soft x-ray scattering of $\text{LaNiO}_3\text{-DyScO}_3$



- $q = (\frac{1}{4} \frac{1}{4} \frac{1}{4})$ magnetic reflection at the Dy M_5 resonance below $T_{ind} \sim 10$ K
- Magnetic order induced into interfacial layers only.

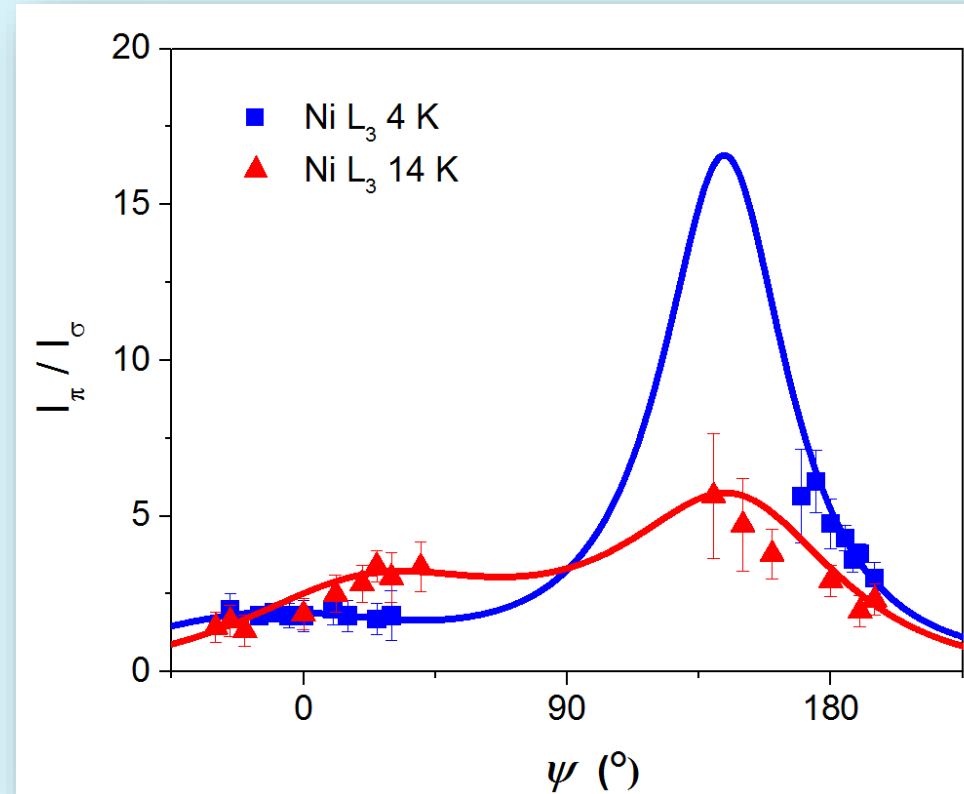
Resonant soft x-ray scattering of $\text{LaNiO}_3\text{-DyScO}_3$



$$I_{\mu\nu} = \left| \sum_i e^{i\mathbf{q}\cdot\mathbf{r}_i} F_i(E) \varepsilon_\mu \times \varepsilon_\nu^* \cdot \hat{\mathbf{m}}_i \right|^2$$

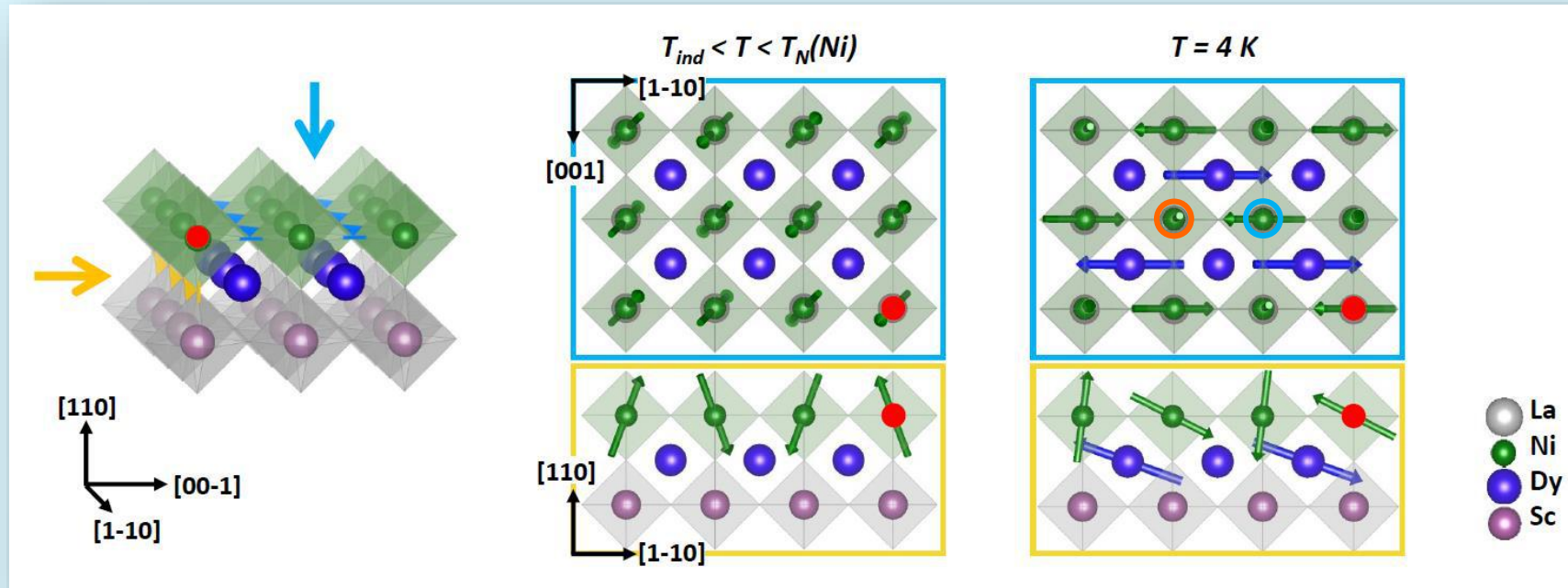
- Best description of ψ dependence by a collinear antiferromagnetic model
→ Dy moments form an $\sim 25^\circ$ with the b axis.
- Close to one out of the two Ising axis in bulk DyScO_3
- “up zero down zero”

Feedback to the Ni magnetic order



Azimuthal dependence for $T > T_{\text{ind}}$ and $T > T_{\text{ind}}$ is different

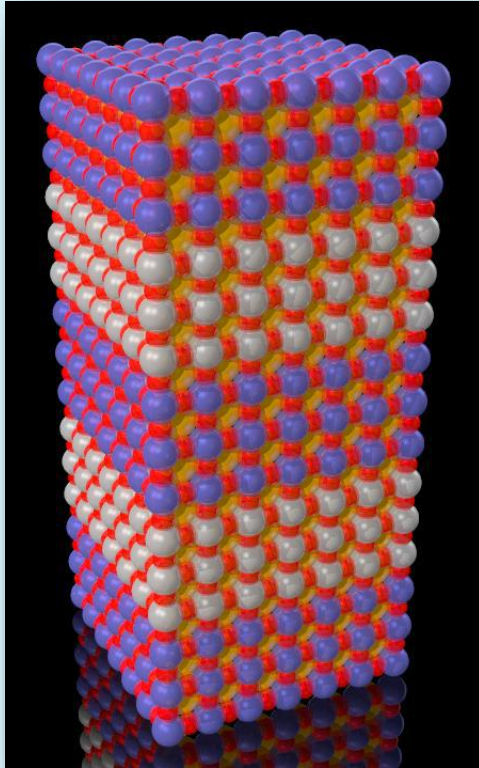
Proposed magnetic order



Interaction across the interface generate two inequivalent Ni sites

- gaining energy from Ni-Dy exchange energy
- orientation determined by Ni-Ni exchange (Ni-Dy frustrated)

Summary & Conclusion



For a future rational design of complex transition-metal oxide heterostructures it is important to **identify and understand interface reconstruction mechanisms**. X-ray spectroscopy provides valuable insights.

Examples of spin, orbital, charge, and lattice reconstructions in vanadate and nickelate heterostructures:

- Importance of **structural details** on electronic instabilities (orbital order / metal-insulator transition)
- Depth profile of interfacial **charge doping depends on chemistry**
- Topotactic anion exchange synthesis offers many new possibilities.

**Create atomic-scale Quantum Materials
with desired properties**

Many thanks to my collaborators

Soft x-ray spectroscopy: Dep. of B. Keimer (MPI-FKF), E. Goering (Dep. G. Schütz (MPI-IS)
E. Schierle, E. Weschke (HZB, Berlin)
R. Sutarto, F. He (CLS)

PLD and MBE growth: G. Christiani, G. Logvenov (MPI-FKF)

Soft chemistry/target preparation: R. Merkle, A. Fuchs (MPI-FKF)

Theory: H. Menke, D. Mantadakis, P. Hansmann (MPI-FKF, FAU Erlangen)
B. Geisler, R. Pentcheva (U-Duisburg-Essen)
M. Haverkort (U-Heidelberg)

Electron microscopy: F. Misják, U. Kaiser (U-Ulm)
Y. E. Suyolcu, Y. Wang, P. A. van Aken (MPI-FKF)

Discussion: G. A. Sawatzky (UBC Vancouver), B. Lotsch,
V. Katukuri, N. Bogdanov, A. Alavi (MPI-FKF)

